



HiPRWind
***High Power, high Reliability,
Off-shore Wind Technology***

PROJECT DELIVERABLE REPORT

DELIVERABLE D1.3

Final Design of the floating Platform

Document Identifier:	HiPRWind_D1.3_Final Design of the floating Platform.docx
Preparation Date:	May 30, 2014
Document Status:	FINAL
Author(s):	Gunther Auer, Javier Pascual, Raul Manzananas
Dissemination Level:	PU



**Project co-funded by the European Community
in the 7th RTD Framework Programme, Energy**
Grant Agreement 256812, Call FP7-ENERGY-2010-1



DOCUMENT SUMMARY SHEET

Template Details	
Type of Document:	Deliverable
Document Reference #:	D1.3
Title:	Final Design of the floating Platform
Version Number:	2.0
Release Date:	May 30, 2014
Delivery Date:	
Author(s):	Gunther Auer, Javier Pascual, Raul Manzananas(Acciona Energía)
Document Identifier:	HiPRWind_D1.3_Final Design of the floating Platform.docx
Document Status:	FINAL
Dissemination Level:	PU - Public

Project Details	
Project Acronym:	HiPRWind
Project Title:	High Power, High Reliability Offshore Wind Technology
Project Number:	256812
Call Identifier:	FP7-ENERGY-2010-1
Call Theme:	Information and Communication Technologies
Project Coordinator:	Fraunhofer Institute for Wind Energy and Energy Systems Technology
Partners:	<p> IDESIA - Ingenieria y Diseno Europeo S.A., Spain NTNU – Norwegian University of Science & Technology, Norway Acciona Energia S.A. / Spain SINTEF Energi AS / Norway Technip France SAS, France National Renewable Energy Centre, UK ABB Schweiz AG, Switzerland TECNALIA, Spain Wölfel Beratende Ingenieure GmbH & Co. KG, Germany Dr. techn. Olav Olsen AS, Norway Bureau Veritas, France Micromega Dynamics SA, Belgium Universität Siegen, Germany TWI Limited, UK I-Techs.p.r.l., Belgium Acciona Windpower S.A., Spain Vicinay Cadenas S.A., Spain </p>
Instrument:	Collaborative Project
Contract Start Date:	November 1, 2010
Duration:	60 Months

Abstract

This document contains the detailed final design of the HiPRWind floating platform with the relevant design data. Detail documentation are provided in Annexes A to F.

Keywords: Final Design, Floating Platform, RAO, Fatigue, Stress Concentration Factor, Seakeeping, Structural Calculation, Mooring, Chain, Towing, Corrosion Protection, Access System, Ballast System, Fully Coupled Model, Uncoupled Model, Damper, Towing, Dynamic cable, Load Case, Stress Analysis, Nodes

Revision History

Version:	Date:	Status:	Comments
1.0	03/10/2013	Draft	Gunther Auer
2.0	30/05/2014	Final	J. Giebhardt (approved)

Copyright notice

© 2010-13 the HiPRWind Consortium. All rights reserved. **HiPRWind**– an acronym for **H**igh **P**ower, **H**igh **R**eliability Offshore **W**ind Technology – is a Collaborative Project co-financed by the European Commission under FP7 RTD Grant Agreement no. 256812. For general information see www.hiprwind.eu. In accordance with the Dissemination Level indicated on the cover page, you are permitted to copy and use this document, including this copyright notice, but modifying the document or re-distributing it by another name or in another context is not allowed. The contents are reserved by default and may not be disclosed to 3rd parties, except as mandated by the EC Grant Agreement for review and dissemination purposes. Trademarks and other rights on third-party products mentioned in this report are acknowledged and owned by their respective holders. The information in this document represents views and findings of the HiPRWind Consortium Partners at the date of issue. The HiPRWind Consortium does not guarantee that any information contained herein is error-free nor does it make any warranties, express, implied, or statutory, by issuing this document.

Table of Contents

1	Introduction.....	10
2	Structural and Seakeeping Calculations	11
2.1	Seakeeping:	11
2.1.1	<i>Uncoupled Model</i>	11
2.1.2	<i>Fully Coupled Model</i>	12
2.2	Structural calculations.....	15
2.2.1	<i>Fatigue life assessment</i>	15
2.2.2	<i>Load case analysis</i>	17
2.2.3	<i>Stress analysis</i>	18
2.2.3.1	Introduction.....	18
2.2.3.2	Individual joints	19
2.2.3.3	Tower support assembly	19
2.2.4	<i>Results structural calculations</i>	20
2.2.4.1	Introduction.....	20
2.2.4.2	Individual joints	20
2.2.4.3	Tower support assembly	20
2.2.4.4	Discussion of results for structural calculations.....	20
2.2.5	<i>Conclusion for structural calculations</i>	20
2.2.6	<i>Braces</i>	21
2.2.6.1	Model description for Brace structural calculations.....	22
2.2.6.2	Results – diagonal braces.....	23
2.2.6.3	Results – lower braces	26
2.2.6.4	Stress reduction by brackets.....	29
2.2.7	<i>Design check under extreme conditions by BV</i>	32
2.2.7.1	Load cases for extreme conditions.....	32
2.2.7.2	Methodology:.....	33
2.2.7.3	Modeling	33
2.2.7.4	Model	34
2.2.7.5	Results design check.....	41
2.2.7.6	Conclusions design check	42
2.2.8	<i>Dampers</i>	43
2.2.9	<i>Substructure Brace System and wind turbine tower support</i>	47
2.2.10	<i>Door opening in tower base</i>	48
2.2.11	<i>Hatch opening in bottom plate</i>	49
2.2.12	<i>Ballast system</i>	50
2.2.13	<i>Access system</i>	52
2.2.14	<i>Corrosion protection system</i>	54
2.2.15	<i>Mooring</i>	57
2.2.15.1	Mooring installation	58

2.2.15.2	Calculations for the Mooring chains	64
2.2.16	Towing	71
2.2.17	Dynamic CABLE	75
3	References.....	79
4	ANNEX A.....	Error! Bookmark not defined.
5	ANNEX B	Error! Bookmark not defined.
6	ANNEX C	Error! Bookmark not defined.
7	ANNEX D.....	Error! Bookmark not defined.
8	ANNEX E	Error! Bookmark not defined.
9	ANNEX F	Error! Bookmark not defined.

List of Figures

FIGURE 1 RAOs FOR PITCH AND HEAVE	12
FIGURE 2 INTEGRATED MODEL WITH THE AW77 WIND TURBINE MOUNTED ON THE SEMISUBMERSIBLE STRUCTURE	12
FIGURE 3 LOCATION OF SEMISUBMERSIBLE FLOATING PLATFORM NODES AND MEMBERS IN THE BLADED MODEL	13
FIGURE 4 SAMPLES FOR DIFFERENT MODES FOR EIGENFREQUENCIES	14
FIGURE 5 SAMPLE OF LIFE TIME WEIGHTED EQUIVALENT LOADS	15
FIGURE 6 SAMPLE OF RAINFLOW CYCLE EXCEEDANCE DIAGRAM FOR THE COMPONENTS	15
FIGURE 7 NOMENCLATURE FOR NODES ON SEMISUBMERSIBLE STRUCTURE	18
FIGURE 8 PART OF COLUMN SELECTED FOR LOCAL MODEL	22
FIGURE 9 (A) SHOWS THE OUTER GEOMETRY OF THE LOCAL MODEL IN ABAQUS, WHILE (B) SHOWS THE COHERENT MESH.	22
FIGURE 10 (A) SHOWS THE INNER GEOMETRY OF THE LOCAL MODEL IN ABAQUS, WHILE (B) SHOWS THE COHERENT MESH	23
FIGURE 11 VON MISES STRESS FOR OUTER GEOMETRY UNDER AXIAL LOADING OF DIAGONAL BRACE. THE MAXIMUM STRESS VALUE OVER THE CROSS SECTION IS SHOWN. (STRESS VALUES ARE IN Pa)	23
FIGURE 12 VON MISES STRESS FOR GEOMETRY WITHOUT OUTER SHELL UNDER AXIAL LOADING. THE MAXIMUM STRESS VALUE OVER THE CROSS SECTION IS SHOWN. (STRESS VALUES ARE IN Pa)	24
FIGURE 13 VON MISES STRESS FOR INNER GEOMETRY, BRACE REMOVED, UNDER AXIAL LOADING. THE MAXIMUM STRESS VALUE OVER THE CROSS SECTION IS SHOWN. (STRESS VALUES ARE IN Pa)	24
FIGURE 14 VON MISES STRESS FOR MOMENT ABOUT LOCAL “HORIZONTAL” AXIS OF DIAGONAL BRACE. THE MAXIMUM STRESS VALUE OVER THE CROSS SECTION IS SHOWN. (STRESS VALUES ARE IN Pa)	25
FIGURE 15 VON MISES STRESS FOR MOMENT ABOUT LOCAL “VERTICAL” AXIS OF DIAGONAL BRACE. THE MAXIMUM STRESS VALUE OVER THE CROSS SECTION IS SHOWN. (STRESS VALUES ARE IN Pa)	26
FIGURE 16 VON MISES STRESS FOR OUTER GEOMETRY UNDER AXIAL LOADING OF LOWER BRACE. THE MAXIMUM STRESS VALUE OVER THE CROSS SECTION IS SHOWN. (STRESS VALUES ARE IN Pa)	26
FIGURE 17 VON MISES STRESS FOR INNER GEOMETRY UNDER AXIAL LOADING OF LOWER BRACE. THE MAXIMUM STRESS VALUE OVER THE CROSS SECTION IS SHOWN. (STRESS VALUES ARE IN Pa)	27
FIGURE 18 VON MISES STRESS FOR INNER GEOMETRY (BRACE REMOVED) UNDER AXIAL LOADING OF LOWER BRACE. THE MAXIMUM STRESS VALUE OVER THE CROSS SECTION IS SHOWN. (STRESS VALUES ARE IN Pa)	27
FIGURE 19 PLOT OF VON MISES STRESS FOR MOMENT ABOUT LOCAL HORIZONTAL AXIS OF LOWER BRACE. THE MAXIMUM STRESS VALUE OVER THE CROSS SECTION IS SHOWN. (STRESS VALUES ARE IN Pa)	28
FIGURE 20 PLOT OF VON MISES STRESS FOR MOMENT ABOUT LOCAL VERTICAL AXIS OF LOWER BRACE. THE MAXIMUM STRESS VALUE OVER THE CROSS SECTION IS SHOWN. (STRESS VALUES ARE IN Pa)	29
FIGURE 21 PROPOSED BRACKET SYSTEM.....	30
FIGURE 22 PLOT OF VON MISES STRESS FOR AXIAL LOAD OF LOWER BRACE WITH BRACKETS. THE MAXIMUM STRESS VALUE OVER THE CROSS SECTION IS SHOWN. (STRESS VALUES ARE IN Pa)	31
FIGURE 23 COMPARISON OLD VERSUS NEW SOLUTION FOR THE BRACKETS FOR THE LOWER BRACES	32
FIGURE 24 EXTREME CONDITIONS.....	32
FIGURE 25 BV METHODOLOGY	33
FIGURE 26 HYDRODYNAMIC MODEL	35
FIGURE 27 STRUCTURAL MODEL.....	36
FIGURE 28 BV SOFTWARE MARS.....	37
FIGURE 29 FEA COLUMN TOWER CONNECTION	37
FIGURE 30 MOORING LINE CHARACTERISTICS	40
FIGURE 31 EXAMPLE OF TENSION MATRIX COMPUTED	41
FIGURE 32 WELDING ON BOTH SIDES OF A PLATE AT A CROSSING	42
FIGURE 33 DAMPER COMPONENTS FROM CAD MODEL	45
FIGURE 34 FINAL CALCULATIONS FOR DAMPER DIMENSIONS.....	45
FIGURE 35 FINAL DAMPER VALUES FOR HYDRODYNAMIC ANALYSIS.....	46
FIGURE 36 WADAM CALCULATIONS.....	46
FIGURE 37 CFD CALCULATIONS	46
FIGURE 38 LOCATION OF PRESSURE SENSORS.....	47
FIGURE 39 DAMPER AND COLUMN TANK TESTING	47
FIGURE 40 RESULTING NEW DAMPER DESIGN	47
FIGURE 41 CENTRAL CONNECTION	48
FIGURE 42 CALCULATION FOR TOWER SUPPORT STRUCTURE	48
FIGURE 43 TOWER DOOR FRAME	49

FIGURE 44 HATCH OPENING IN TRANSITION PIECE BOTTOM	49
FIGURE 45 BALLAST SYSTEM IN COLUMN	50
FIGURE 46 BALLAST TANK SECTION IN COLUMN WITH CENTRAL PIPE	51
FIGURE 47 BALLAST SYSTEM SCHEMATIC	51
FIGURE 48 OUTER COLUMN ACCESS SYSTEM.....	52
FIGURE 49 PLATFORM DESIGN FOR INTERIOR OF COLUMNS	53
FIGURE 50 RESCUE SCENARIOS FOR COLUMN.....	53
FIGURE 51 CENTRAL ACCESS PLATFORM MATERIAL	54
FIGURE 52 SACRIFICIAL ANODE CALCULATION	55
FIGURE 53 COMPARISON SACRIFICIAL ANODES AND IMPRESSED CURRENT SYSTEM.....	56
FIGURE 54 SIMULATIONS FOR DEFECT IN ONE MOORING LINE.....	58
FIGURE 55 TANKS TEST COMPARISON TO NUMERICAL MODEL.....	58
FIGURE 56 TANK TEST CONFIGURATION AND QTF RESULTS.....	59
FIGURE 57 GIS WITH BATHYMETRY OF BIMEP AREA.....	59
FIGURE 58 SLOPES IN THE AREA OF DEPLETION	60
FIGURE 59 SEABED COMPOSITION, SEDIMENT STRUCTURE	60
FIGURE 60 CONSTELLATION AT ARRIVAL OF FLOATER ON SITE	61
FIGURE 61 PREINSTALLED CHAIN SEGMENTS, RED PART BUOY SUSTAINED	61
FIGURE 62 CONNECTION OPERATION FIRST LINE.....	61
FIGURE 63 CONNECTION OPERATION SECOND LINE.....	62
FIGURE 64 START CONNECTION OPERATION THIRD LINE.....	62
FIGURE 65 MOORING LINE FIXTURE AND TENSIONING DETAIL OF CAD MODEL	63
FIGURE 66 MOORING LINE FAIRLEAD.....	63
FIGURE 67 THIRD MOORING LINE TENSIONING ROLLER	64
FIGURE 68 CHAIN CHARACTERISTICS.....	65
FIGURE 69 ANNUAL PARTIAL DAMAGES AT CONNECTION BETWEEN CHAINS. LINE 1.....	68
FIGURE 70 ANNUAL PARTIAL DAMAGES AT CONNECTION BETWEEN CHAINS. LINE 2.....	69
FIGURE 71 ANNUAL PARTIAL DAMAGES AT CONNECTION BETWEEN CHAINS. LINE 3.....	69
FIGURE 72 ANNUAL PARTIAL DAMAGES AT CONNECTION BETWEEN STRUCTURE AND LINE 1.....	70
FIGURE 73 ANNUAL PARTIAL DAMAGES AT CONNECTION BETWEEN STRUCTURE AND LINE 2.....	70
FIGURE 74 ANNUAL PARTIAL DAMAGES AT CONNECTION BETWEEN STRUCTURE AND LINE 3.....	70
FIGURE 75 ROUTE FOR TOWING OPERATION	71
FIGURE 76 CALCULATIONS FOR ALTERNATIVE TOWING SCENARIOS	72
FIGURE 77 TOWING SPEEDS FOR DIFFERENT DRAFTS AND WIND SPEEDS.....	72
FIGURE 78 TOWING ARRANGEMENT.....	73
FIGURE 79 TOWING BRACKET COMPONENTS	74
FIGURE 80 TOWING BRACKET INTEGRATED IN COLUMN WALL AT HEIGHT OF RING STIFFENER.....	75
FIGURE 81 DYNAMIC CABLE STUDY	76
FIGURE 82 RESULTS FOR EXTREME CONDITIONS FOR THE DESIGN CALCULATIONS FROM BILBAO-BISCAY BUOY (2136).....	77
FIGURE 83 GEOMETRY AND LOADING DIRECTIONS FOR MODEL OF THE JOINTS THAT CONNECT THE LOWER AND DIAGONAL BRACES WITH THE COLUMNS. THE GREEN PLANE IS THE REFERENCE PLANE FOR THE DEFINITION OF IN-PLANE BENDING AND OUT-OF-PLANE BENDING.	ERROR! BOOKMARK NOT DEFINED.
FIGURE 84 GEOMETRY FOR MODEL OF THE JOINTS THAT CONNECT THE UPPER BRACES AND TOWER SUPPORT BRACES WITH THE COLUMNS.	ERROR! BOOKMARK NOT DEFINED.
FIGURE 85 LOADING DIRECTIONS FOR THE MODEL OF THE JOINTS THAT CONNECT THE UPPER BRACES AND TOWER SUPPORT BRACES WITH THE COLUMNS AND THE JOINTS THAT CONNECT THE TOWER SUPPORT BRACES WITH THE TOWER.	ERROR! BOOKMARK NOT DEFINED.
FIGURE 86 MAXIMUM PRINCIPAL STRESS (Pa) FOR AN AXIAL LOAD AT JOINTS BETWEEN COLUMNS AND DIAGONAL BRACES (MODEL 3).....	ERROR! BOOKMARK NOT DEFINED.
FIGURE 87 MAXIMUM PRINCIPAL STRESS (Pa) FOR AN IN-PLANE BENDING MOMENT AT JOINTS BETWEEN COLUMNS AND DIAGONAL BRACES (MODEL 3).....	ERROR! BOOKMARK NOT DEFINED.
FIGURE 88 MAXIMUM PRINCIPAL STRESS (Pa) FOR AN OUT-OF-PLANE BENDING MOMENT AT JOINT BETWEEN COLUMNS AND DIAGONAL BRACES (MODEL 3).....	ERROR! BOOKMARK NOT DEFINED.
FIGURE 89 MAXIMUM PRINCIPAL STRESS (Pa) AT NODES 61, 64, 65 AND 66 FOR AN AXIAL LOAD OF 1N.....	ERROR! BOOKMARK NOT DEFINED.
FIGURE 90 MAXIMUM PRINCIPAL STRESS (Pa) AT NODES 61, 64, 65 AND 66 FOR AN AXIAL LOAD OF 1N.....	ERROR! BOOKMARK NOT DEFINED.
FIGURE 91 MAXIMUM PRINCIPAL STRESS (Pa) AT NODES 73, 74 AND 75 FOR AN AXIAL LOAD OF 1N.....	ERROR! BOOKMARK NOT DEFINED.
FIGURE 92 MAXIMUM PRINCIPAL STRESS (Pa) AT NODE 75 FOR AN AXIAL LOAD OF 1N.....	ERROR! BOOKMARK NOT DEFINED.
FIGURE 93 MAXIMUM PRINCIPAL STRESS (Pa) AT NODES 76, 77 AND 78 FOR AN AXIAL LOAD OF 1N.....	ERROR! BOOKMARK NOT DEFINED.
FIGURE 94 MAXIMUM PRINCIPAL STRESS (Pa) AT NODE 78 FOR AN AXIAL LOAD OF 1N.....	ERROR! BOOKMARK NOT DEFINED.

FIGURE 95 MAXIMUM PRINCIPAL STRESS (PA) AT NODES 61, 64, 65 AND 66 FOR AN IN-PLANE BENDING MOMENT OF 28.6Nm.....	ERROR! BOOKMARK NOT DEFINED.
FIGURE 96 MAXIMUM PRINCIPAL STRESS (PA) AT NODES 61, 64, 65 AND 66 FOR AN IN PLANE BENDING MOMENT OF 28.6Nm.....	ERROR! BOOKMARK NOT DEFINED.
FIGURE 97 MAXIMUM PRINCIPAL STRESS (PA) AT NODE 75 FOR AN IN PLANE BENDING MOMENT OF 28.6Nm.....	ERROR! BOOKMARK NOT DEFINED.
FIGURE 98 MAXIMUM PRINCIPAL STRESS (PA) AT NODE 75 FOR AN IN PLANE BENDING MOMENT OF 28.6Nm.....	ERROR! BOOKMARK NOT DEFINED.
FIGURE 99 MAXIMUM PRINCIPAL STRESS (PA) AT NODE 78 FOR AN IN PLANE BENDING MOMENT OF 28.6Nm.....	ERROR! BOOKMARK NOT DEFINED.
FIGURE 100 MAXIMUM PRINCIPAL STRESS (PA) AT NODE 78 FOR AN IN PLANE BENDING MOMENT OF 28.6Nm.....	ERROR! BOOKMARK NOT DEFINED.
FIGURE 101 MAXIMUM PRINCIPAL STRESS (PA) AT NODES 61, 64, 65 AND 66 FOR AN IN PLANE BENDING MOMENT OF 28.6Nm, FOR THE OTHER NODES.	ERROR! BOOKMARK NOT DEFINED.
FIGURE 102 MAXIMUM PRINCIPAL STRESS (PA) AT NODES 61, 64, 65 AND 66 FOR AN IN PLANE BENDING MOMENT OF 28.6Nm, FOR THE OTHER NODES.	ERROR! BOOKMARK NOT DEFINED.
FIGURE 103 MAXIMUM PRINCIPAL STRESS (PA) AT NODES 75 FOR AN IN PLANE BENDING MOMENT OF 28.6Nm, FOR THE OTHER NODES.	ERROR! BOOKMARK NOT DEFINED.
FIGURE 104 MAXIMUM PRINCIPAL STRESS (PA) AT NODES 75 FOR AN IN PLANE BENDING MOMENT OF 28.6Nm, FOR THE OTHER NODES.	ERROR! BOOKMARK NOT DEFINED.
FIGURE 105 MAXIMUM PRINCIPAL STRESS (PA) AT NODES 78 FOR AN IN PLANE BENDING MOMENT OF 28.6Nm, FOR THE OTHER NODES.	ERROR! BOOKMARK NOT DEFINED.
FIGURE 106 MAXIMUM PRINCIPAL STRESS (PA) AT NODES 78 FOR AN IN PLANE BENDING MOMENT OF 28.6Nm, FOR THE OTHER NODES.	ERROR! BOOKMARK NOT DEFINED.
FIGURE 107 MAXIMUM PRINCIPAL STRESS (PA) AT NODES 61, 64, 65 AND 66 FOR AN OUT OF PLANE BENDING MOMENT OF 28.6Nm.....	ERROR! BOOKMARK NOT DEFINED.
FIGURE 108 MAXIMUM PRINCIPAL STRESS (PA) AT NODES 61, 64, 65 AND 66 FOR AN OUT OF PLANE BENDING MOMENT OF 28.6Nm.....	ERROR! BOOKMARK NOT DEFINED.
FIGURE 109 MAXIMUM PRINCIPAL STRESS (PA) AT NODE 75 FOR AN OUT OF PLANE BENDING MOMENT OF 28.6Nm.....	ERROR! BOOKMARK NOT DEFINED.
FIGURE 110 MAXIMUM PRINCIPAL STRESS (PA) AT NODE 78 FOR AN OUT OF PLANE BENDING MOMENT OF 28.6Nm.....	ERROR! BOOKMARK NOT DEFINED.
FIGURE 111 MAXIMUM PRINCIPAL STRESS (PA) AT NODES 61, 64, 65 AND 66 FOR AN OUT OF PLANE BENDING MOMENT OF 28.6Nm, FOR THE OTHER NODES.	ERROR! BOOKMARK NOT DEFINED.
FIGURE 112 MAXIMUM PRINCIPAL STRESS (PA) AT NODES 61, 64, 65 AND 66 FOR AN OUT OF PLANE BENDING MOMENT OF 28.6Nm, FOR THE OTHER NODES.	ERROR! BOOKMARK NOT DEFINED.
FIGURE 113 MAXIMUM PRINCIPAL STRESS (PA) AT NODE 75 FOR AN OUT OF PLANE BENDING MOMENT OF 28.6Nm, FOR THE OTHER NODES. PEAK STRESS IS $1.21 \cdot 10^2$ Pa.	ERROR! BOOKMARK NOT DEFINED.
FIGURE 114 MAXIMUM PRINCIPAL STRESS (PA) AT NODE 78 FOR AN OUT OF PLANE BENDING MOMENT OF 28.6Nm, FOR THE OTHER NODES. PEAK STRESS IS $1.44 \cdot 10^2$ Pa.	ERROR! BOOKMARK NOT DEFINED.
FIGURE 115 MAXIMUM PRINCIPAL STRESS (PA) AT NODES 61, 64, 65 AND 66 FOR AN OUT OF PLANE BENDING MOMENT OF 28.6Nm, FOR THE OTHER NODES 2.	ERROR! BOOKMARK NOT DEFINED.
FIGURE 116 MAXIMUM PRINCIPAL STRESS (PA) AT NODES 61, 64, 65 AND 66 FOR AN OUT OF PLANE BENDING MOMENT OF 28.6Nm, FOR THE OTHER NODES 2.	ERROR! BOOKMARK NOT DEFINED.
FIGURE 117 MAXIMUM PRINCIPAL STRESS (PA) AT NODE 75 FOR AN OUT OF PLANE BENDING MOMENT OF 28.6Nm, FOR THE OTHER NODES 2. PEAK STRESS IS $5.9 \cdot 10^1$ Pa.....	ERROR! BOOKMARK NOT DEFINED.
FIGURE 118 MAXIMUM PRINCIPAL STRESS (PA) AT NODE 78 FOR AN OUT OF PLANE BENDING MOMENT OF 28.6Nm, FOR THE OTHER NODES 2. PEAK STRESS IS $8.0 \cdot 10^1$ Pa.....	ERROR! BOOKMARK NOT DEFINED.
FIGURE 119 LOAD CASE 1.....	ERROR! BOOKMARK NOT DEFINED.
FIGURE 120 LOAD CASE 7.....	ERROR! BOOKMARK NOT DEFINED.
FIGURE 121 LOAD CASE 8.....	ERROR! BOOKMARK NOT DEFINED.
FIGURE 122 LOAD CASE 9.....	ERROR! BOOKMARK NOT DEFINED.

List of Tables

TABLE 1: VALUES FOR A AND M FOR CATHODIC PROTECTION (CP) AND IN SEAWATER.....	17
TABLE 2: MATERIAL PROPERTIES FOR STEEL (ANDERSON (03/01/2012, 12:34)).....	21
TABLE 3: LOADING DIRECTIONS FOR THE APPLIED MOMENTS IN GLOBAL COORDINATE SYSTEM	21
TABLE 4: COMPUTED MASS VALUES	36
TABLE 5: STRUCTURAL BEAM CHARACTERISTICS	37
TABLE 6 TABLE WITH MAXIMUM PRESSURE VALUES FOR GIVEN PERIODS	44
TABLE 7: ISOLATION SPECIFICATIONS	52
TABLE 8: FAIRLEAD AND ANCHOR POINTS IN LOCAL COORDINATES FRAME FOR AVERAGED POSITION.....	65
TABLE 9: 84MM AND 92MM CHAIN CHARACTERISTICS.....	65
TABLE 10: LOAD CASES AND PROBABILITY OF OCCURRENCE.....	66
TABLE 11: VELOCITY COEFFICIENTS OF WIND TURBINE	66
TABLE 12: ANNUAL DAMAGES AND FATIGUE LIVES AT CONNECTION BETWEEN CHAINS.	68
TABLE 13: ANNUAL DAMAGE AND FATIGUE LIFE AT CONNECTION BETWEEN LINES AND STRUCTURE.	68
TABLE 14: LARGEST PARTIAL DAMAGES AT CONNECTION BETWEEN CHAINS.....	69
TABLE 15: LARGEST PARTIAL DAMAGES AT CONNECTION LINES AND STRUCTURE.....	70
TABLE 16 TABLE WITH OFFERS FROM DIFFERENT CABLE SUPPLIERS.....	78
TABLE 17: AXIAL LOAD AT JOINT BETWEEN COLUMNS AND LOWER HORIZONTAL BRACES, WITHOUT SUPPORTING BRACKET.....	ERROR! BOOKMARK NOT DEFINED.
TABLE 18: IN-PLANE BENDING MOMENT AT JOINT BETWEEN COLUMNS AND LOWER HORIZONTAL BRACES, WITHOUT SUPPORTING BRACKET	ERROR! BOOKMARK NOT DEFINED.
TABLE 19: OUT-OF-PLANE BENDING MOMENT AT JOINT BETWEEN COLUMNS AND LOWER HORIZONTAL BRACES, WITHOUT SUPPORTING BRACKET	ERROR! BOOKMARK NOT DEFINED.
TABLE 20: AXIAL LOAD AT JOINT BETWEEN COLUMNS AND LOWER HORIZONTAL BRACES, WITH SUPPORTING BRACKET.....	ERROR! BOOKMARK NOT DEFINED.
TABLE 21: IN-PLANE BENDING MOMENT AT JOINT BETWEEN COLUMNS AND LOWER HORIZONTAL BRACES, WITH SUPPORTING BRACKET	ERROR! BOOKMARK NOT DEFINED.
TABLE 22: OUT-OF-PLANE BENDING MOMENT AT JOINT BETWEEN COLUMNS AND LOWER HORIZONTAL BRACES, WITH SUPPORTING BRACKET	ERROR! BOOKMARK NOT DEFINED.
TABLE 23: AXIAL LOAD AT JOINT BETWEEN COLUMNS AND DIAGONAL BRACES.....	ERROR! BOOKMARK NOT DEFINED.
TABLE 24: IN-PLANE BENDING MOMENT AT JOINT BETWEEN COLUMNS AND DIAGONAL BRACES.....	ERROR! BOOKMARK NOT DEFINED.
TABLE 25: OUT-OF-PLANE BENDING MOMENT AT JOINT BETWEEN COLUMNS AND DIAGONAL BRACES.....	ERROR! BOOKMARK NOT DEFINED.
TABLE 26: AXIAL LOAD AT TOWER SUPPORT ASSEMBLY.....	ERROR! BOOKMARK NOT DEFINED.
TABLE 27: IN-PLANE BENDING MOMENT AT TOWER SUPPORT ASSEMBLY FOR COLUMN 1.....	ERROR! BOOKMARK NOT DEFINED.
TABLE 28: OUT-OF-PLANE BENDING MOMENT AT TOWER SUPPORT ASSEMBLY FOR COLUMN 1.....	ERROR! BOOKMARK NOT DEFINED.
TABLE 29: IN-PLANE BENDING MOMENT AT TOWER SUPPORT ASSEMBLY FOR COLUMN 2.....	ERROR! BOOKMARK NOT DEFINED.
TABLE 30: OUT-OF-PLANE BENDING MOMENT AT TOWER SUPPORT ASSEMBLY FOR COLUMN 2.....	ERROR! BOOKMARK NOT DEFINED.
TABLE 31: IN-PLANE BENDING MOMENT AT TOWER SUPPORT ASSEMBLY FOR COLUMN 3.....	ERROR! BOOKMARK NOT DEFINED.
TABLE 32: OUT-OF-PLANE BENDING MOMENT AT TOWER SUPPORT ASSEMBLY FOR COLUMN 3.....	ERROR! BOOKMARK NOT DEFINED.
TABLE 33: FATIGUE CALCULATION CHAIN.....	ERROR! BOOKMARK NOT DEFINED.
TABLE 34: MAXIMUM TENSIONS AT THE CONNECTION POINT BETWEEN LINE AND FLOATING STRUCTURE.....	ERROR! BOOKMARK NOT DEFINED.
TABLE 35: MAXIMUM TENSIONS AT THE CONNECTION POINT BETWEEN LINES.	ERROR! BOOKMARK NOT DEFINED.
TABLE 36: ANNUAL PARTIAL DAMAGES AT THE CONNECTION POINT BETWEEN LINE AND FLOATING STRUCTURE.....	ERROR! BOOKMARK NOT DEFINED.
TABLE 37: ANNUAL PARTIAL DAMAGES AT THE CONNECTION POINT BETWEEN 84 MM AND 92 MM CHAINS.....	ERROR! BOOKMARK NOT DEFINED.

1 Introduction

The current document is a DRAFT version of the Deliverable D1.3 Final Design of the floating HiPRWind Platform. Due to the fact that certain design details need to be finalized in dependence of the final details of the marine operations and the dynamic cable design that have not been determined by the date of closing Version 1, there are certain gaps and uncertainties in this DRAFT version that will have to be clarified in the final version of the Document.

There is also a second round of turbine loads present that needs to be used to determine the safety concentration factors for the fatigue check in a second iteration to check that the design actually is valid as it is now, or if minor changes need to be implemented to enhance the fatigue performance of certain unions.

The Final Design of the HiPRWind floating platform contains several main aspects as the structural design influenced by all relevant aspects from Met-ocean, Geophysical and Geotechnical conditions at the site of employment, to the Mooring, Transport, Sea-keeping and Stability, Load-Out, Marine Operations, Turbine and Control analysis and their respective design implications. The fatigue analysis was done and the required testing of the welds of the structure to ensure the quality of the build was defined. The Design was calculated and the construction drawings were created from the model.

2 Structural and Seakeeping Calculations

The structural design of the floater is divided in two different main sections, one is the Seakeeping and the other is composed of the Structural Calculations, both with their respective analysis, calculations and design implications.

2.1 Seakeeping:

During the detailed engineering phase a complex simulation has been carried out taking into account dynamic wind in a simplified way into the uncoupled model.

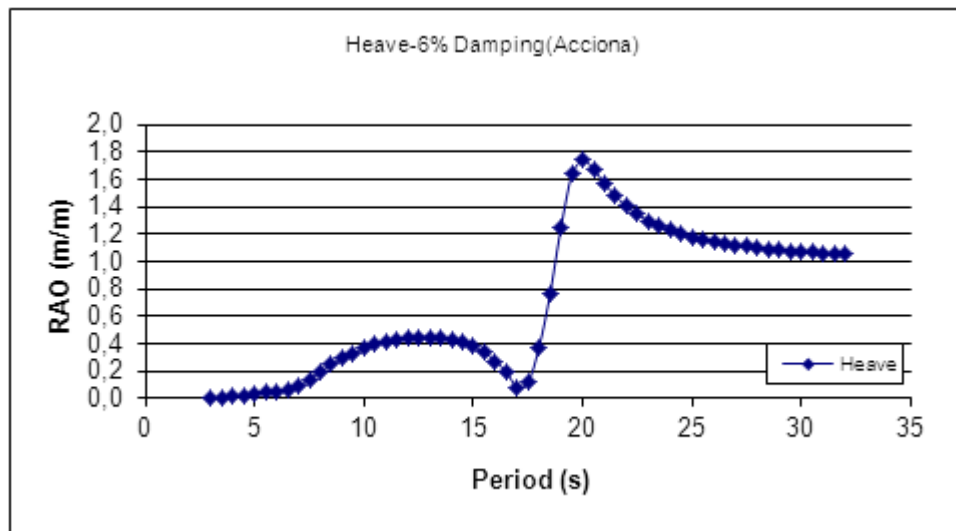
2.1.1 Uncoupled Model

SIMO-RIFLEX which is an uncoupled tool has been used for the uncoupled model. The dynamic behavior of the floater is calculated without taking into account the real-time influence of the wind turbine, which means that the wind turbine loads are calculated separately and introduced in the calculation as dynamic loads but not calculated at each time step. This uncoupled tool is well-known software, extensively used in the OIL&GAS industry with advanced hydrodynamic settings and dynamic mooring implementation. SIMO-RIFLEX has been used to design the floater itself and the mooring system.

To perform the analysis of the movements of the floater in time domain simulation (SIMO-RIFLEX) a previous analysis in the frequency domain had to be done to determine the Response Amplitude Operators (RAOs). This was performed with WADAM, software for hydrodynamic calculations done in the frequency domain developed by DNV.

The response amplitude operator of motion shows the platform behavior of the Semisubmersible structure.

In the following the results of the calculation for the 3 degrees of freedom are shown with pitch and heave.



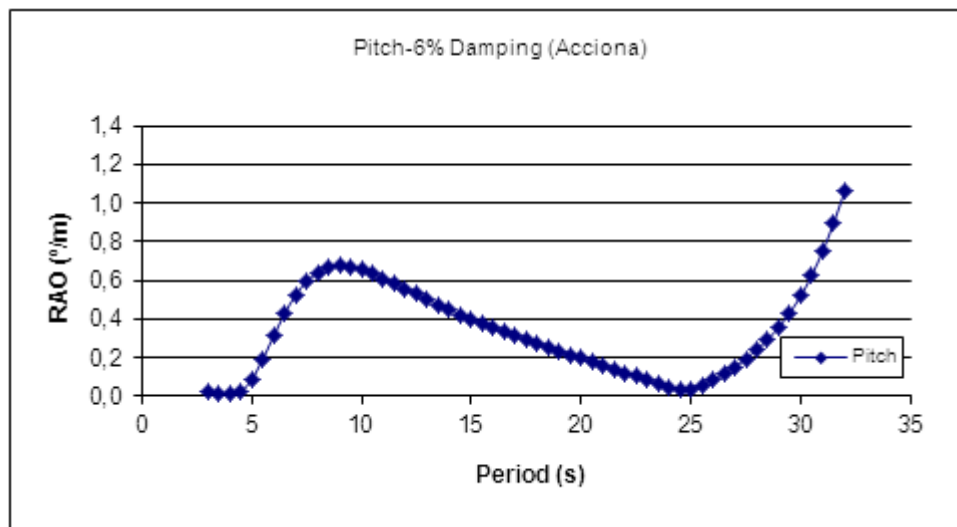


Figure 1 RAOs for pitch and heave

These RAOs were then later on used in SIMO-RIFLEX to carry out the final analysis of the mooring system, in Bladed to validate the dynamic behavior of the platform and to obtain the time series that were used for all the fatigue calculations. Compare also with chapter 2.2.15.2.

2.1.2 Fully Coupled Model

Bladed was used for the integrated wave and wind response analyses.

Fully coupled model with Bladed was calculated and the results used in several other calculations (e.g. in the fatigue calculations).

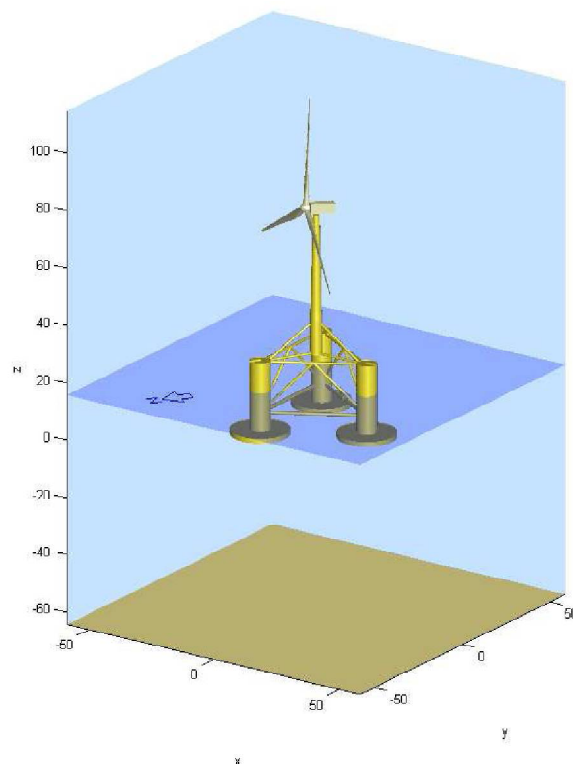


Figure 2 Integrated model with the AW77 wind turbine mounted on the semisubmersible structure

On basis of this combined model a series of calculations was performed with results that were later on used for the calculation of the platform (e.g. braces, columns, interconnections, etc.).

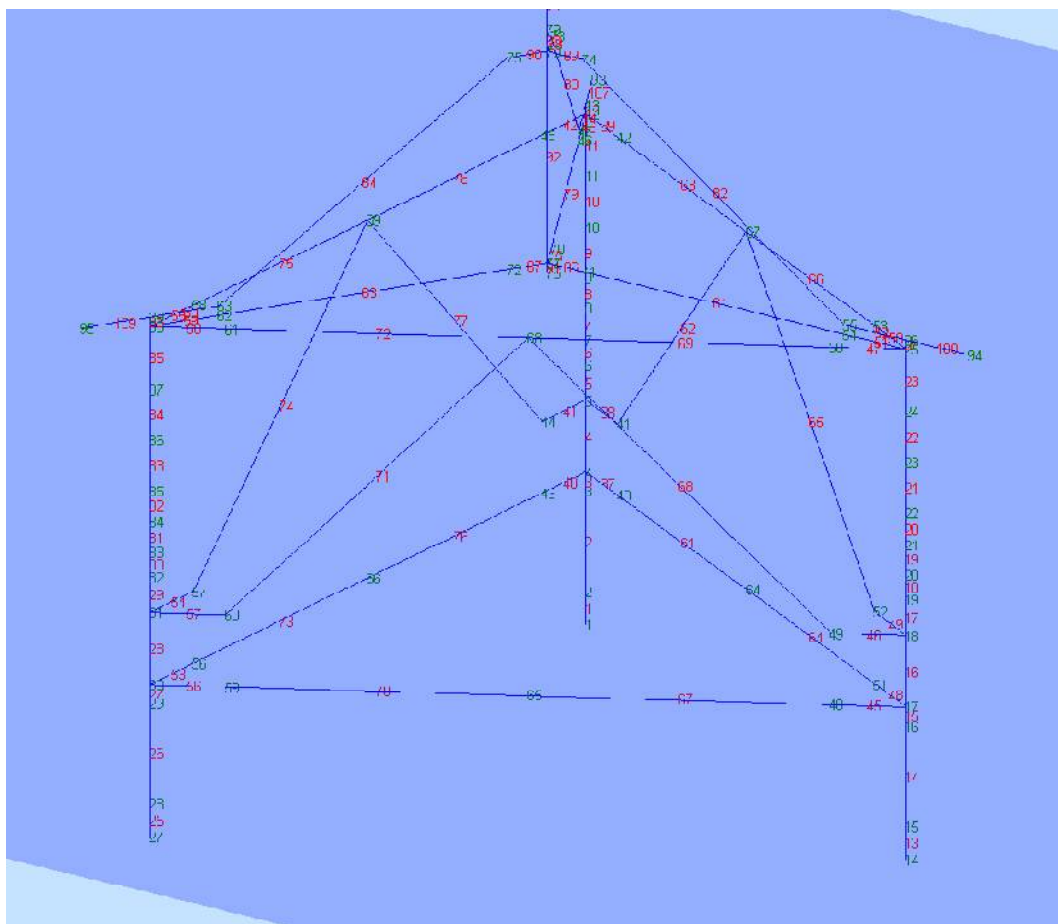


Figure 3 Location of semisubmersible floating platform nodes and members in the Bladed Model

The location of semisubmersible floating platform nodes and members in the Bladed Model are given in the figure above. For each of the nodes and members the forces and moments were determined.

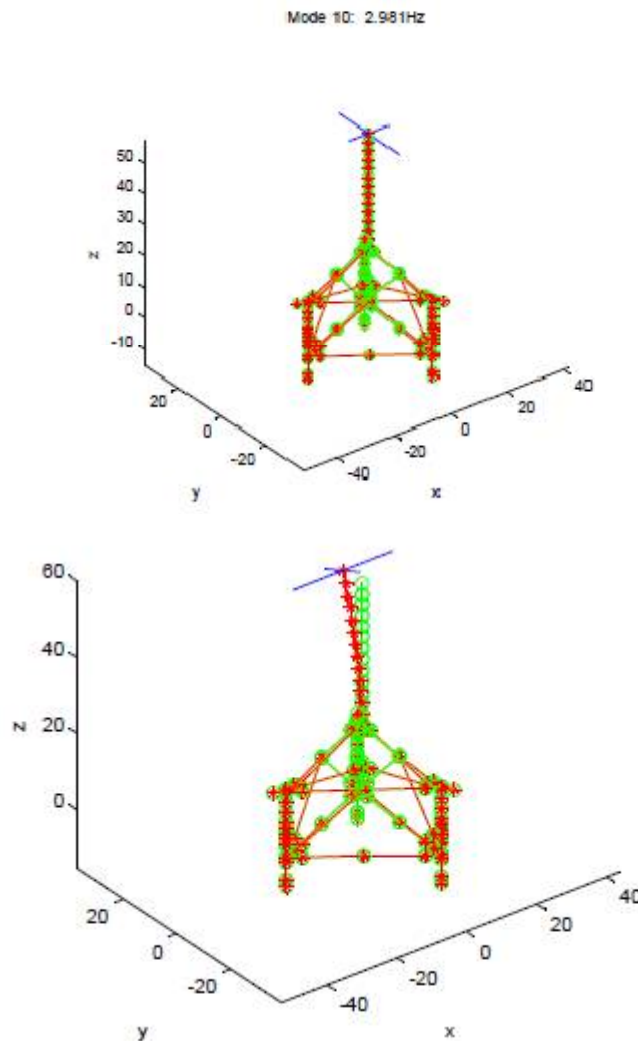


Figure 4 Samples for different modes for Eigenfrequencies

Different modes for Eigenfrequencies were investigated and the vibration analysis was performed for different frequencies. A complete series of extreme load histograms were elaborated for the components. The ultimate site specific loads were calculated to determine if the components will withstand the ultimate limit states.

Furthermore the fatigue loads were determined. These were used as basis for the fatigue load analysis of unions and components (e.g. of different braces vs. column).

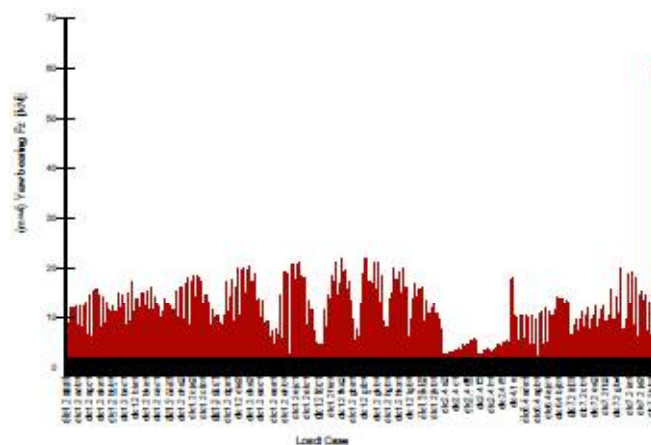


Figure 5 Sample of life time weighted equivalent loads

The Lifetime Equivalent Loads were determined. These are of maximum interest for the fatigue analysis. A visual way to show these fatigue analysis is the rainflow cycle exceedance diagram that was created for all important components in the load path (e.g. blade, hub, etc.)

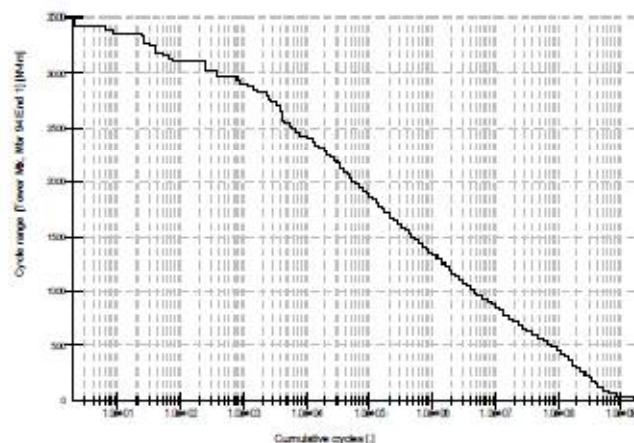


Figure 6 Sample of Rainflow cycle exceedance diagram for the components

Uncoupled and coupled tools were validated through a code-to-code comparison and advantages and disadvantages of both tools have been discussed in order to share and use the results in further design phases adequately. The use of both tools has been a successfully finished design task. With this comparison the consortium managed to assure the reliability of many calculations and the accuracy of the results.

These analyses, with both uncoupled and coupled tool, have been used as a basis for extreme loadcases (compare with Figure 24 Extreme Conditions) and the fatigue assessment of the substructure (hot spots), basically for design of the braces and their transition details, and for the design of the wind turbine support (transition piece) where high dynamic loads were expected.

2.2 Structural calculations

2.2.1 Fatigue life assessment

The fatigue life of the joints in the floating support structure was assessed according to the procedure suggested in DNV-RP-C203[16]. This document allows for the estimation of fatigue damage using SN curves. SN curves show the relation between a stress range (S) and a number of cycles to failure (N). The general form of an SN curve is given as

$$N = \frac{a}{(\Delta\sigma)^m}$$

where N is the number of cycles to failure, $\Delta\sigma$ is the stress range and a and m are constants given in DNV-RP-C203 [16]. The stress range was calculated by TWI, using Finite Element Analyses (FEA) and load case data provided by Acciona Windpower (AW). For each joint an FEA model was set up and three peak values for the stress were calculated: One for an applied axial force (F_a^{FEA}); one for an applied in-plane bending moment (M_{ip}^{FEA}); and one for an applied out-of-plane bending moment (M_{op}^{FEA}), see also **Error! Reference source not found.**. The results were used to determine transfer functions between the calculated peak stresses and the applied loads as follows

$$T_a = \frac{\sigma_a^{FEA}}{F_a^{FEA}}, \quad T_{ip} = \frac{\sigma_{ip}^{FEA}}{M_{ip}^{FEA}}, \quad T_{op} = \frac{\sigma_{op}^{FEA}}{M_{op}^{FEA}}$$

where T_a , T_{ip} and T_{op} are the transfer functions for the axial force, the in-plane bending moment and out-of-plane bending moment respectively. Similarly, σ_a^{FEA} , σ_{ip}^{FEA} and σ_{op}^{FEA} are the peak stresses calculated for the axial force, the in-plane bending moment and out-of-plane bending moment respectively. Using the transfer functions, the peak stresses corresponding to the load cases provided by AW were obtained:

$$\sigma_a^{AW} = T_a F_a^{AW}, \quad \sigma_{ip}^{AW} = T_{ip} M_{ip}^{AW}, \quad \sigma_{op}^{AW} = T_{op} M_{op}^{AW}$$

where σ_a^{AW} , σ_{ip}^{AW} , and σ_{op}^{AW} are the peak stresses corresponding to the axial force F_a^{AW} , in-plane bending moment M_{ip}^{AW} and out-of-plane bending moment M_{op}^{AW} as provided by AW, respectively. The loads provided by AW are cyclic loads, so therefore the corresponding peak stresses can be interpreted as stress ranges, i.e. $\sigma_a^{AW} = \Delta\sigma_a^{AW}$, $\sigma_{ip}^{AW} = \Delta\sigma_{ip}^{AW}$ and $\sigma_{op}^{AW} = \Delta\sigma_{op}^{AW}$. This allows for the calculation of the number of cycles to failure for each load case:

$$N_a^f = \frac{a}{(\Delta\sigma_a^{AW})^m}, \quad N_{ip}^f = \frac{a}{(\Delta\sigma_{ip}^{AW})^m}, \quad N_{op}^f = \frac{a}{(\Delta\sigma_{op}^{AW})^m}$$

with N_a^f , N_{ip}^f and N_{op}^f denoting the number of cycles to failure for the axial load, in-plane bending moment and out-of-plane bending moment respectively. AW has supplied an expected number of cycles per load range, which can be expressed as a fraction of the number of cycles to failure for that load range. This is known as damage D . Per load case many load ranges and their expected number of cycles are given, which means that the total damage per load case is a summation over the load ranges:

$$D_a = \sum_{j=1}^{j=n} \left(\frac{N_a^e}{N_a^f} \right)_j, \quad D_{ip} = \sum_{j=1}^{j=n} \left(\frac{N_{ip}^e}{N_{ip}^f} \right)_j, \quad D_{op} = \sum_{j=1}^{j=n} \left(\frac{N_{op}^e}{N_{op}^f} \right)_j$$

where D_a , D_{ip} and D_{op} are the damages as a results of the axial force, in-plane bending moment and out-of-plane bending moment respectively. N_a^e , N_{ip}^e and N_{op}^e indicate the expected number of cycles per load range for the axial force, in-plane bending moment and out-of-plane bending moment respectively. Finally, n is the number of load ranges.

The values for constants a and m are given in [16] for a range of situations. Two aspects were considered when selecting the appropriate values. The first aspect was the classification of the geometry. It was chosen to base the calculations on the Class D curve for the welded joints and on the Class C curve for the non-welded details. The second aspect was the environment of the structure. It was chosen to calculate the fatigue life based on the SN curves in air, in seawater with cathodic protection (CP) and in seawater for free corrosion. The values of a and m for these situations are given as follows:

Table 1: Values for a and m for cathodic protection (CP) and in seawater.

Environment	Class C				Class D			
	N	$\Delta\sigma$	$\log a$	m	N	$\Delta\sigma$	$\log a$	m
Air	$\leq 10^7$	≥ 73	12.592	3	$\leq 10^7$	≥ 53	12.164	3
	$> 10^7$	< 73	16.320	5	$> 10^7$	< 53	15.606	5
Seawater with CP	$\leq 10^6$	≥ 116	12.192	3	$\leq 10^6$	≥ 83	11.764	3
	$> 10^6$	< 116	16.320	5	$> 10^6$	< 83	15.606	5
Seawater free corrosion			12.115	3			11.687	3

2.2.2 Load case analysis

The load case data was provided by AW. AW had generated a model to predict the force and the moment histories in the floating support structure, using software package Bladed. For all main intersections in the model, a file was provided containing the expected number of cycles per load range for each component of force and moment [18]. The force and moment components were defined in a global coordinate system. The numbering of the nodes and members in the AW model is shown in Figure 7[17]. All members connect two nodes. Of the two nodes, the one with the lowest node number is being referred to as end 1, whereas the node with the highest node number is being referred to as end 2. The files containing the load case data are named according to the following format:

Mbr <member number> End <end number>_1DMarkov.xls

Thus, in order to assess the joint corresponding to node 54 in Figure 7, the load case data in file 'Mbr 67 End 1_1DMarkov.xls' was required.

When applying the axial force, in-plane bending moment and out-of-plane bending moment to some of the joints, the directions of the loads happened to correspond to the global x, y and z directions, see for example the joints indicated with nodes 59 and 46 in Figure 7. If that was the case, it was straightforward to use the transfer functions T_a , T_{ip} and T_{op} to obtain the stress ranges $\Delta\sigma_a^{AW}$, $\Delta\sigma_{ip}^{AW}$ and $\Delta\sigma_{op}^{AW}$. For other joints it was necessary to resolve the vectors given by AW into components of the local coordinate system in order to obtain F_a^{AW} , M_{ip}^{AW} and M_{op}^{AW} .

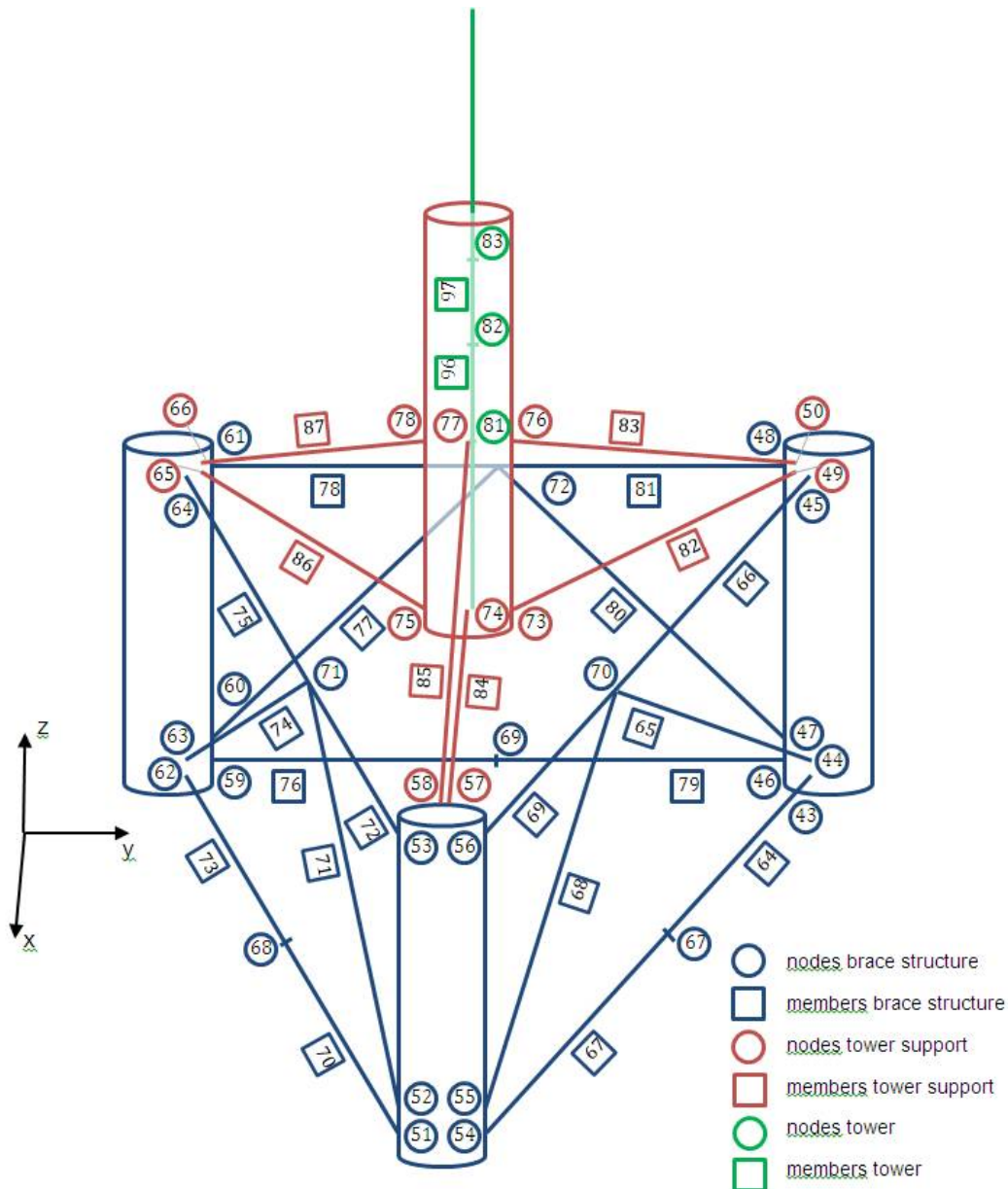


Figure 7 Nomenclature for nodes on Semisubmersible structure

2.2.3 Stress analysis

2.2.3.1 Introduction

To obtain the transfer functions T_a , T_{ip} and T_{op} , FEA models were set up in ABAQUS 6.11. The joints of the brace structure were assessed individually; however, due to the complex design of carrying loads in the tower support structure, the joints in this part were assessed as an assembly. The geometry and material properties for the models were provided by Olav Olsen [15] (Table 2). For each joint three different load cases were considered: An axial load, an in-plane bending moment and an out-of-plane bending moment. The loads are applied to reference points which are connected to the braces with kinematic coupling constraints. The displacement of the reference point in axial direction is constrained. The models were meshed using quadratic shell elements. The size of the elements at the joints was limited to a maximum of $2t$, where t is the thickness of the joint, based on previous work carried out by Smith et al and Smith and Maddox [19, 20].

2.2.3.2 Individual joints

The joints connecting the lower and diagonal braces to the columns (corresponding to nodes 43, 44, 46, 47, 51, 52, 54, 55, 62, 63, 59 and 60 in Figure 7) were assessed individually. The geometry used for the FEA calculations is shown in **Error! Reference source not found.**. There is a difference between the two joints that connect the column to the lower braces. The joint on the left in **Error! Reference source not found.** is a plain joint, whereas the joint on the right is supported by a bracket between the column and the brace. The addition of the bracket was proposed by Anderson [14] and fatigue life for this joint was assessed with and without the bracket.

The directions of the loads for one of the joints are shown in **Error! Reference source not found.**. The green reference plane defines in-plane bending and out-of-plane bending. The boundary conditions were applied to the centers of the top and bottom plates. At the bottom plate, the displacements in x, y and z direction and rotation around the z axis were fixed. At the top plate, the displacements in x and y directions were fixed. The top and bottom plate had an artificially high stiffness of ten times the stiffness of the material.

The following loads were applied to the reference point in order to obtain the transfer functions:

$$F_a^{FEA} = 1 \text{ N}$$

$$M_{ip}^{FEA} = 1 \text{ Nm}$$

$$M_{op}^{FEA} = 1 \text{ Nm}$$

2.2.3.3 Tower support assembly

The joints that are part of the tower support (corresponding to nodes 45, 48, 49, 50, 53, 56, 57, 58, 61, 64, 65, 66, 73, 74, 75, 76, 77 and 78 in Figure 7) were assessed as an assembly. **Error! Reference source not found.** shows the geometry of the FEA model, which includes all three columns. Only one of the columns was meshed with small elements at the joints, in order to keep the computation time limited.

The loads were applied to the tower, as fatigue of the joints was expected to be entirely related to the dynamic loads from the tower [21]. Due to a close to linear relation between the bending moment and the shear force in the tower, a shear force was applied in the model. Based on calculations by Olav Olsen, the loads were applied at 30.8m from the point where the tower intersects with the diagonal tower support braces (node 81 in Figure 7). For the applied shear forces, the corresponding bending moments were calculated, in order to obtain the transfer functions[22]. It was chosen to the load case data at node 82 in Figure 7, which means that the data in file 'Mbr 96 End 2_1DMarkov.xls' was required. Node 82 was located 2.2m above the intersection point between the tower and the tower support braces. The bending moments were calculated as follows:

$$M_x = F (a - x)$$

where F is the applied shear force, M_x the corresponding bending moment, a is the arm between the point where the force is applied and the intersection point and x is the arm between the point at which the load case data was considered and the intersection point. The applied forces were all 1N, which leads to the following loads:

$$F_a^{FEA} = 1 \text{ N}$$

$$M_{ip}^{FEA} = 28.6 \text{ Nm}$$

$$M_{op}^{FEA} = 28.6 \text{ Nm}$$

The directions of the axial and shear forces are shown in **Error! Reference source not found.** and listed in Table 3. Boundary conditions were applied to the centers of the bottom planes of the columns. For the column with the fine mesh the center was fixed in x, y and z directions. The center of one of the other columns was fixed in x and z directions and the center of the remaining column was fixed in z direction.

2.2.4 Results structural calculations

2.2.4.1 Introduction

The maximum principal stresses were evaluated to obtain the peak stresses that were needed to calculate the transfer functions. The model consists of shell elements and it was therefore necessary to extract the stresses on the outer layer of the elements, which in this case was SPOS (The faces with normals along the underlying element normals define the SPOS face). To visualize the stresses in the joint, only the required brace was displayed. This means that all other components, including parts of the brace that sit inside the column, were made invisible. This way the peak stresses were not influenced by averaging stresses from other elements.

2.2.4.2 Individual joints

Three models were used to assess the joints between the columns and the lower horizontal and diagonal braces. Model 1 was for the joints between the columns and the lower horizontal braces (nodes 43, 46, 51, 54, 59 and 62 in Figure 7), model 2 was for the same joints but with the supporting bracket and model 3 was for the joints between the columns and the diagonal braces (nodes 44, 47, 52, 55, 60 and 63 in Figure 7). The peak stresses were obtained from the FEA models and the damage was calculated for two different environments. The results are given in **Error! Reference source not found.** to **Error! Reference source not found.**. The corresponding stress plots are shown in **Error! Reference source not found.** to **Error! Reference source not found.**.

2.2.4.3 Tower support assembly

The different models that were used to obtain the peak stresses for the tower support assembly are named A, B, C, D, E and F, as indicated in **Error! Reference source not found.**. The damage is calculated for the SN-curves in air. The results are presented in **Error! Reference source not found.** to **Error! Reference source not found.**, with the corresponding stress plots shown in **Error! Reference source not found.** to **Error! Reference source not found.**.

As only one of the columns in the model was meshed with small elements, results of different models were used to assess the fatigue life for a given load case. The model that was used for the results in **Error! Reference source not found.** to **Error! Reference source not found.** is given in the column 'Model'.

2.2.4.4 Discussion of results for structural calculations

The fatigue life for the joints in the structure can be easily evaluated by looking at the final column of **Error! Reference source not found.** to **Error! Reference source not found.**. The cases that lead to a damage that exceeds 1 are indicated in red.

The damage exceeds 1 for the joints between the columns and the lower horizontal braces. This is the case for assessment in seawater with cathodic protection and for seawater without cathodic protection. The addition of the supporting bracket does substantially improve the fatigue life, but even with cathodic protection the damage exceeds 1 for this case. Values for the damage are below 2 though, so the joints are not expected to fail within 10 years.

Another joint that experiences damage exceeding 1, is the joint between the columns and the diagonal braces. This, however, is only the case when there is no cathodic protection.

2.2.5 Conclusion for structural calculations

The critical joints in the floating support structure are the joints indicated with node 43, 51, 54 and 62 in Figure 7 Nomenclature for nodes on Semisubmersible structure. Even with cathodic protection and supporting brackets the damage of these joints will exceed 1.

Other critical joints are the ones indicated with 44, 52, 55 and 63 in Figure 7 Nomenclature for nodes on Semisubmersible structure, but only in the case when no cathodic protection is used.

Since there has been a second set of loads been produced for the present design a second iteration of these present calculations will have to be performed. It is expected that the final version of this document will then show the final results for those nodes mentioned above will be uncritical in all cases. Cathodic protection will be implemented anyhow. In case that the above results are confirmed and the values remain high for some nodes, small design changes (compare also with 2.2.6.4 and 2.2.6.4) could be to reduce the values at the relevant nodes and implemented to achieve a high safety margin for the design.

Table 2: Material properties for steel (Anderson (03/01/2012, 12:34)).

Young's modulus, Pa	$2 \cdot 10^{11}$
Poisson's ratio	0.33

Table 3: Loading directions for the applied moments in global coordinate system

	M_x	M_y	M_z
In plane loading for column 1	-0.866025404	0.5	0
Out of plane loading for column 1	-0.5	-0.866025404	0
In plane loading for column 2	0	-1	0
Out of plane loading for column 2	-1	0	0
In plane loading for column 3	0.866025404	0.5	0
Out of plane loading for column 3	0.5	-0.866025404	0

The SCF (stress concentration factors) have been used to verify the design. These SCF were calculated for axial, "in plane" and "out of plane" bending moments according to the schematics that can be seen in **Error! Reference source not found.**

With the respective loading the fatigue calculations could be performed on basis of the SCF.

These analyses, with both uncoupled and coupled tool, have been used as basis for extreme load cases and fatigue assessment of the substructure (hot spots), basically for design of the braces and their transition details and for the design of the wind turbine support (Transition Piece) where high dynamic loads were expected. Results for the detailed design are shown in the following.

2.2.6 Braces

A local linear finite element analysis for the connection of lower and diagonal braces to the columns of the floater has been performed. The local analysis has been performed to check the structural behavior of the structure and to identify locations with stress concentrations. The location of stress concentrations are as expected and the general local design seems reasonable.

2.2.6.1 Model description for Brace structural calculations

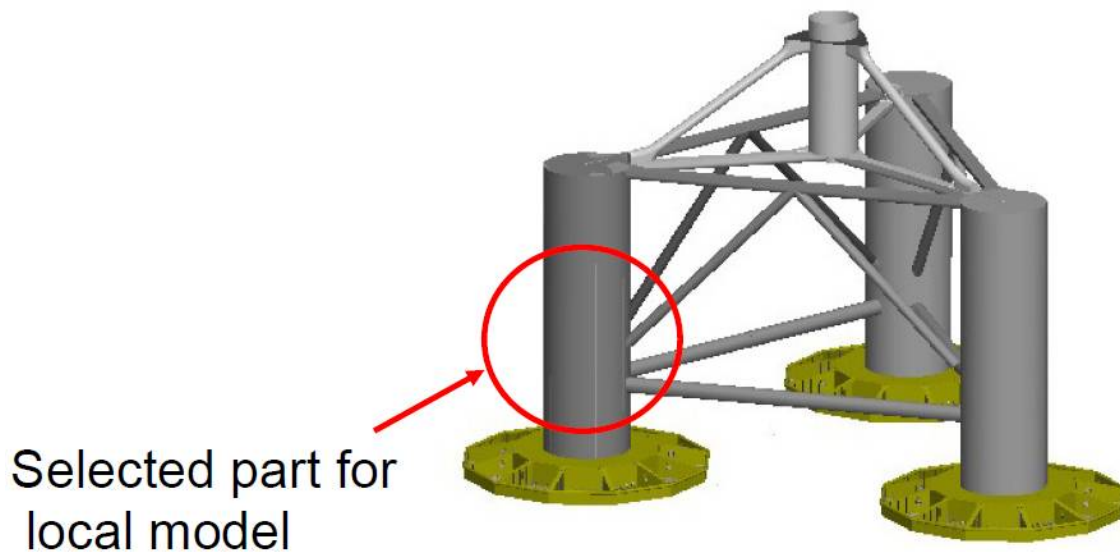


Figure 8 Part of column selected for local model

The selected part for the local analysis of lower and diagonal brace connection are shown in Figure 8. The ABAQUS model used for the local analysis is shown in Figure 9 and Figure 10. In principal the model contains 4-node general purpose shell elements with full integration (ABAQUS: S4). These elements are suitable for both thick and thin shells. Some 3-noded triangular elements have been included in complex areas. Thicknesses, dimensions etc. are found in relevant spreadsheets.

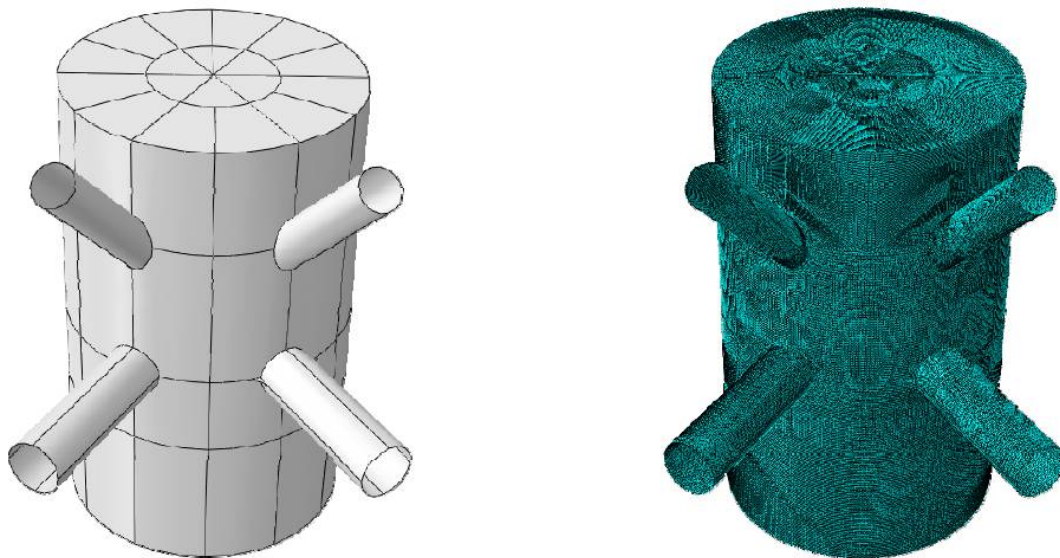


Figure 9 (A) shows the outer geometry of the local model in ABAQUS, while (B) shows the coherent mesh.

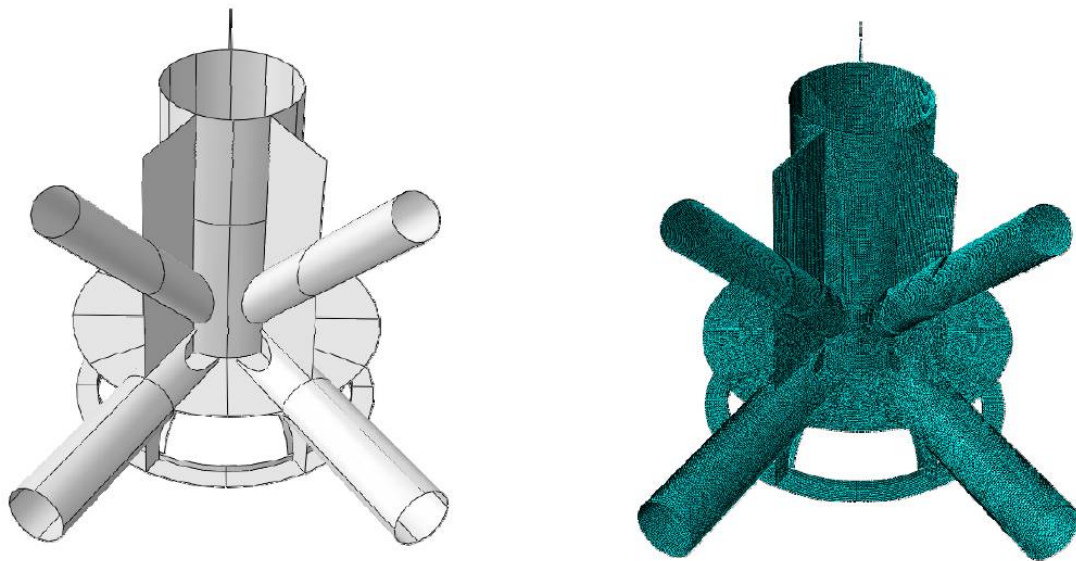


Figure 10 (A) shows the inner geometry of the local model in ABAQUS, while (B) shows the coherent mesh

2.2.6.2 Results – diagonal braces

2.2.6.2.1 Axial load:

Stress levels in the diagonal braces when under axial loading are shown in Figure 11, Figure 12 and Figure 13.

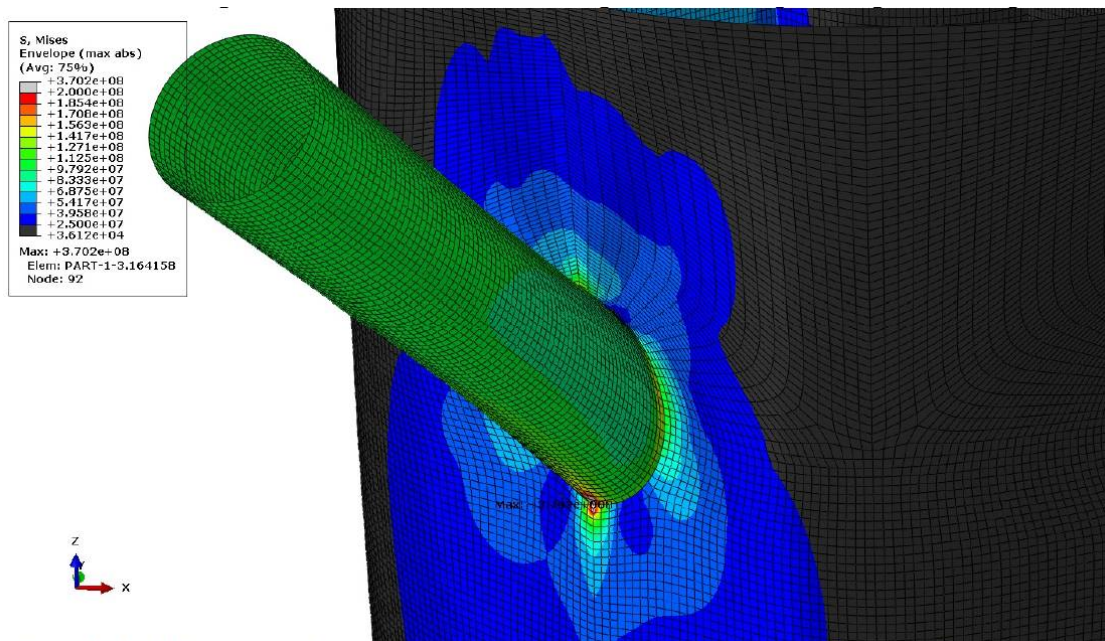


Figure 11 Von Mises stress for outer geometry under axial loading of diagonal brace. The maximum stress value over the cross section is shown. (Stress values are in Pa)

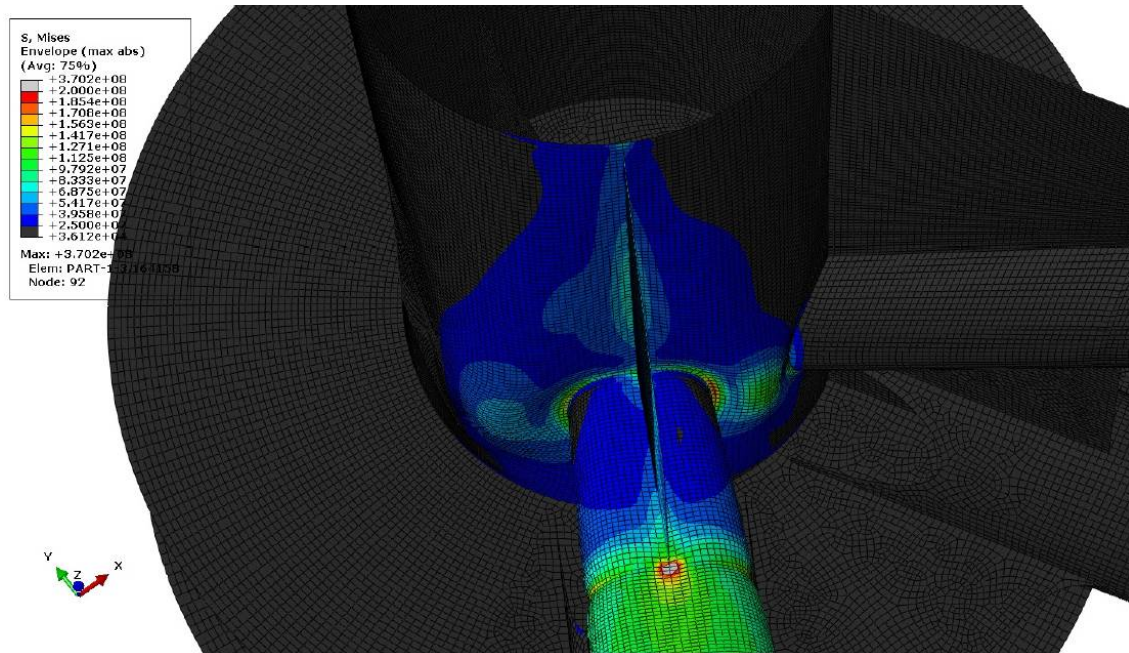


Figure 12 Von Mises stress for geometry without outer shell under axial loading. The maximum stress value over the cross section is shown. (Stress values are in Pa)

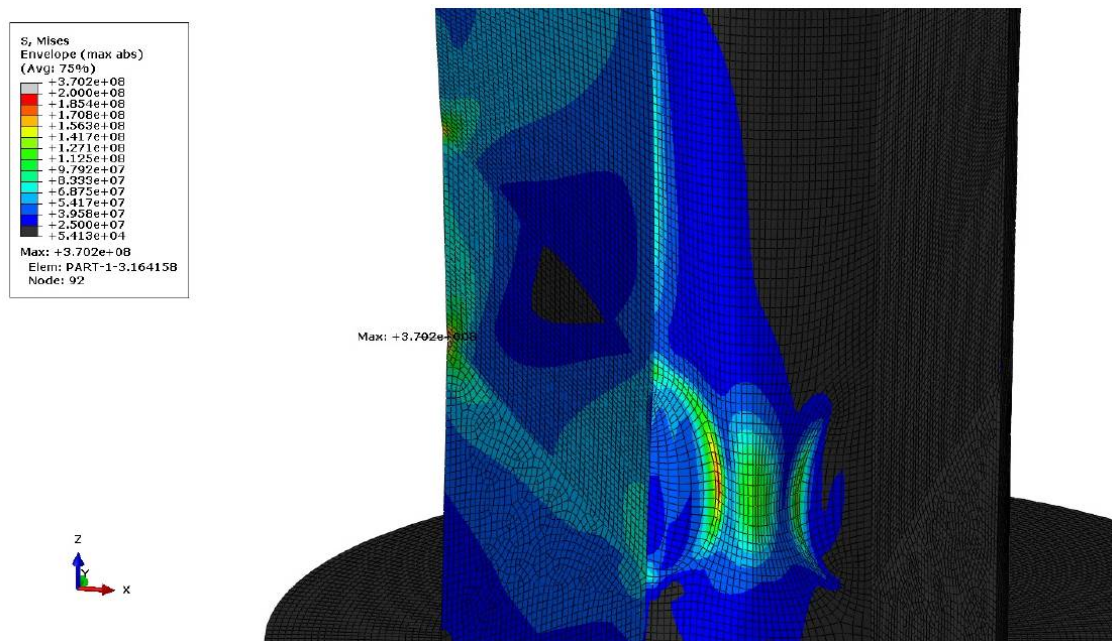
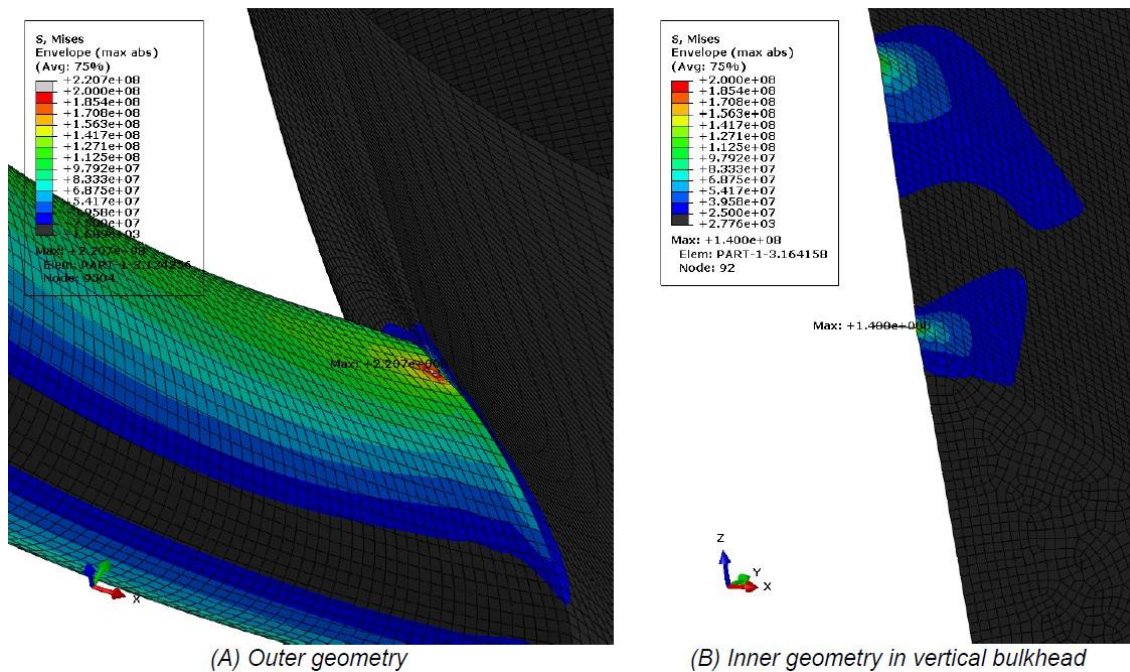


Figure 13 Von Mises stress for inner geometry, brace removed, under axial loading. The maximum stress value over the cross section is shown. (Stress values are in Pa)

2.2.6.2.2 Moment about local “horizontal” axis:

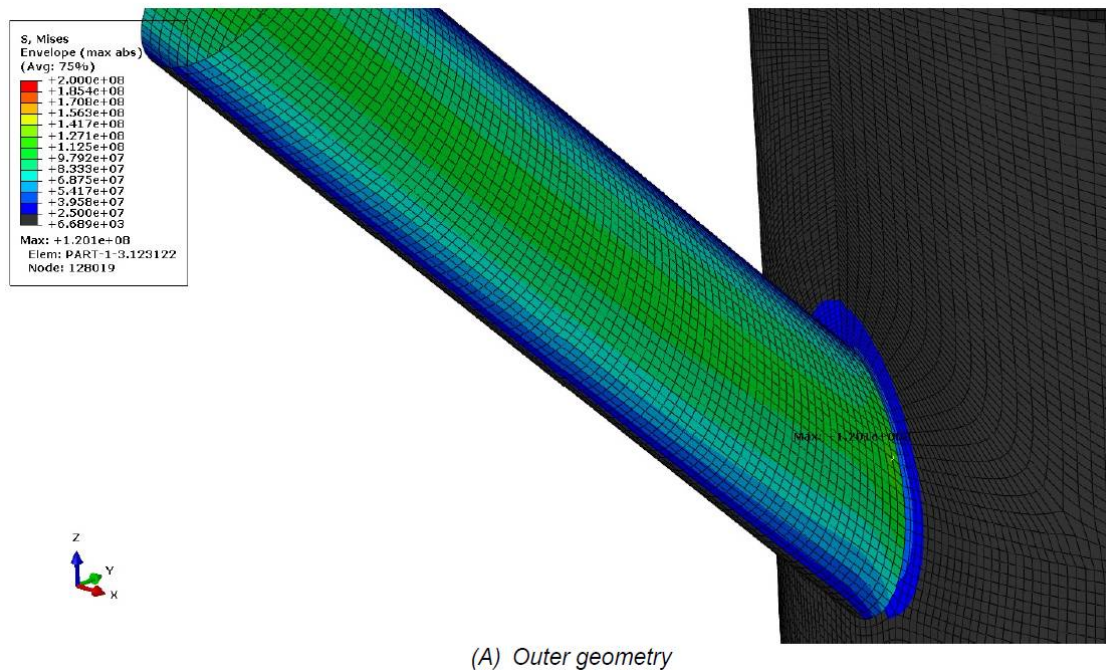
Stress plots for moment about local “horizontal” axis are shown in Figure 14.



(A) Outer geometry (B) Inner geometry in vertical bulkhead
Figure 14 Von Mises stress for moment about local “horizontal” axis of diagonal brace. The maximum stress value over the cross section is shown. (Stress values are in Pa)

2.2.6.2.3 Moment about local “vertical” axis:

Von Mises stress plots for a moment about local “vertical” are shown in Figure 15.



(A) Outer geometry

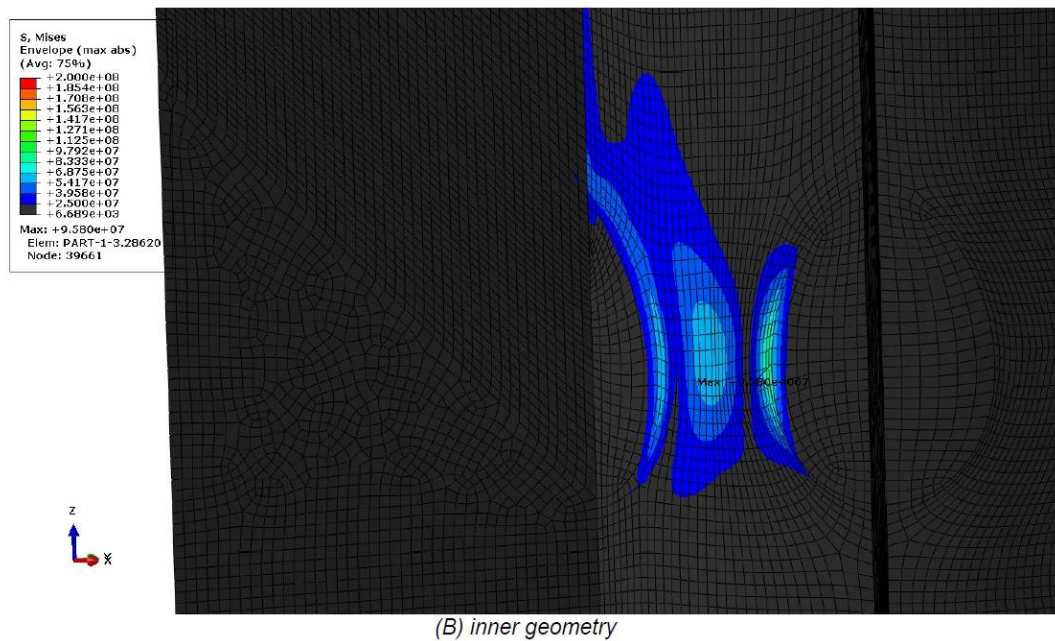


Figure 15 Von Mises stress for moment about local “vertical” axis of diagonal brace. The maximum stress value over the cross section is shown. (Stress values are in Pa)

2.2.6.3 Results – lower braces

2.2.6.3.1 Axial load:

Von Mises stress plots for axial loading of lower brace are given in Figure 16, Figure 17 and Figure 18.

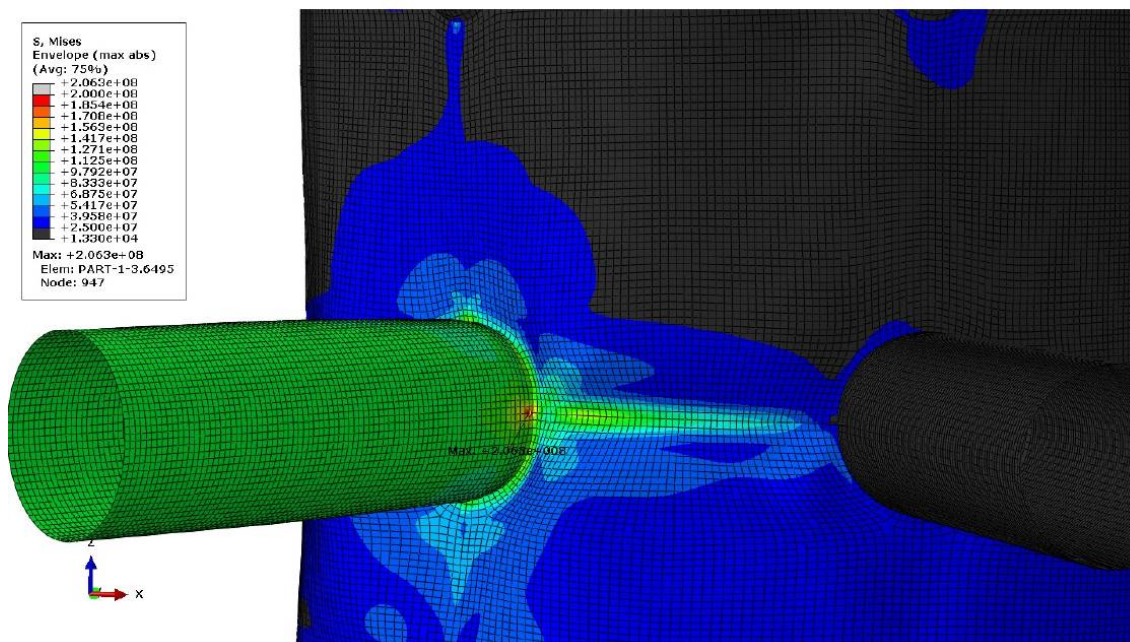


Figure 16 Von Mises stress for outer geometry under axial loading of lower brace. The maximum stress value over the cross section is shown. (Stress values are in Pa)

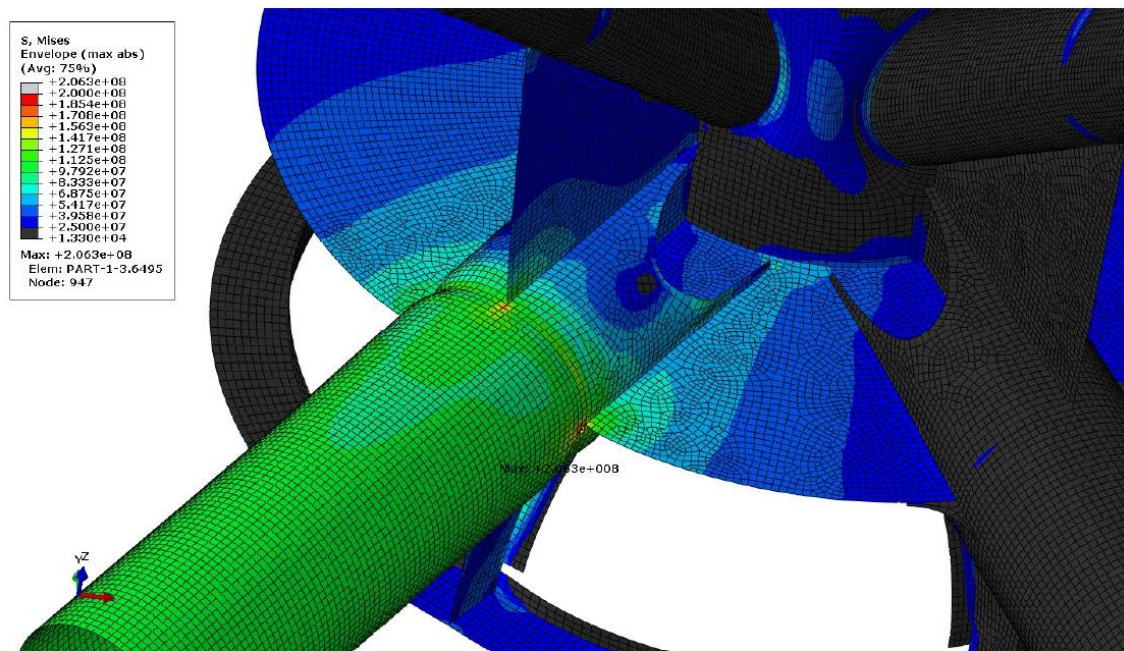


Figure 17 Von Mises stress for inner geometry under axial loading of lower brace. The maximum stress value over the cross section is shown. (Stress values are in Pa)

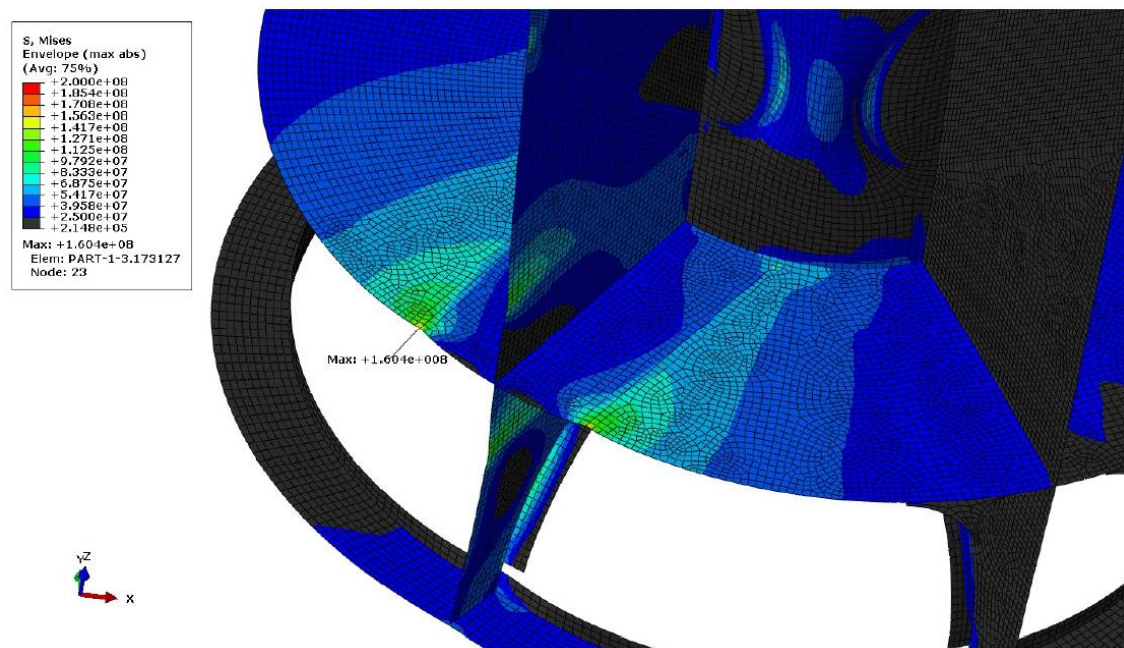
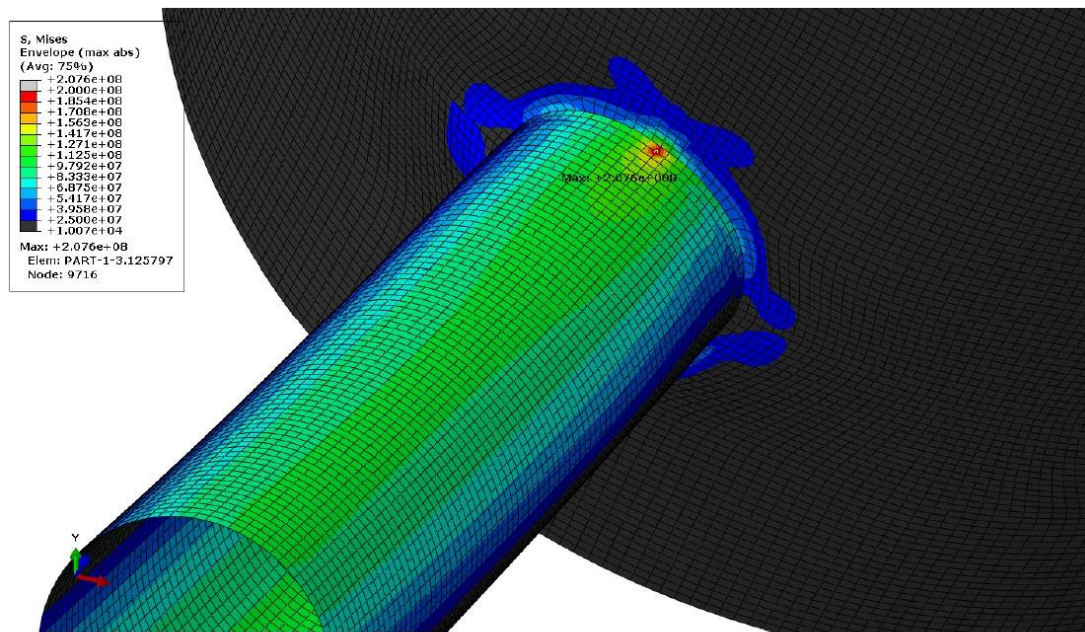


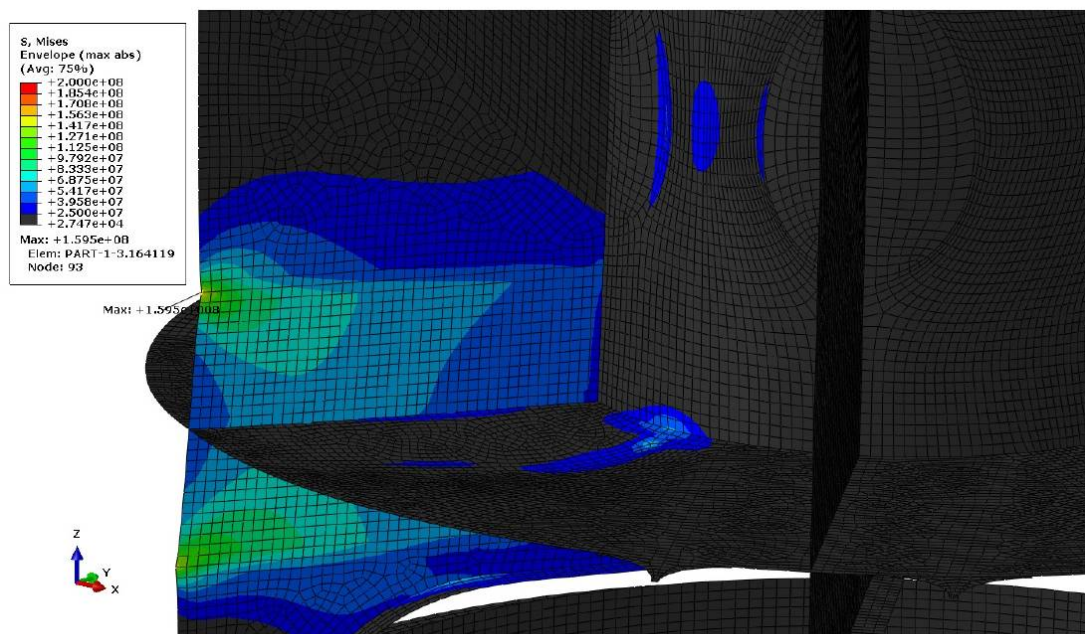
Figure 18 Von Mises stress for inner geometry (brace removed) under axial loading of lower brace. The maximum stress value over the cross section is shown. (Stress values are in Pa)

2.2.6.3.2 Moment about local horizontal vertical axis:

Results for moment about local vertical axis of lower brace are given in Figure 19.



(A) Outer geometry



(B) Inner geometry

Figure 19 Plot of Von Mises stress for moment about local horizontal axis of lower brace. The maximum stress value over the cross section is shown. (Stress values are in Pa)

2.2.6.3.3 Moment about local horizontal axis:

Von Mises stress plots for bending about local vertical axis are given in Figure 20.

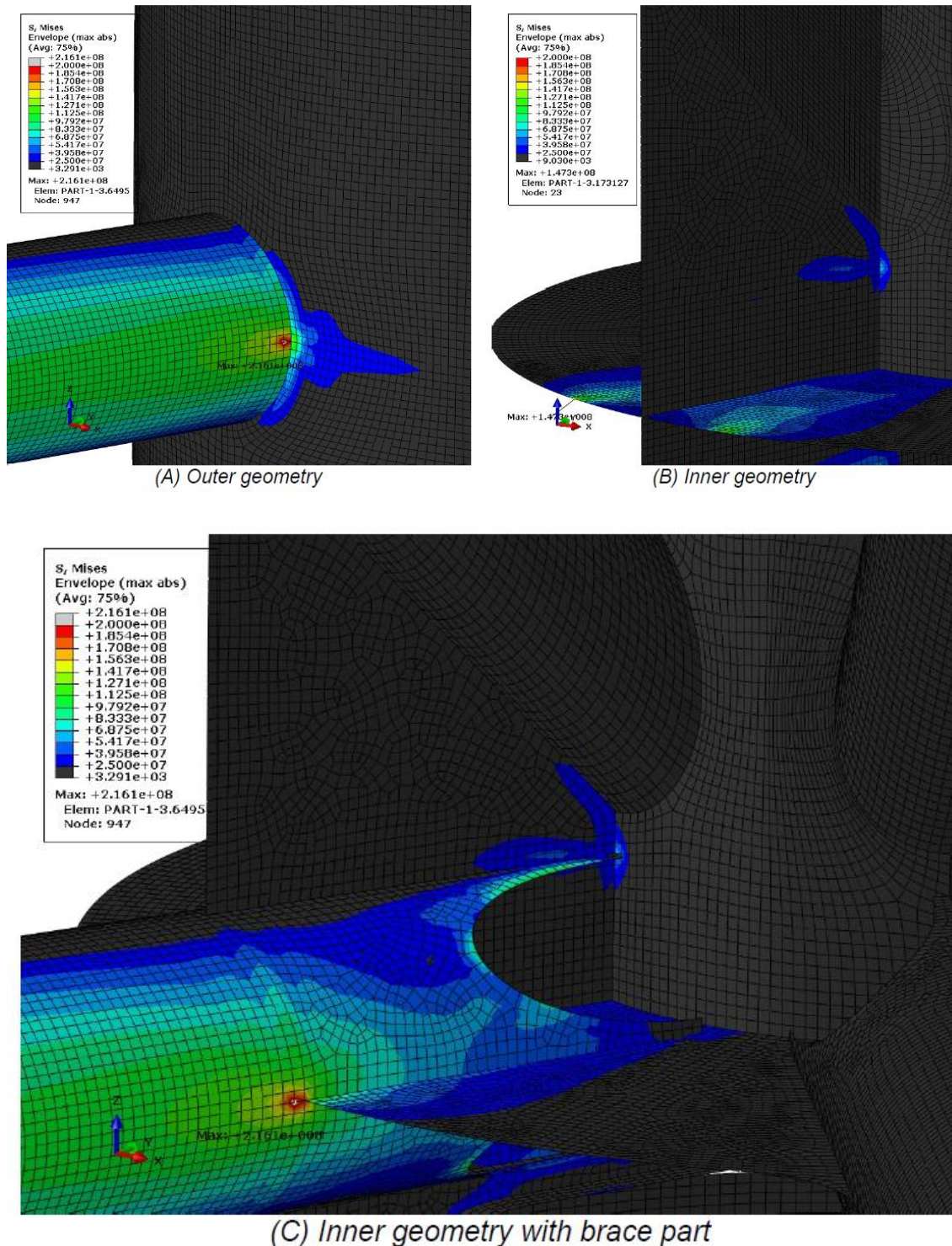


Figure 20 Plot of Von Mises stress for moment about local vertical axis of lower brace. The maximum stress value over the cross section is shown. (Stress values are in Pa)

2.2.6.4 Stress reduction by brackets

The stress concentrations found above have to be considered with respect to fatigue. If the fatigue life of the structure is not satisfactory some modifications have to be carried out. In that respect some preliminary studies of possible bracket designs have been conducted. The brackets are placed in the horizontal plane at the intersection between lower brace and the outer shell. The brackets are shown in

Figure 21. The brackets are 15 mm thick and the height of the bracket toe is approximately 15 mm from the central line of the shell surface.

The bracket is approximately 300 mm long and 300 mm wide. Several other bracket configurations have also been studied and it is very important to have a small height at the bracket toe.

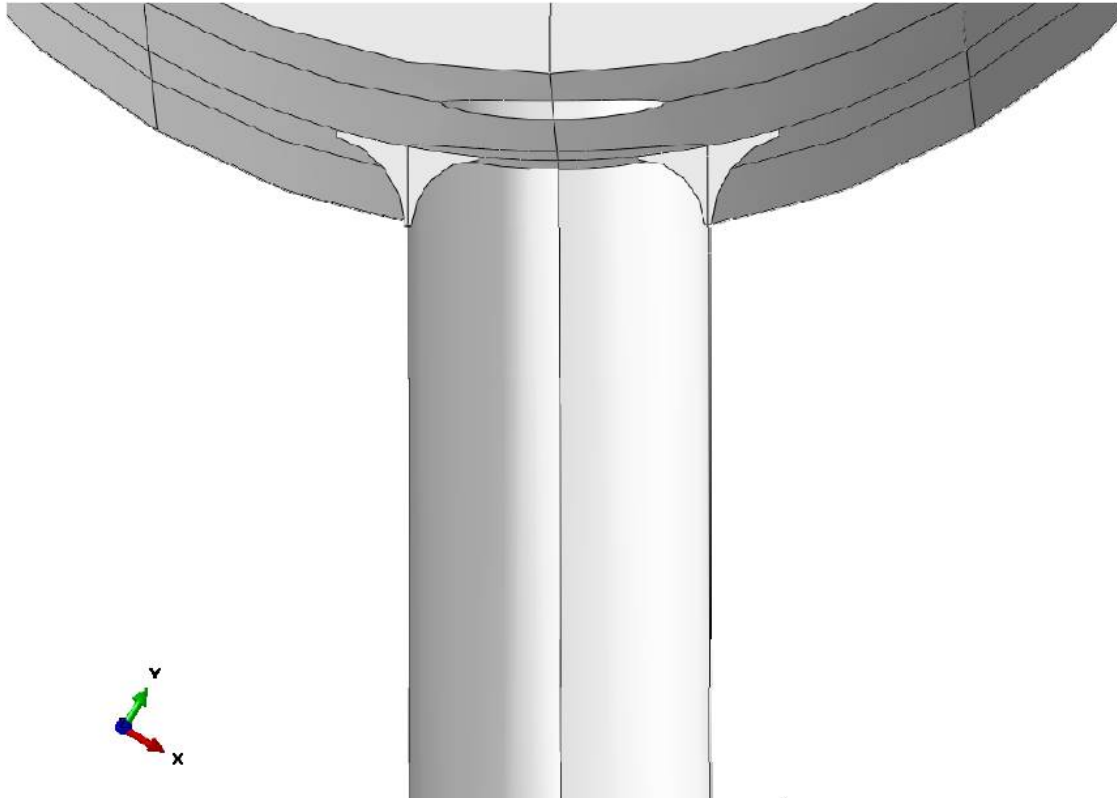


Figure 21 Proposed bracket system

Results for axial loading of the lower brace with the proposed brackets are presented in Figure 22. The maximum stress concentration in the horizontal brace is reduced from 206 MPa to approximately 165 MPa, and it is moved from the outer shell intersection to the bracket toe. There is a stress concentration of approximately 200 MPa in the brackets, but this concentration is in an area without welding so it would not be critical with respect to fatigue. Similar stress concentration reductions are observed for local bending of the lower brace about the vertical axis. A corresponding bracket definition should be used in the vertical plane if the stress concentrations due to bending about the horizontal axis should be reduced. Similar definitions of brackets can also be used for the connection of diagonal braces to the column.

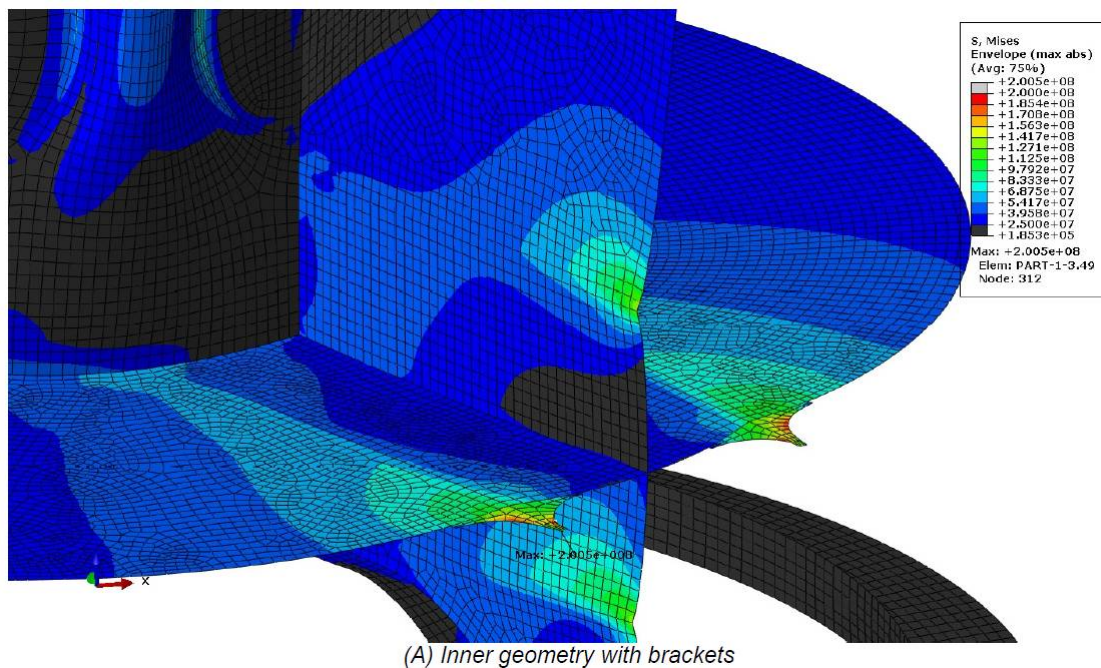
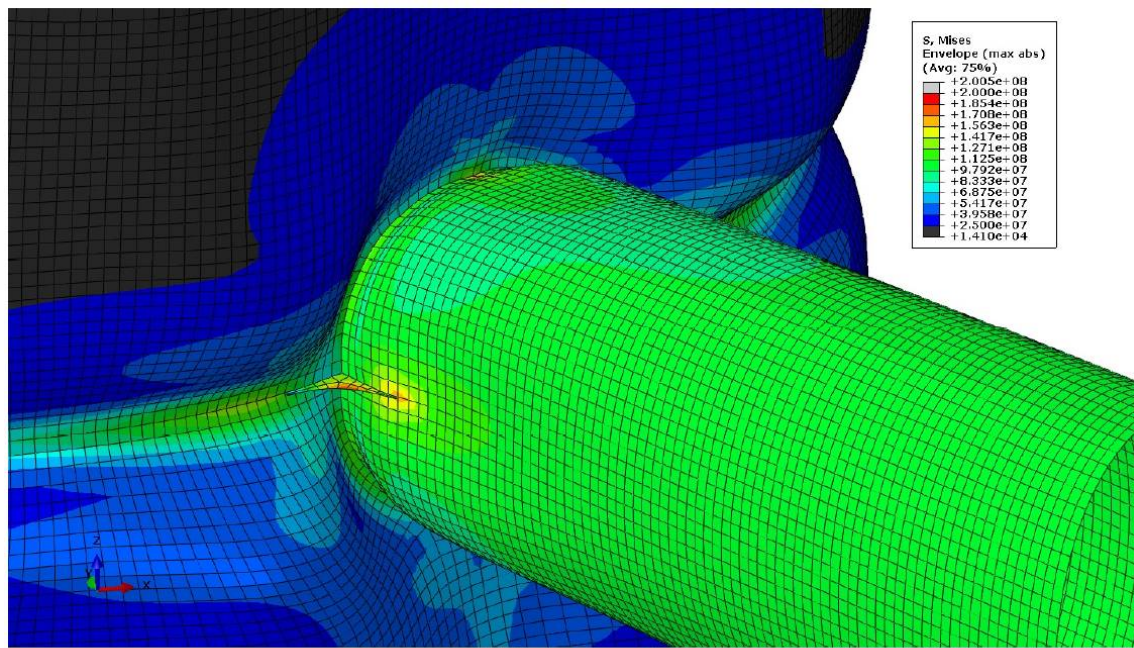


Figure 22 Plot of Von Mises stress for axial load of lower brace with brackets. The maximum stress value over the cross section is shown. (Stress values are in Pa)

Another change has been done for the interior brackets to reduce stress in the critical hot spots of the unions in the interior. In the critical areas material has been removed and smaller brackets are used now.

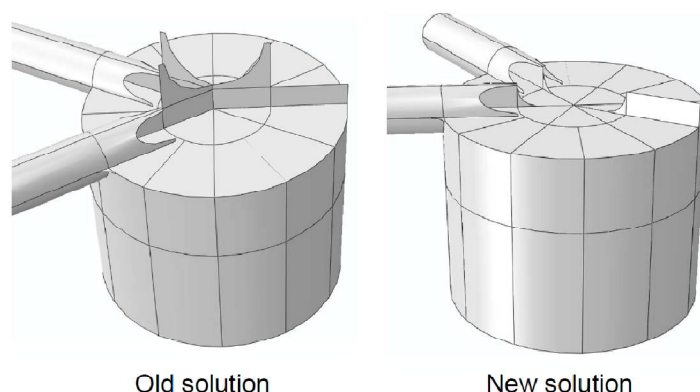


Figure 23 Comparison old versus new solution for the brackets for the lower braces

2.2.7 Design check under extreme conditions by BV

BV performed a design check for the design of the floating structure for extreme conditions. The evaluation has been done differently to the design check performed by Olav Olson to allow a cross check for the design and to verify if there were additional hot spots that had to be taken care of especially in the zones of the structural tubular connections which were deemed to be the most critical.

2.2.7.1 Load cases for extreme conditions

The load cases used for the final check of the structure are taken from the extreme load cases matrix.

Id	Hs	Tp	Gam ma	Dir_w aves	V_wind	Dir_wind	V_curr	Dir_curr	Comments	RP wave	RP wind	RP current
1	13.36	16.16	6.36	316.1	30.94	285.8	1.02	268.2	Max surge	61,00	41,88	1,24
2	9.8	14.77	3.82	314.1	25.01	291.4	0.91	268.5	Max surge	1,04	0,18	0,39
3	5.32	15.65	7.0	306.6	11.4	221.1	0.27	227.7	Min surge	0,01	0,01	0,01
4	5.02	16.03	7.0	303.8	14.54	259.5	0.84	254	Min sway	0,01	0,01	0,19
5	7.36	14.49	4.47	320.2	25.01	283.7	1.04	261.7	Min sway	0,01	0,18	1,73
6	5.19	16.71	7.0	302.5	11.4	222.4	0.51	236.9	Min sway	0,01	0,01	0,02
7	11.48	15.09	6.1	319.0	25.95	300.8	0.97	277.9	Min pitch	4,61	0,25	0,55
8	10.61	16.02	4.65	319.2	2.69	285.3	0.99	268.5	Min pitch	2,13	0,68	0,62
9	10.24	15.63	4.62	317.0	25.01	289.3	1.03	268.5	Min pitch	1,54	0,18	1,39
10	7.62	11.63	6.1	315.6	19.67	315.5	0.35	315.3	Max pitch	0,15	0,02	0,01
11	9.327	14.79 5	4.048	316.9	29.523	277.5	1.102	264.1	Max Acel X	0,70	2,63	5,10
12	9.372	16.18 6	5.115	316.5	31.068	276.8	0.901	267.8	Max wind speed	0,72	61,00	0,28

Figure 24 Extreme Conditions

The whole load cases were discussed and validated for mooring extreme analysis. In the structural point of view only load cases 1, 7, 8 and 9 were relevant for the wave return period. It was also assumed that wind forces are always maximum in load cases 1, 7, 8 and 9 (maximum thrust force from the thrust coefficient relative to wind) [26]. Wind forces are applied at turbine point $X=0$, $Y=0$, $Z=60\text{m}$ (above free surface) and $F_{\text{wind}} = 265 \text{ kN}$; $M_{\text{wind}} = 17254 \text{ kNm}$. Wind force is assumed in the same direction as wind direction, moment is defined perpendicular at the force.

2.2.7.2 Methodology:

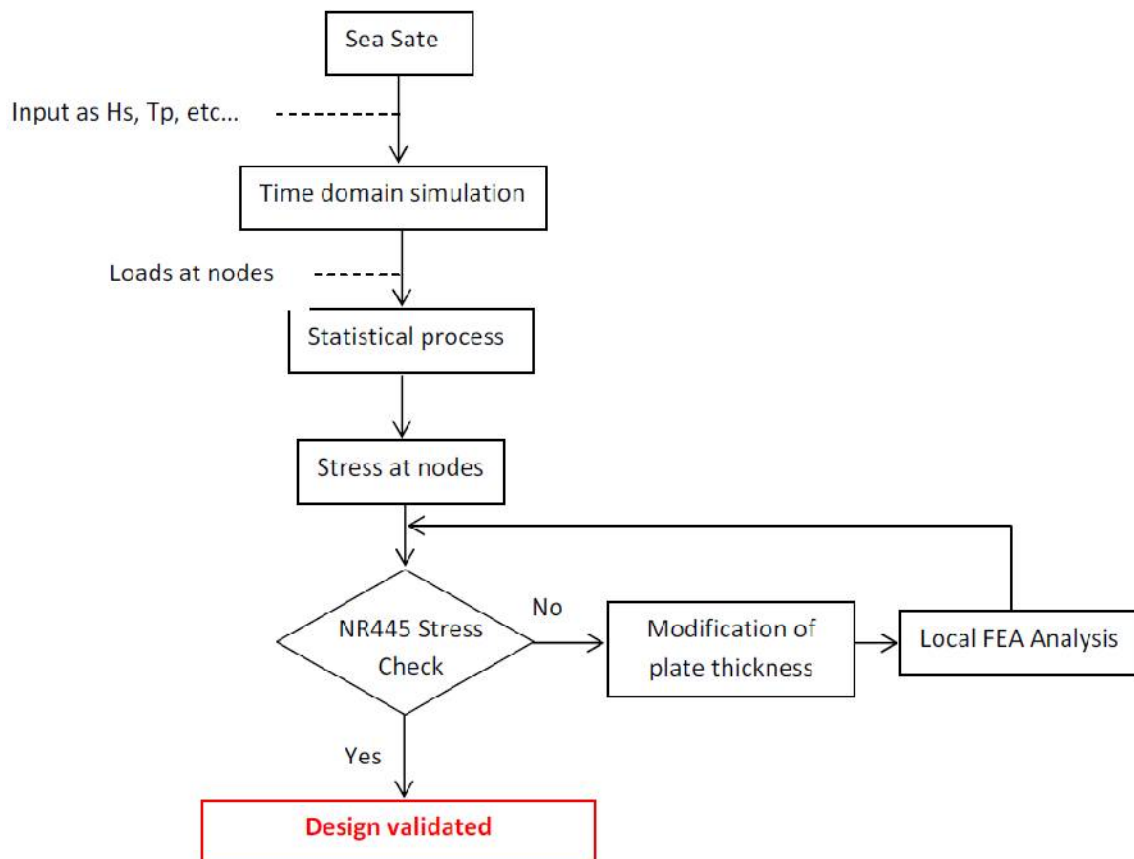


Figure 25BV Methodology

This methodology is different from the one chosen by Olav Olsen (design wave analysis with DNV criteria). This will allow to identifying possible other hot spots in the structure. The check focuses on most probable critical points that are structural tubular connections.

2.2.7.3 Modeling

a. Time domain analysis

For each load case, non-linear time domain simulations of 3h were performed. Wave forces come either from hydrodynamic panels for columns, either from Morison elements for braces and columns. For columns, only Morison damping term was considered in Morison elements. The structure was modeled by beams and FEA was performed for the 3h simulation. Outputs were internal forces and moments in beams.

b. Statistical post-processing

From 3h simulations, combined stresses in beams were computed using the formula 5.3.1 of Bureau Veritas NR445 – Rule for classification of offshore units, Part B, Section 3 [4]. For beams, combined stresses (based on Von Mises formulation) were defined as following:

$$\sigma_{combined} = \sqrt{\sigma_{axial}^2 + 3\tau^2}$$

Where:

$$\sigma_{axial} = \max\left(\frac{N}{S} \pm \frac{M_y}{I_y} \cdot \frac{D}{2} \pm \frac{M_z}{I_z} \cdot \frac{D}{2}\right)$$

$$\tau = \sqrt{\left(\frac{T_y}{S}\right)^2 + \left(\frac{T_z}{S}\right)^2}$$

and:

N: axial force in X axis

Ty: shear force in Y axis

Tz: shear force in Z axis

D: equivalent diameter of the beam

S: area of the beam section

Iy: inertia in Y axis

Iz: inertia in Z axis

Then extreme stresses with an occurrence probability of 0.001 were calculated and fitted on a Weibull probability distribution. Extreme stresses were then compared to BV NR445 criteria. This way of proceeding resulted in an evaluation of stresses coming from the current combination of forces that occurs in a representative sea state.

c. Validation of the design:

At critical points (brace connections at columns and tower), a comparison was done between the calculated extreme stresses with an occurrence probability of 0.001 and the criteria defined in 5.2.1 of BV NR445. If the criterion was not matched, a local FEM with modified plate thicknesses was computed to check the stresses according to BV NR445. The check was done using the safety factor “design” $\alpha=0,6$. The material strength proposed by Olav Olsen and used here was $R_e=275\text{MPa}$. Probable plate thicknesses that went over the criteria were modified until BV NR445 criterion was validated.

2.2.7.4 Model

a. Hydrodynamic Model:

The model is shown in red:

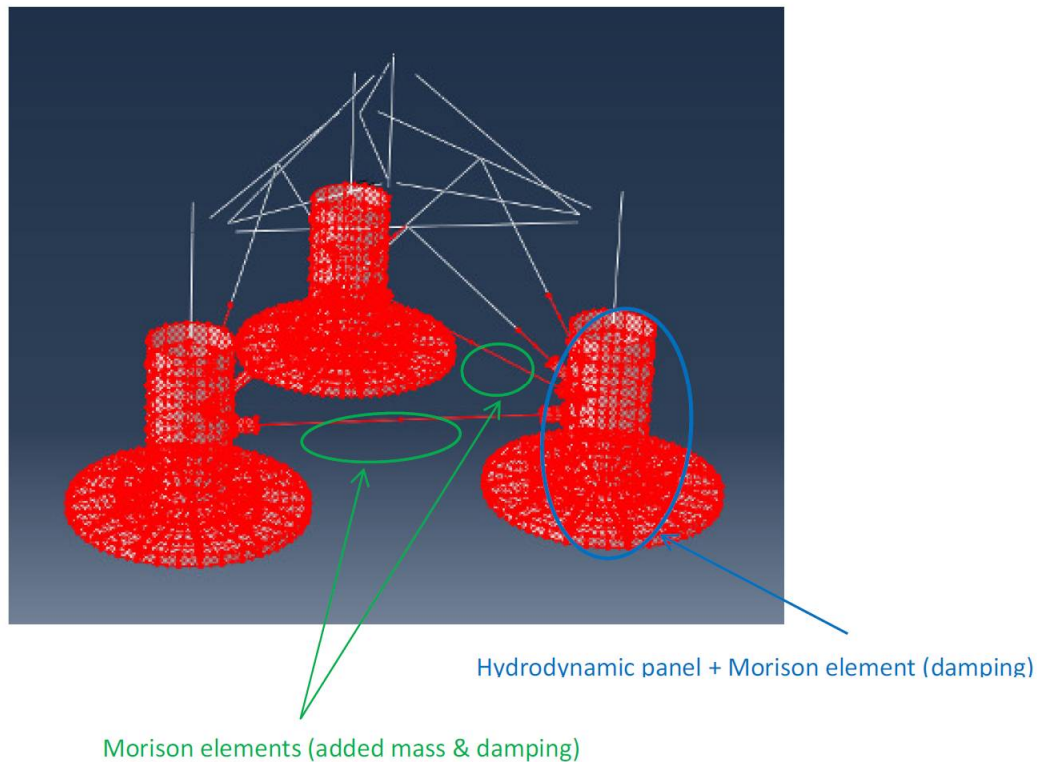


Figure 26 Hydrodynamic Model

For panels below $z=0$, all pressure components were considered: Froude-Krylov, radiation and diffraction. For panels above $z=0$, only Froude-Krylov pressures were calculated. Morison forces were computed when the element was wet.

b. Structural model:

Beam model:

Each part of the structure (braces, columns, and tower) was modeled with beams. The characteristics are described below. In order to adjust whole mass and inertia of the model, punctual masses were used. Green points show punctual mass for decks, stiffeners, dampers and rotor assembly.

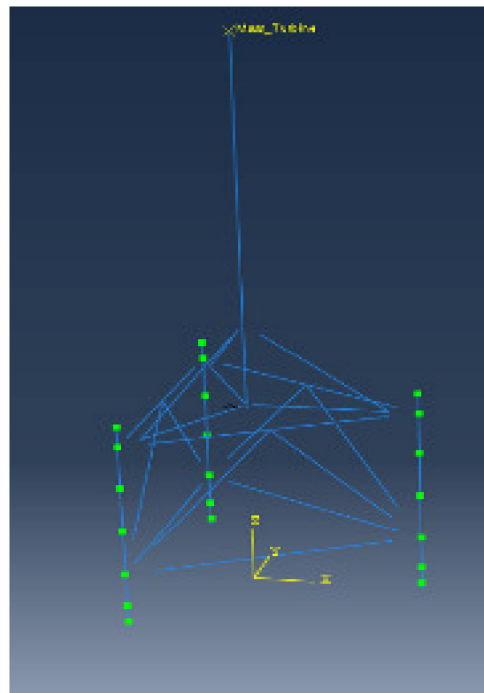


Figure 27 Structural Model

The final computed mass values of the structure are given in the following table.

Table 4: Computed Mass Values

	Bv	Olav Olsen	Error
$M_{\text{structural}} \text{ [t]}$	900.32	920.000	-2.1%
$M_{\text{tot}} \text{ [t]}$	3115.67	3333.738	-6.5%
$R_x \text{ [m]}$	20.65	20.857	-1.0%
$R_y \text{ [m]}$	20.65	20.857	-1.0%
$R_z \text{ [m]}$	19.19	20.207	-5.0%

References for inertia and masses:

- 2012-04-19 - “HiPRWind Main Structure Specification rev.2 April 2012.pdf”
- 2011-12-19 - “WTG FLOATER SEMI Rev-01 191211.xls”

Beam conversion:

The characteristics (inertia, area) of each beam have been calculated with different methods depending on the type of section studied.

- For simple sections such as the tower or cylinder braces, characteristics have been found analytically.
- for columns, inertias and areas have been calculated using BV software Mars :

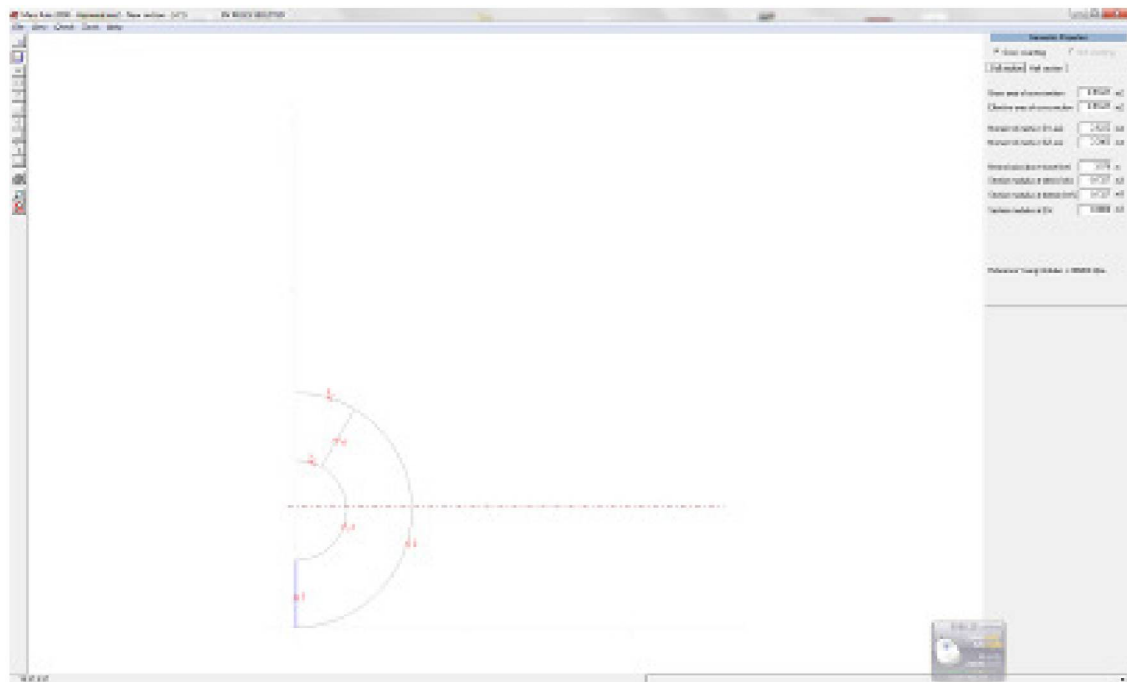


Figure 28 BV Software Mars

For connections a FEA has been performed. Here an example for column-tower connection:

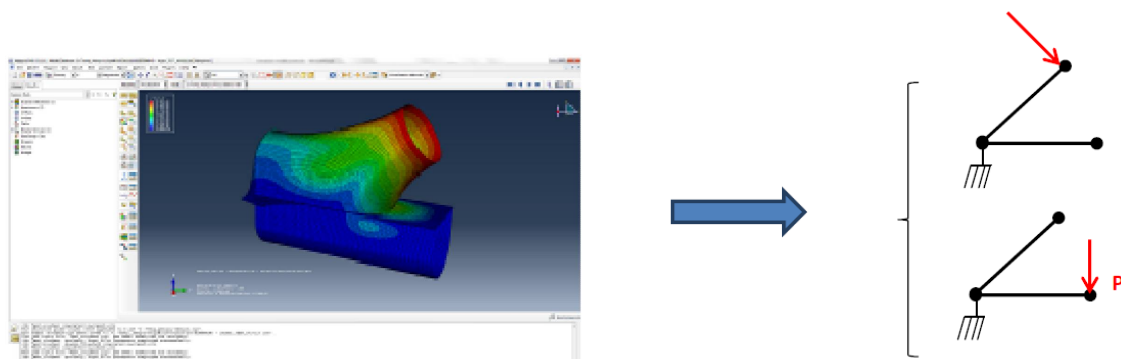


Figure 29 FEA column tower connection

Assuming a cantilevered beam, the relation between applied force P and displacement is:

$$y(L) = -\frac{PL^3}{3EI}$$

Inertias have been calculated in both Y and Z directions assuming X in the axis of the beam and assuming $E=210 \times 10^{12} \text{ Pa}$ for steels. Areas have been calculated from the mass of the element assuming $\rho=7850 \text{ kg/m}^3$, M found with plate FEM and

$$A = \frac{M}{\rho L_{\text{element}}}$$

All beam characteristics are given as follows:

Table 5: Structural Beam Characteristics

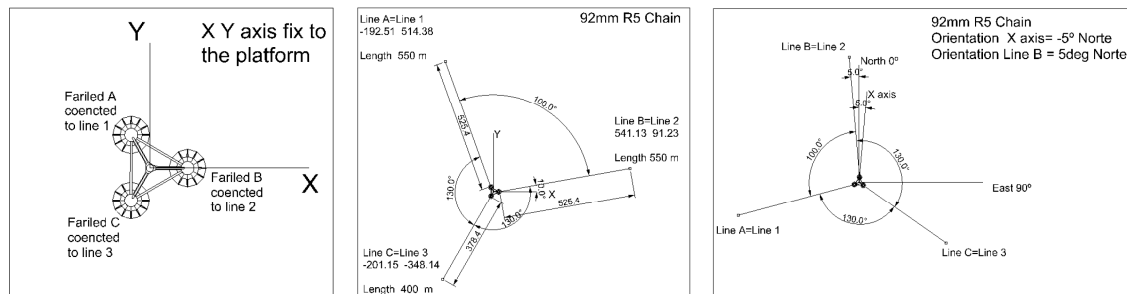
Structural Beam Characteristics		Material		
		rho	7.85E+03	[kg/m3]
		E	2.10E+11	[Pa]
Tower support connections (Diag Braces)	Cylinder	D	0.900000	[m]
		t	0.016000	[m]
		I	0.008684	[m4]
		S	0.046048	[m2]
	Column connection	IHor	0.015163	[m4]
		IVer	0.018875	[m4]
		J	0.034038	[m4]
		M	1.077.756	[t]
		L	2.840.840	[m]
		S	0.050083	[m2]
	Tower connection	IHor	0.012054	[m4]
		IVer	0.009796	[m4]
		J	0.021850	[m4]
		M	3.298.788	[t]
		L	2.777.000	[m]
		S	0.156817	[m2]
Tower + Tower connections (Hor braces)	U-Shaped	IHor	0.007178	[m4]
		IVer	0.006600	[m4]
		J	0.013778	[m4]
		S	0.056986	[m2]
	Column connection	IHor	0.012004	[m4]
		IVer	0.008922	[m4]
		J	0.020926	[m4]
		M	1.239.000	[t]
		L	2.750.000	[m]
		S	0.059478	[m2]
	Tower connection	IHor	0.026267	[m4]
		IVer	0.009552	[m4]
		J	0.035819	[m4]
		M	3.611.333	[t]
		L	2.930.000	[m]
		S	0.162711	[m2]
Tower		D	4.000.000	[m]
	Section 1 (upper)	t	0.040000	[m]
		I	0.975550	[m4]
		S	0.515692	[m2]
	Section 2	t	0.030000	[m]
	Section 2	I	0.737187	[m4]
		S	0.387746	[m2]
	Section 3	t	0.025000	[m]

		I	0.616635	[m4]
		S	0.323528	[m2]
	Section 4 (lower)	t	0.020000	[m]
		I	0.495165	[m4]
		S	0.259148	[m2]
Column	S0	D	3.010.000	[m]
		t	0.010000	[m]
		I	0.106030	[m4]
		M	1.665.258	[t]
		L	2.200.000	[m]
		S	0.096425	[m2]
	S1	I voile ext	2.296.300	[m4]
		I perp voile ext	2.626.108	[m4]
		J	4.922.408	[m4]
		M	26.494.286	[t]
		L	6.000.000	[m]
		S	0.562511	[m2]
	S2	I voile ext	2.583.400	[m4]
		I perp voile ext	2.996.912	[m4]
		J	5.580.312	[m4]
		M	30.283.030	[t]
		L	6.000.000	[m]
		S	0.642952	[m2]
	S3	I voile ext	2.788.500	[m4]
		I perp voile ext	3.373.357	[m4]
		J	6.161.857	[m4]
		M	36.407.136	[t]
		L	6.000.000	[m]
		S	0.772975	[m2]
	S41	I voile ext	2.811.100	[m4]
		I perp voile ext	3.378.364	[m4]
		J	6.189.464	[m4]
		M	4.085.701	[t]
		L	0.800000	[m]
		S	0.650589	[m2]
	S42	I voile ext	2.721.100	[m4]
		I perp voile ext	2.928.570	[m4]
		J	5.649.670	[m4]
		M	4.364.663	[t]
		L	1.161.500	[m]

Braces		S	0.478698	[m2]
	S43	D	7.000.000	[m]
		t	0.020000	[m]
		I	2.670.913	[m4]
		M	12.491.742	[t]
		L	3.546.500	[m]
		S	0.448697	[m2]
	Inter Column Hor	D	1.300.000	[m]
		t	0.020000	[m]
		I	0.016475	[m4]
		S	0.082275	[m2]
	Inter Column Diag	D	0.900000	[m]
		t	0.015000	[m]
		I	0.004084	[m4]
		S	0.042664	[m2]
	Inter Column U-shaped	IHor	0.007178	[m4]
		IVer	0.006600	[m4]
		J	0.013778	[m4]
		S	0.056255	[m2]

c. Mooring system:

The characteristics of the mooring lines



The mooring response was assumed to be quasi-static. For each line, the line tensions were preprocessed with BV mooring code for different offsets of the platform. Then, at each time step of the simulation, tensions at mooring points were interpolated in these pre-calculated tables.

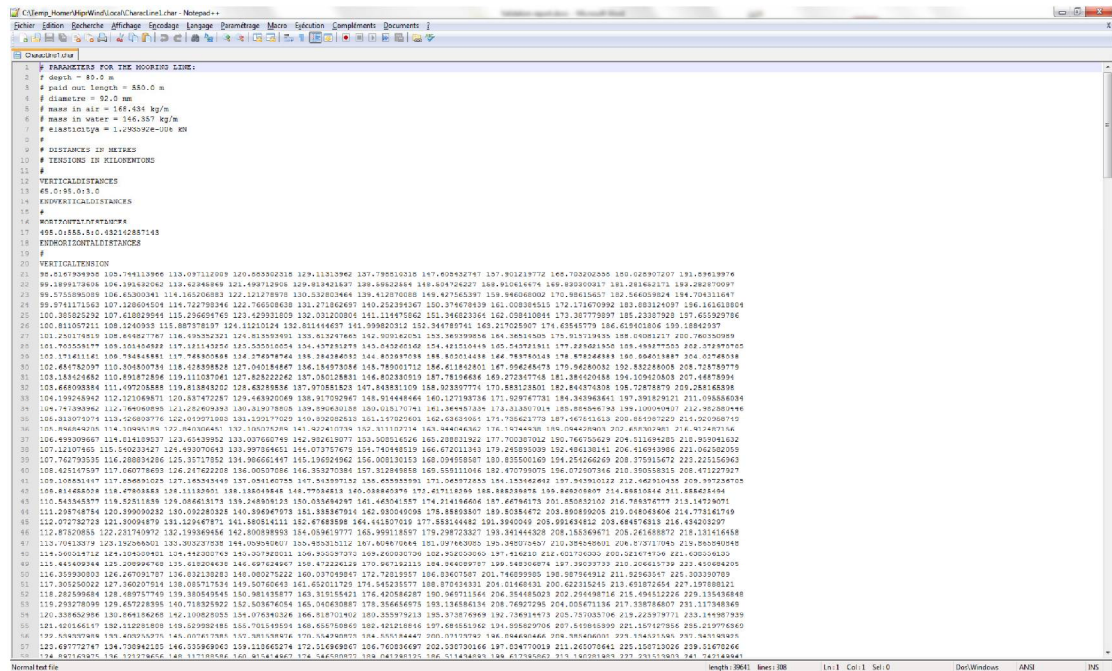


Figure 31 Example of tension matrix computed

2.2.7.5 Results design check

The stresses in different elements were checked within NR445 criteria. For $R_e=275\text{MPa}$ was chosen with a safety factor “design” $\alpha=0.6$, and maximum admissible stress was $\sigma_{\text{adm}} = 181.5\text{ MPa}$. A “Utilization factor” was calculated, which is the ratio between computed value from calculation by admissible value of σ_{adm} . This ratio must be under one. Results are presented from the most critical areas to the less critical ones and are given for each load case in Pascal:

2.2.7.6 Conclusions design check

a. General

For each load case, the NR445 criteria are respected. This means that proposed thicknesses in steel 275 MPa are acceptable.

b. Steel grades

Considering the environmental conditions, steel of grade A or B were accepted (it depends on the measured temperature at BIMEP site off Bilbao, since the air temperature can lower down to 0°C, therefore grade B is recommended). Grade Z is required where connections demand welding in both sides of a plate at a crossing as displayed by Olav Olsen. See Figure 32.

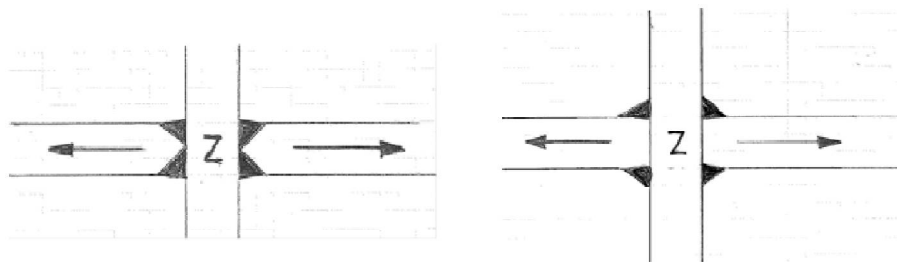


Figure 32 Welding on both sides of a plate at a crossing

c. Welding

For welding the proposed solutions of Olav Olsen are acceptable:

- double continuous fillet welding with $a = \max(0.25 \cdot \text{thickness}; 3.5\text{mm})$ are accepted for:
 - all welding of principal and secondary stiffening to inner and outer plates, outside connections areas and passages through other stiffening or plates,
- Full penetration welding for all connections (at least 10% at each extremity of stiffeners' spans) and butt-weld of main parts plates (columns, braces, decks).

2.2.8 Dampers

Final Damper design calculations with the resulting dimensions were undertaken.

Analysis of dynamic damper plate pressure

The final Analysis of dynamic damper plate pressure was performed.

Maximum dynamic resultant pressures, on the thin rim, were found by combining panel pressure RAOs for corresponding panels in POSTRESP (DNV software). A summary of the pressure resultants found are given in the Table 6 below. This table also contains the maximum pressures found at the top and bottom of the plate in addition to the relevant wave amplitude calculated in accordance with DNV-RP-C103 [25]. This was based on the results presented in Table 6. It seems reasonable to consider a resulting pressure of 25 kPa when dimensioning the outer rim plate.

Table 6 Table with Maximum pressure values for given periods

		<i>Pressure calculated by WADAM</i>					
<i>Periode</i>	<i>Wave length</i>	<i>Top of plate</i>		<i>Bottom of plate</i>		<i>Pressure difference</i>	
T (s)	λ (m)	p_d/a (Pa)	p_d (Pa)	p_d/a (Pa)	p_d (Pa)	$\Delta p_d/a$ (Pa)	Δp_d (Pa)
6.0	56	3913	15710	1974	7925	3025	12145
6.5	66	4413	20125	2469	11259	3150	14365
7.0	76	4876	24923	2929	14971	3199	16352
7.5	88	5313	30091	3369	19081	3196	18101
8.0	100	5723	35557	3795	23578	3153	19589
8.5	113	6102	41225	4206	28416	3080	20808
9.0	126	6445	46984	4598	33519	2984	21753
9.5	141	6755	52774	4968	38813	2874	22453
10.0	156	7031	58511	5314	44222	2753	22910
10.5	172	7277	64157	5635	49681	2627	23161
11.0	188	7496	69678	5932	55140	2500	23238
11.5	205	7691	75047	6205	60547	2373	23155
12.0	222	7866	80258	6457	65882	2249	22947
12.5	240	8023	85296	6689	71113	2129	22634
13.0	257	8163	90139	6902	76215	2014	22239
13.5	275	8290	94808	7097	81164	1905	21786
14.0	293	8405	99292	7278	85979	1802	21288
14.5	311	8509	103590	7443	90612	1706	20769
15.0	329	8604	107711	7596	95092	1615	20218
15.5	347	8691	111660	7736	99390	1531	19670
16.0	365	8770	115428	7866	103530	1452	19111
16.5	383	8843	119038	7986	107502	1378	18550
17.0	401	8910	122485	8096	111295	1309	17995
17.5	418	8971	125767	8199	114944	1245	17454
18.0	436	9028	128911	8294	118430	1186	16935
		128911		118430		23238	

The final design for the Dampers was determined and the manufacturing drawings for the components have been created.

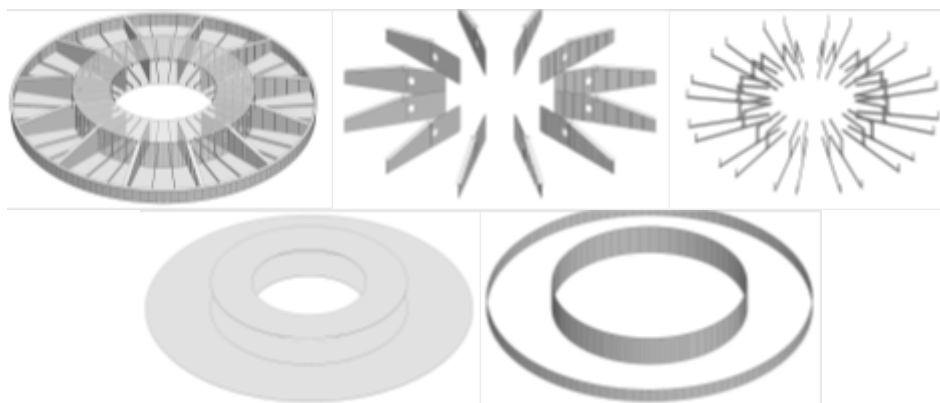


Figure 33 Damper components from CAD model

Column diameter	7.00	m
Damper plate outer diameter	0	m
Nuber of segments	12	
Diameter of the tank section	12	m
Total tank volume	417	m3
tank height	2	m
Outer rim height	1	m
Pressure height	15	m
Segment angle	0.523599	rad
Segment area	0	m2
Total area	0	m2
Equivalent diameter of damper	0	
Tank segment		
Tank segment floor area	5.792957	m2
Tank Segment volume	11.58591	m3
Total tank volume 1 column	139.031	m3
Tank floor thickness	15	mm
Tank floor plate weight	1.364241	t
ST1 length	4.34816	m
St1 weight/m	18.5	
ST2 length	3.726994	m
St21 weight/m	25.4	
Weight stiffeners	0.175107	t
Side wall length	2.50	m
Side wall area	5	m2
Side wall thickness	12	mm
Side wall weight	0.471	t
End wall area	6.211657	m2
End wall thickness	15	mm
End wall weight	0.731423	t
Stiffeners 2X length	3.105829	
Weight pr/m	28.3	
Stiffeners weight	0.17579	t
s1	3.105829	m
s2	0	m
h	-5.79555	m
Plate area	-9	m2
Plate thickness	12	mm
plate weight	-0.8478	t
stiff distance	-1.15911	
ds	-0.62117	
Is1	2.484663	
Weight pr/m	25.4	
Is2	1.863497	
Weight pr/m	28.3	
Is3	1.242331	
Weight pr/m	33.5	
Is4	0.621166	
Weight pr/m	36.7	
Weight of stiffeners	0.180262	
Girder web area	-9	m2
Thickness	12	mm
Girder flange area	-1.8	m2
Thickness	13	mm
Weight of girder	-1.03149	t
board plate area	0	m2
Thickness	15	mm
Weight of rim board	0	t
Pipe weight	0.3	t
Contingency factor weight	1.2	
Weight one segment	3.057881	t
calculated weight of damper	36.69457	t
Estimated weight (incl. Cont. Factor)	44.03349	
Weight of all damper plates	132.1005	t

Figure 34 Final calculations for damper dimensions

For the hydrodynamic analysis of the dampers the following data has been

used in WADAM.

Calculation of equivalent damper data for hydrodynamic analyses			
Tank volume	139.031	m3	
Entrapped water in outer part			
F	6.211657	m2	
f	0	m2	
Volume	-12	m3	
Equivalent volume one damper			
Area plate	-38.4845		
Equivalent height	0.129117	m	
Volume of steel	5.609361	m3	
Volume water	-10.5784	m3	

Figure 35 Final Damper values for hydrodynamic analysis

From the WADAM calculation the RAOs for movements and forces are retrieved. WADAM calculations as well give the forces in different braces, the added mass of the complete structure and the potential damping.

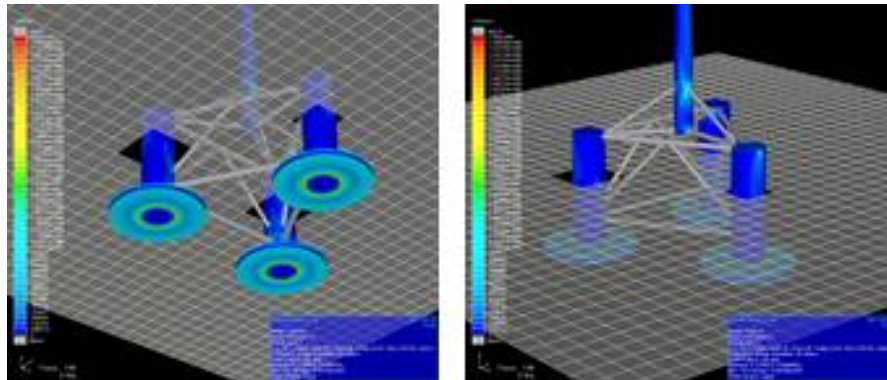


Figure 36 WADAM calculations

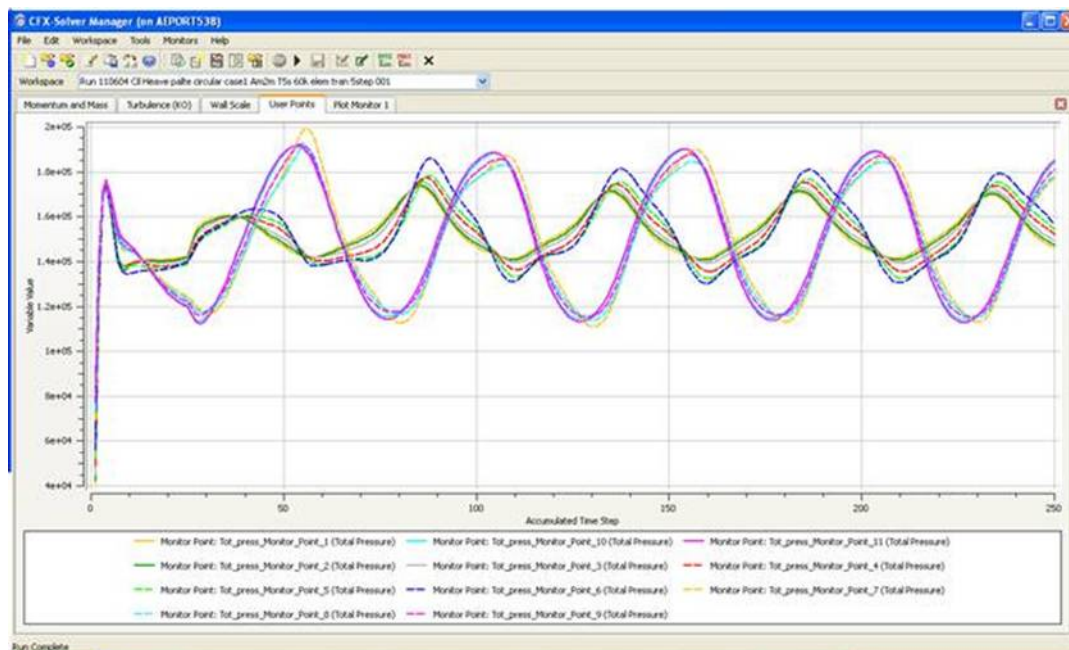


Figure 37 CFD calculations

Acciona Energía, not using HiPRWind resources, did undertake additional numerical calculations and CFD modeling (see Figure 37) that was further correlated to specific tank testing and decay tests for the proposed dampers and other possible solutions. One additional feature that was correlated in between numerical and CFD against tank testing was the pressure at the different damper plates (upper and lower plates). These tests were performed by attaching pressure sensors to the different plates and thus understand all damping coefficients and forces for structural input. See Figure 32 and Figure 33.



Figure 38 Location of Pressure sensors



Figure 39 Damper and Column tank testing

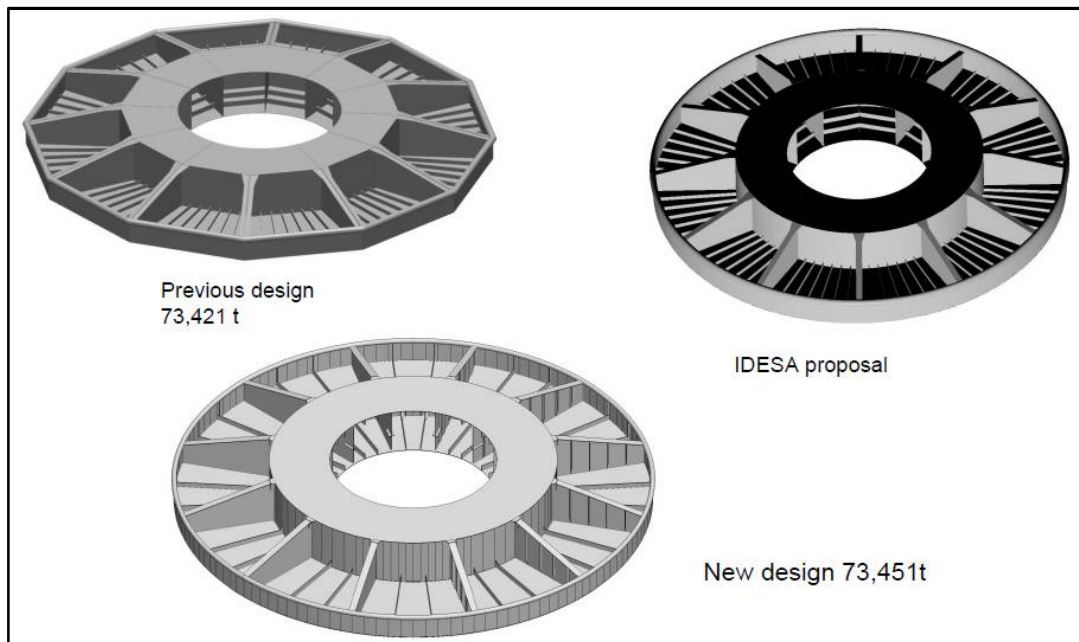


Figure 40 Resulting new damper design

2.2.9 Substructure Brace System and wind turbine tower support

The tower base and support braces tie the turbine tower rigidly to the floater structure. The design of these structures is related entirely to the loads from tower. And the design moment for the tower base is also used for preliminary design of the tower support. The support of the tower base is constituted by

the 3 diagonal braces and the 3 horizontal braces that are connected to the 3 columns in common support points. The gravity load from the turbine, tower and tower support structure is carried as compression loads in the diagonal braces. The dynamic moment from the tower is counteracted by horizontal moment pairs at the lower horizontal brace support and at the upper diagonal brace support. The diagonal brace is dimensioned for the axial reaction force from the tower moment by a nominal axial stress of approx. 60 MPa, as for the tower. The tower support base which is a column with diameter equal to the tower bottom, transfer the horizontal reaction forces to the braces. The column will be exposed to a shear force required to translate the tower moment to upper and lower horizontal reaction forces. The Tower moment will decrease to zero at the bottom of the support column. This means that the plate thickness can be reduced toward the bottom of the column.

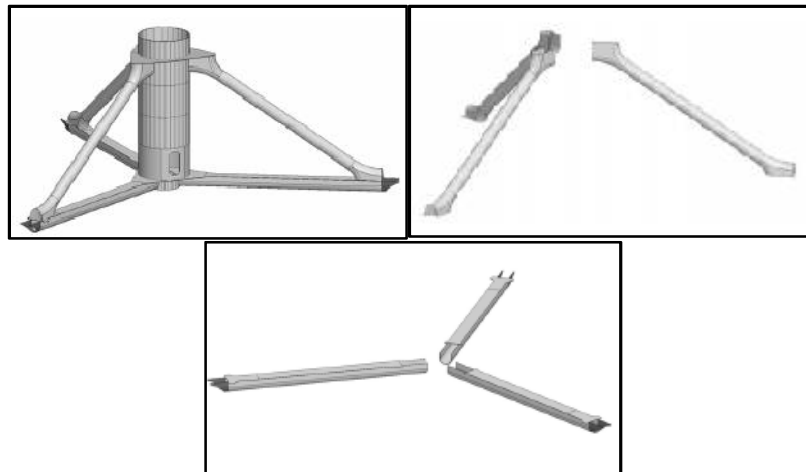


Figure 41 Central connection

The design for the central connection was finalized as well and the final dimensions been calculated.

Tower support structure		Upper brace level on support column		Rotor tip level above keel line	
Horizontal brace system length	16,735 m	Upper brace level on support column	36.00 m	Rotor tip level above keel line	37.000 m
Brace angle	6.594 rad	Relative rotor clearance factor	0.030	Bottom Tower flange level	34.000 m
Tower base diameter	4.30 m	Clearance to rotor tip	2.00 m	Bottom level support column	35.0 m
Brace system height	11,300 m	Height of base above upper brace conn.	1.20 m	Tower support column height	11,000 m
Tower braces Top - U-shaped		Tower braces Diagonal		Control of Diagonal brace	
Number of braces	3	Number of braces	3	Load according to extreme tower moment	
Brace length	14,71 m	L/D default value	30	Design tower moment	31631214 Nm
Diameter	0.900 m	T/D default value	3.030	Design tower shear force	1070330 N
Height	0.900 m	Vert. dist. from support plate - tower flange	1.50 m	Equivalent moment arm	29.73978 m
Width of top plate	1.000 m	Dist. from deck to support plate	6.50 m	Distance upper/lower support	11.30 m
Default thickness	16 mm	Vert. distance upper/lower supp.	6.00 m	Upper horiz. reaction	3006478 N
Applied thickness	10 mm	Dist. distance brace	14,101 m	Lower horiz. reaction	2016153 N
Weight contingency	30 %	Brace length	17,10 m	Reaction force in diagonal brace	2348178 N
	L/D 16.340	Angle with horizontal	0.59403 rad	Axial stress in diagonal brace	98.3 MPa
	L/D 10.055	Default diameter	0.90 m		
Section area	0.040 m ²	Applied diameter	0.90 m		
Weight one brace	7,740 ton	Default thickness	13.500 mm		
CoG Vertical level	25.95 m	Applied thickness	15.00 mm		
		Weight contingency	10 %		
			L/D ratio 16.72980		
			T/D ratio 0.016601		
		Section area brace	0.036173 m ²		
		Section area steel	0.040 m ²		
		Weight one brace	8.800 ton		
		Upper level connection	36.400 m		
		CoG Vertical level	30.40 m		

Figure 42 Calculation for tower support structure

2.2.10 Door opening in tower base

The door in a Wind Turbine tower and the door in the tower base on HiPRWind have different challenges with respect to design as follows:

- In a normal tower the stress pattern is mainly main stresses in axial direction due to the high bending load. The shear load is small. Accordingly the standard oval design is working good to reduce stress concentrations.

- In the HiPRWind tower base, the bending moment goes from maximum at the top brace connection to zero at lower brace connection. In addition there is a high shear load in the base due to transfer of the horizontal reaction forces through the column. Accordingly there are dominant diagonal directed main stresses in the base cylinder. The Oval door frame will accordingly not work as well as the long axis will not be in the direction of the main stress.
- An analysis of the tower door design was done and an alternative solution for the tower door was proposed to limit the stress in the affected zones of the transition piece shell. In this design a frame is clamped to the shell of the Transition Piece and the door is directly mounted onto this frame structure.

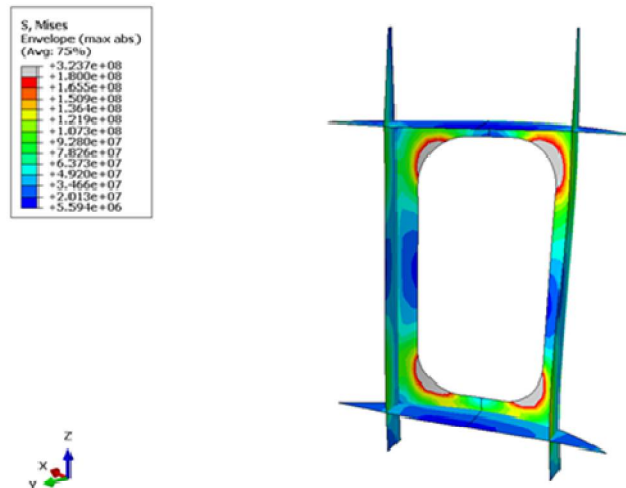


Figure 43 Tower door frame

The new design solution will resolve the issues. Since the structure will be clamped to the shell structure it allows for an adapted design as a secondary structure.

2.2.11 Hatch opening in bottom plate

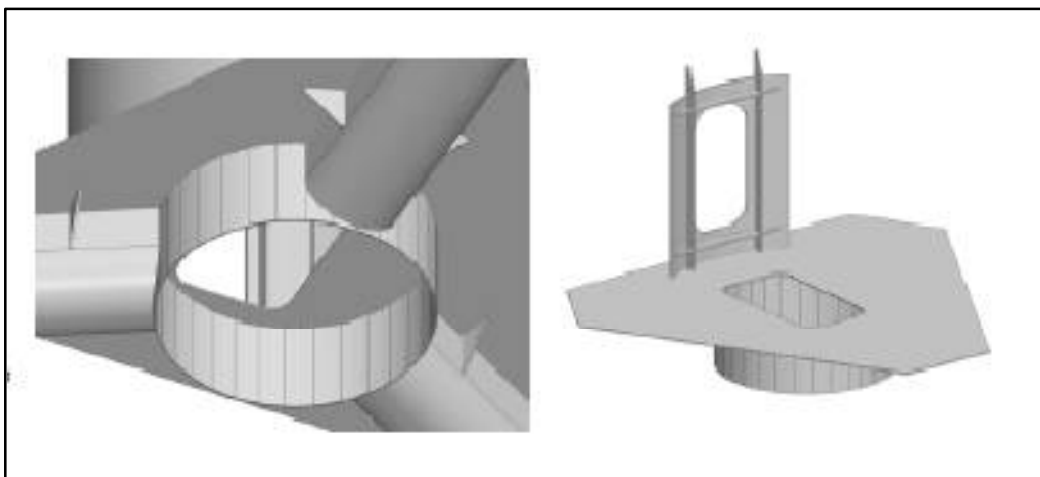


Figure 44 Hatch opening in Transition Piece Bottom

Analysis of the O&M requirements did reveal the need for a hatch in the Transition Piece bottom part to allow for the exchange of components from inside the tower. This is especially important in case of the transformer exchange. It is not likely that a transformer fails, but in case it does an exchange from the inside of the Transition Piece would almost be impossible without such a hatch at the bottom of the structure, since the components are mounted inside before the tower and turbine are installed on top of the Transition Piece. The development of this hatch required some structural analysis since the required

size for this opening is rather large. The calculation has been performed with the help of the CAD model.

2.2.12 Ballast system

The ballast system has been defined; a specification and the detailed drawings were elaborated along with the bill of materials.

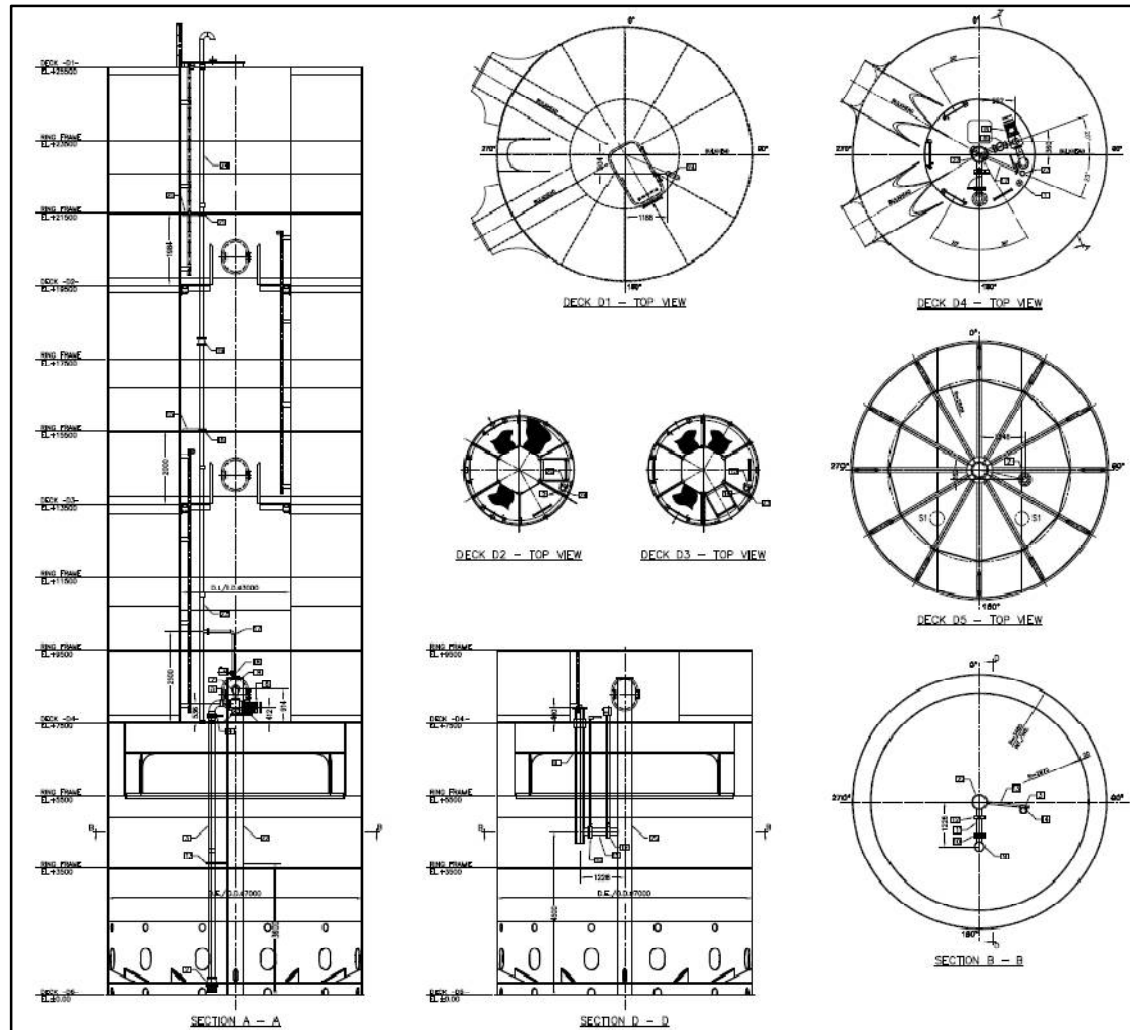


Figure 45 Ballast system in column

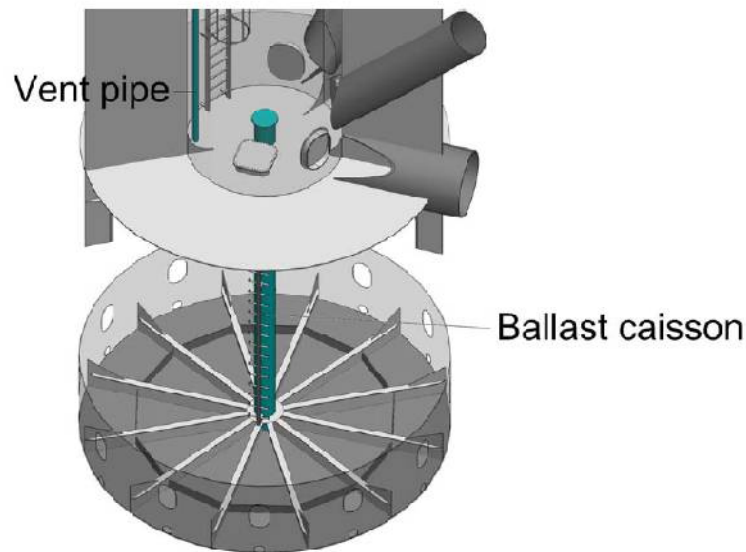


Figure 46 Ballast tank section in column with central pipe

Specification of ballast system has been performed defining the system with all relevant schematics and components:

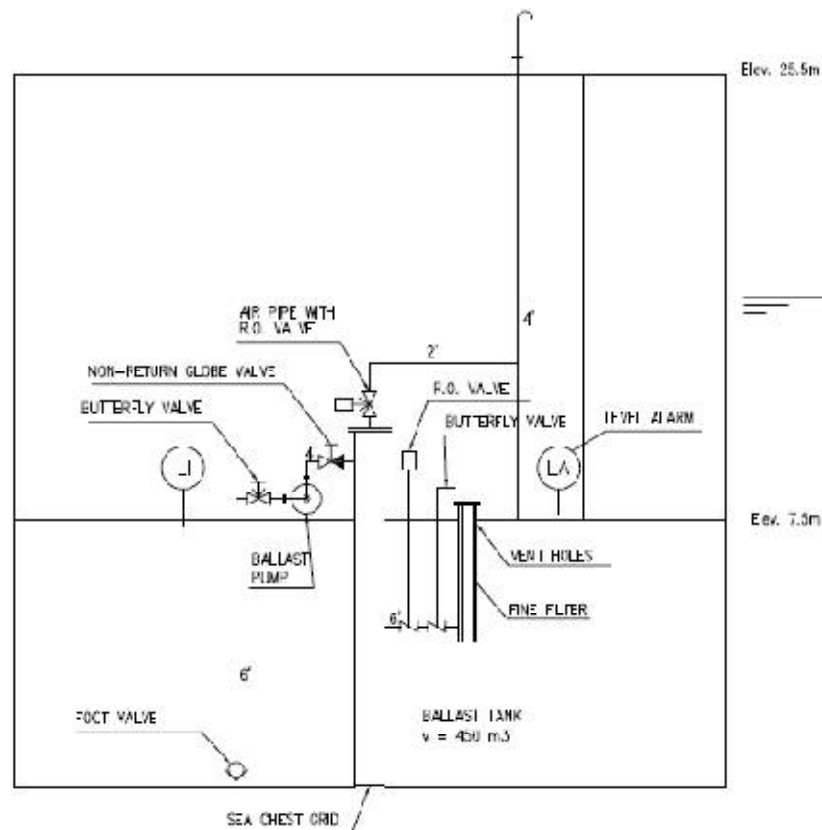


Figure 47 Ballast system schematic

The pumps and electric motors are designed as integrated components. The pumps and electric motors are designed for an easy dismantling overhaul of all maintenance components. Equipment will be supplied according with ISO standards. The pump has in the suction and the discharge zone the possibility to put a manometer to measure the pressure. Motors are fed by 380 V AC, 3 phases, 50 Hz. The electric motors and fittings protection were chosen adequate for the installation site, according to the requirements in Table 7.

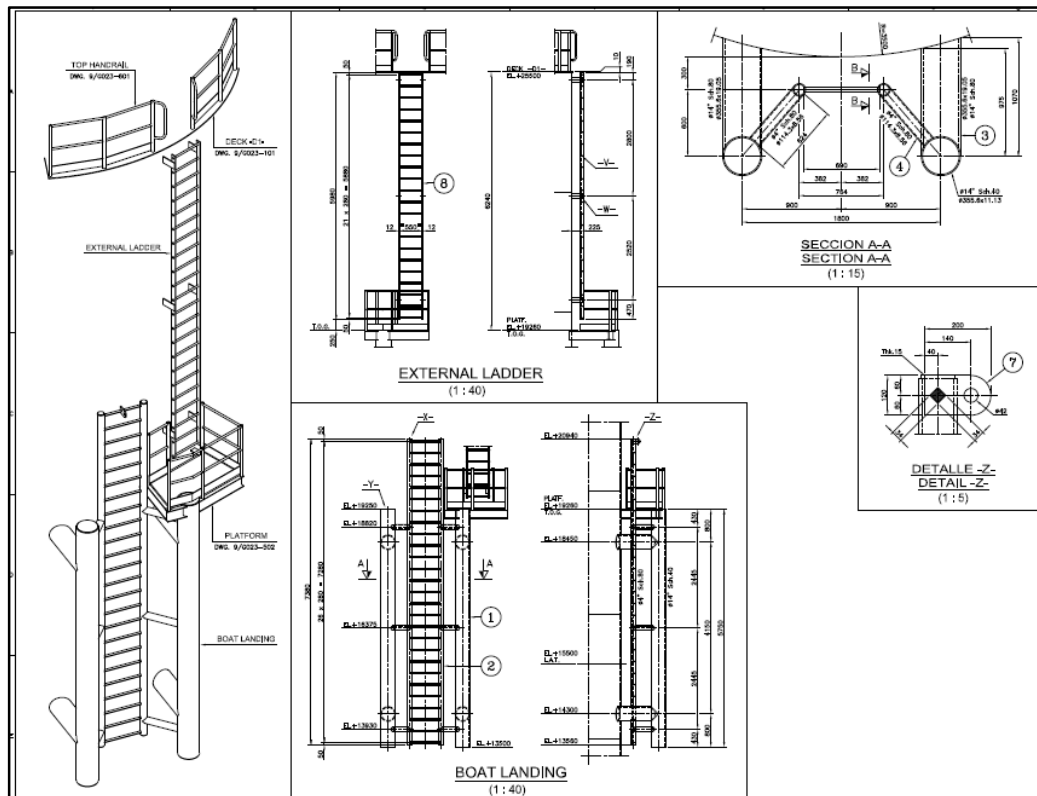
Table 7: Isolation specifications

<i>SITE</i>	<i>MOTOR</i>	<i>JUNCTION BOX</i>
General	IP-44	IP-56
Weather Decks	IP-56	IP-56

Motors isolation will be class F, rate F or better. The components in starter and control boards will be mounted in metallic boxes suitable for marine environment. The range of ambient air temperature in exposed decks is assumed -10 / +40°C. The pump will have connection flanges according DIN 2501.

2.2.13 Access system

The design for exterior (Boat Landing System) and interior Access system inside the columns has been defined. The Design and drawings for the respective ladder and access systems have been calculated and generated

**Figure 48 Outer column access system**

The interior column access and platform design has been finalized, taking in consideration all the aspects of the emergency scenario evaluations and the legal requirements for fixed offshore structures in respect to resting platforms and anchoring points, as well as for guards and rails.

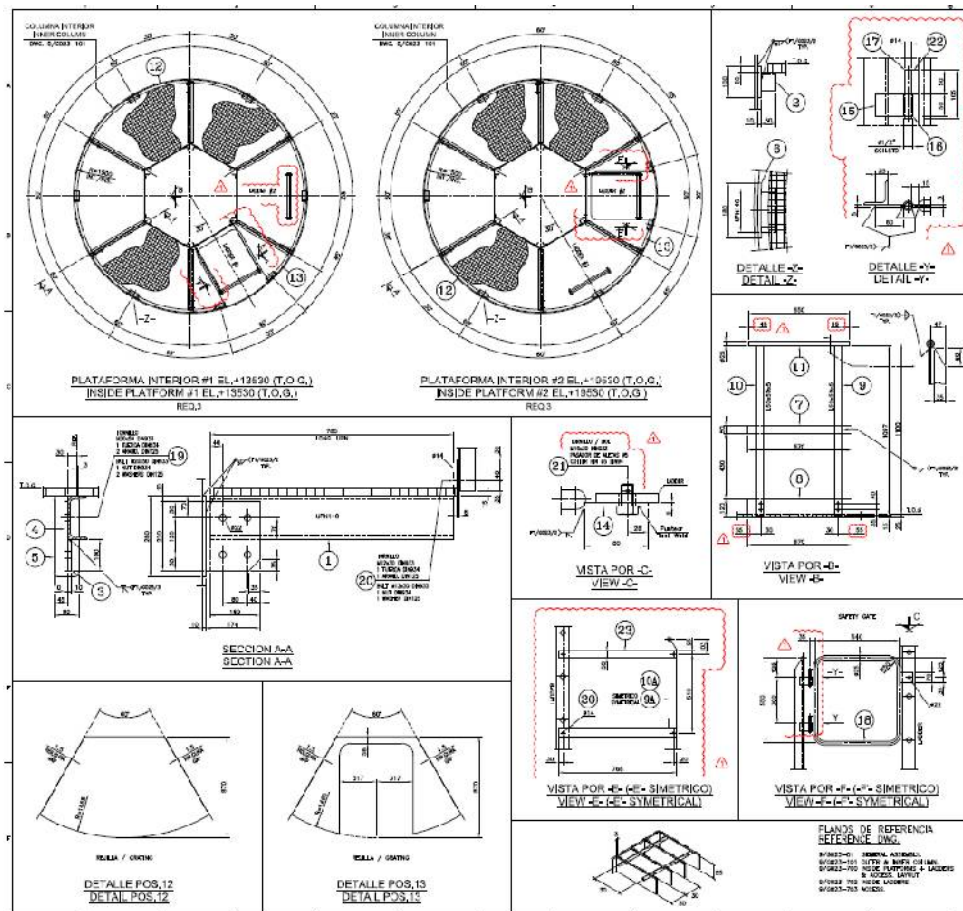


Figure 49 Platform design for interior of columns

An analysis for the escape and rescue from the interior of the columns has been performed. This was based on a Trial performed by Acciona Energía, using non-HiPRWind Resources, with one of its closest Safety consultants in order to assess all risks and casualties. Different commercial equipment's have been investigated and finally a test at a mock up installation has been performed. The test has been done to verify a modified solution with equipment that allows the recuperation of personnel even in case of electricity black outs during a rescue operation. A specially combined rescue rope set up was used that comprised rollers and blocks fitted in a way that safety of the personnel is insured at all-time even in worst case scenarios.

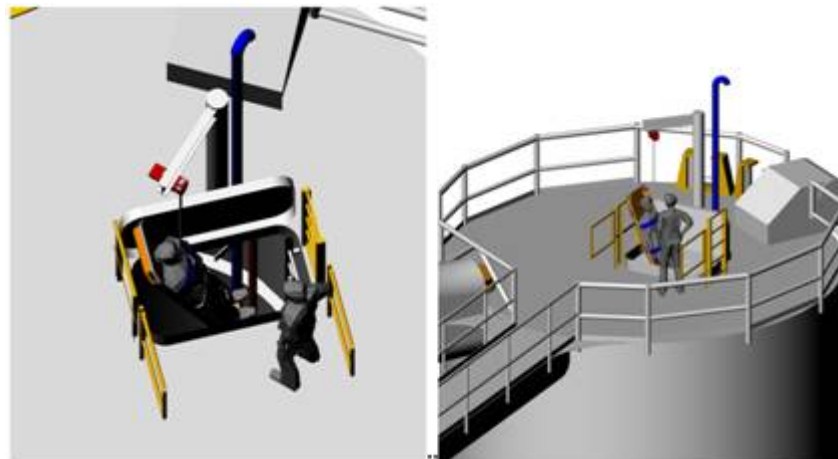


Figure 50 Rescue scenarios for column

CENTRAL ACCESS PLATFORM	MS-level Name		Number	th (mm)	VcG (m)	Weight (ton)	Weight all (ton)	moment (ton)
Web plate	CP MBR		6	15	25,2408	0,104771	0,628626	15,86702
Upper flange	CP MBR		6	10	25,445	0,012994	0,0779628	1,983763
lower flange 1	CP MBR		12	10	25,146	0,007721	0,09264708	2,329703
Lower flange 2	CP MBR		12	10	24,8902	0,007827	0,09392568	2,337829
Backing plate	CP MBR		6	10	25,2816	0,001124	0,00674238	0,170458
transition bracket	CP MBR		12	10	25,495	0,000852	0,01022362	0,260651
					25,21562		0,91012756	22,94943
Edge beams long	CP BEAMS	200x100	2	6	25,3598	0,055814	0,1116286	2,830879
Edge beams short	CP BEAMS	200x100	2	6	25,36	0,127722	0,255444	6,47806
							0,3670726	9,308939
Radial beams Web	CP R-BEAMS		6	20	25,3481	0,133515	0,80109	20,30611
Radial beams flange 1	CP R-BEAMS		6	10	25,455	0,015783	0,0946974	2,410522
Radial beams flange 2	CP R-BEAMS		6	10	25,455	0,015285	0,0917124	2,334539
Radial beams brackets	CP R-BEAMS		6	10	25,3759	0,002366	0,01419624	0,360242
							1,00169604	25,41141
U tube	CP GANGWAY		1	10	25,2216	0,796249	0,796249	20,08267
Top plate	CP GANGWAY		1	10	25,495	0,401334	0,401334	10,23201
Side beams	CP GANGWAY		2	10	25,47	0,067278	0,1345556	3,427131
Cant beams	CP GANGWAY		10	10	25,4326	0,004435	0,0443467	1,127852
Support brackets	CP GANGWAY		2	12	25,3651	0,003714	0,00742856	0,188426
							1,38391386	35,05809
TOTAL					25,31605		3,66281006	92,72787

Figure 51 Central Access Platform Material

For the central platform of the Semisubmersible structure that allows the access towards the Transition Piece a calculation has been performed and the structural materials were defined. The design was adapted to the manufacturing process and the required changes were implemented with their respective drawings.

2.2.14 Corrosion protection system

A comparison has been analysed for the two corrosion protection principles of sacrificial anodes and Impressed Current Cathodic Protection Systems (ICCP). Therefore a calculation of the Corrosion Protection requirements for the existing submerged surface with different Anodes, and different coated surface areas was undertaken.

HiPRWind						
with coating 8m below sea level						
Design parameters						
Structure	Floating					
Design life	5	years				
Operating area	seawater					
Surface area coated and uncoated						
Surface area underwater uncoated	4460					
Surface area underwater coated	630					
Surface area sea bed uncoated	0					
Anode description						
Anode type	Aluminum					
Aluminum alloy capacity	2000	Amp.hrs/kg				
Utilization Factor	0,9					
Hours per year	8760					
Theoretical Anode consumption	4,38	kg/Ampyr				
System requirements						
Safety factor						
Current densities CD uncoated steel in sea water	DNV RP B401					
Initial CD uncoated part	170	mAmp/m ²	DNV RP B401 Table 10-1			
Mean CD uncoated part	80	mAmp/m ²	DNV RP B401 Table 10-2			
Final CD uncoated part	110	mAmp/m ²	DNV RP B401 Table 10-1			
Seabed part	20	mAmp/m ²				
Calculation for coated steel structures:						
Coating breakdown factor	DNV RP B401 Table 10-4 Coating category III					
Initial CD uncoated part	3	mAmp/m ²	factor a: 0,02	0,02	fc mean:	0,05
Mean CD uncoated part	4	mAmp/m ²	factor b: 0,012	0,012	fc final:	0,08
Final CD uncoated part	9	mAmp/m ²				
Current requirements						
	total for all steel work	coated steel sea water	uncoated steel seawater	uncoated steel sea		
Total initial current required	760,3	758,2	2,1	0	Amp/yr	
Total mean current required	359,3	356,8	2,5	0	Amp/yr	
Total final current required	496,1	490,6	5,5	0	Amp/yr	
Anode calculation based on weight						
Required Aluminium weight:	8743,453	kg	based on mean current requirement			
Suitable anode type	P-900-Al					
Quantity required	97,14948148	pcs				
Total net weight	90	kg				
based on mean current requirement	net Al weight:	8730	kg	total		
	97	pcs rounded				
Anode calculation based on current demand						
Initial Current output per anode	4,19	Amp				
Total current output	758,39	Amp	864,5			
Anodes required for initial output	181,47	pcs				
Anodes required for mean output	85,76	pcs	16290	kg	total	
	181	pcs rounded				
Anode calculation based on time						
Total aluminium anode consumption	3330,30	kg/yr	at initial current requirement			
	1573,82	kg/yr	at mean current requirement			
	2173,11	kg/yr	at final current requirement			
Total anode lifetime	4,89	years	at initial current requirement			
	10,35	years	at mean current requirement			
	7,50	years	at final current requirement			
max 181 pcs rounded						

Figure 52 Sacrificial Anode Calculation

A calculation of the required Sacrificial Anode System was undertaken and compared to the requirements for an ICCP System.

Both systems have certain advantages and disadvantages. Some of the most interesting advantages of the ICCP system are its unchanging properties during the lifetime of the structure, while the Sacrificial Anode System is passively reacting to the conditions acting on the chemical principals; the ICCP is actively controlled and can react to changes in the required power output.

- **Sacrificial Anodes** : $0,3 \sim 0,45 \text{ V} * 2,5 \text{ A} = 0,8 \sim 1,1 \text{ Watt}$
- **ICCP Anode** : $24,0 \text{ V} * 120 \text{ A} = 2880 \text{ Watt}$

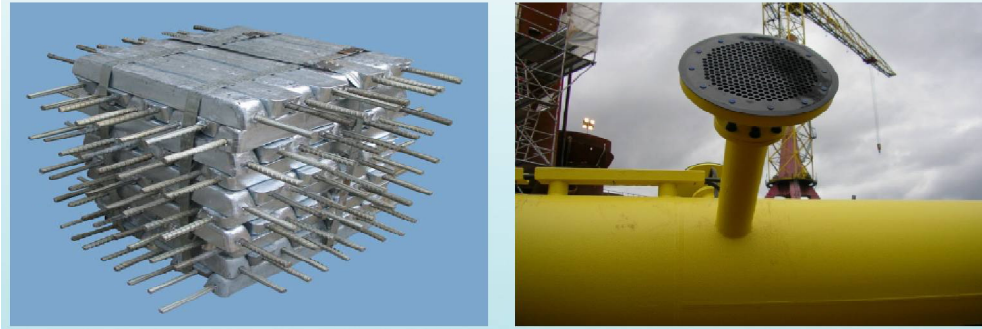


Figure 53 Comparison Sacrificial Anodes and Impressed Current System

In general the ICCP system showed advantages for floating systems with a long operation time. Here the initial purchase cost that is higher for the ICCP system can be compensated by the advantages of the adaptable power output of the system which maintains the system at an optimum protection level, avoiding neither too high current nor too low current. The current demand undergoes certain changes during the lifetime of a structure. In the beginning especially during the initial months, while still Calcium is accumulated on the surface of the structure that will later on protect the surface the current demand is rather high and will then come down to a low level during the main part of the lifetime of the structure until at the end the current demand will rise again due to corrosion effects.

For a lifetime of a structure that exceeds the current 2 years of the HiPRWind project the principal design driver is not the initial current demand, but the lifetime of the anode system and then the size of the anodes needs to be increased significantly and the cost for the additional anode material and for larger fixtures will increase the price for a Sacrificial Anode system considerably and make the ICCP system the preferred choice in spite of additional cost for the current that is required to operate the system.

The ICCP system does need a lot less welding work on the structure. For the surface area of the HiPRWind floating structure a number of less than 21 ICCP Anodes and reference electrodes would have been sufficient to protect the structure, compared to the approximately 167 sacrificial anodes. Since there are so called “shadow areas” where active Anode systems have trouble protecting the surface due to the current distribution in the water towards the structure the final number of anodes and sensors is not entirely depending on the surface area alone, but also on the geometry.

The ICCP system does need some space inside the structure to allocate the control and power system and the remote control needs to be connected to the communication equipment to be able to remotely monitor the parameters and to survey the correct operation of the system. Since there is usually plenty of space in the floating structures that can be used for the location of the equipment this is not an important design criterion.

The active anodes will have to be connected to those cabinets by cables which need to be routed either in the interior of the structure or on the outside. Both cable routes require some additional welding work to attach the cable trays and the protective systems, which should not be neglected in the comparison of the two systems. Especially if the cables are routed on the outside special care has to be taken to protect the cable from wave forces and fatigue loads to avoid system failure. If the cables are routed on the inside of the structure special care needs to be taken to make the protrusion of the cables through bulkheads watertight, this might imply additional cost to the system.

But, since for the current project only a limited time of depletion is foreseen, the financial disadvantages for such a short period depletion and the high operational costs during the initial phase of the depletion led to a sacrificial anode solution. Therefore a conventional sacrificial anode system was designed.

The conventional anode system made from Aluminum sacrificial anodes underlies certain design criteria which do differ a little depending on which design rules will be applied.

The most common rules and guidelines were taken into account for the design of the corrosion protection system considering different painting schemes.

Due to the limited lifetime of the project the main design driver was not the lifetime of the anodes, but the initial current demand. This translates in small anodes, with a high required surface area, resulting in a lot of anodes evenly spread over wide areas of the surface of all members of the structure to protect the complete structure. This requires the installation of the anodes over a wide variety of altitudes or during an early stage of production to avoid welding operations at height during later assembly stages. This will be limited though due to lifting related restrictions and depend on the lifting procedures for certain subassemblies.

2.2.15 Mooring

A final mooring configuration has been designed. An analysis of bathymetry and geophysical studies was combined with the calculations considering the requirements for the design. A simulation model was created in SIMO-RIFLEX. 1st order load transfer functions were calculated in WADAM. The results were checked versus Diodore, Wamit, and the tank testing.

A Turbulent wind model based on onshore turbine loads was assumed. Constant current all over the depth was chosen as a conservative approach. A fully coupled dynamic mooring line was assumed.

Full QTF (Quadratic Transfer Function) calculations were performed and checked with tank testing, in order to take into account the second order forces in the mooring lines. Heave plates quadratic damping for heave and pitch was based again on the tank testing results. The hydrodynamic loads for the Mooring were based on Morison elements. 12 Load-cases were tested with 3h simulations, making 5 different simulations for each load case using different seeds in the generation of waves.

For the design also the defect of one mooring line was investigated and the maximum tension in line 3 was determined to be 3086kN for this extreme case.

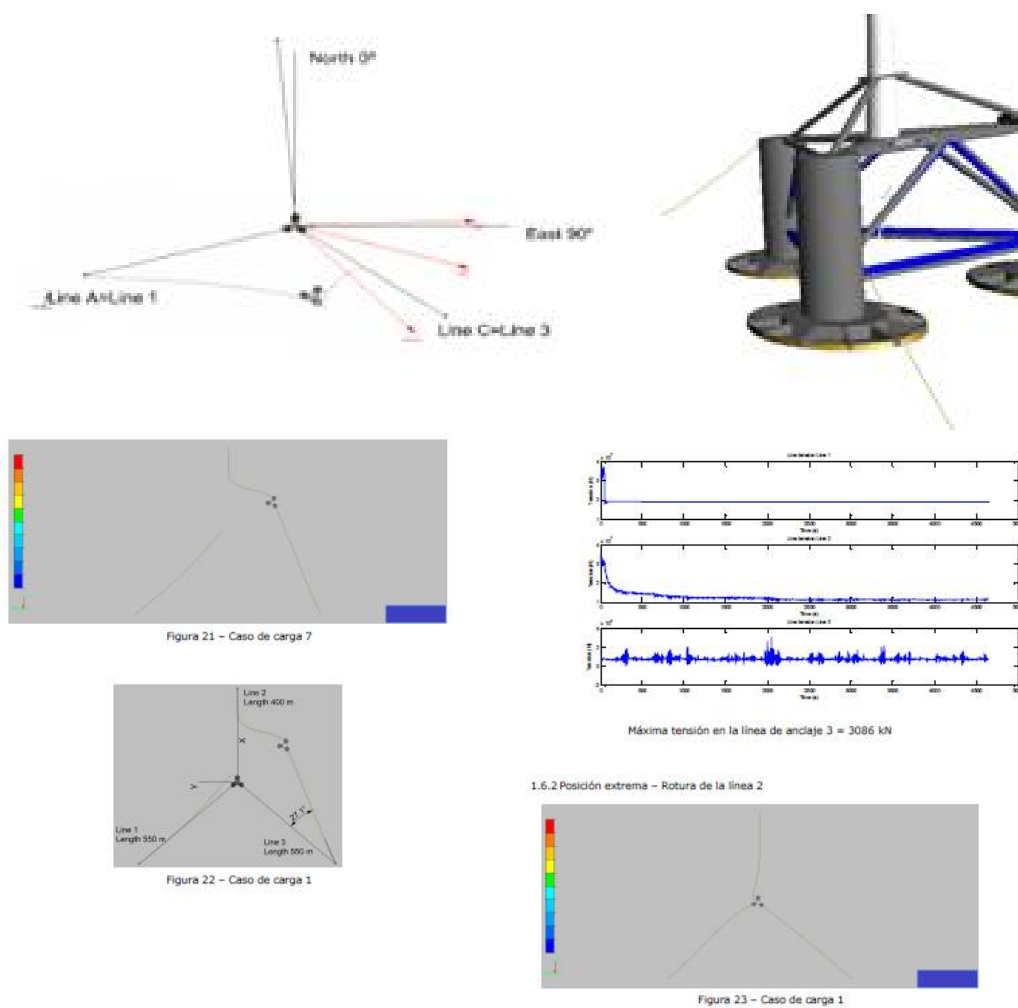


Figure 54 Simulations for defect in one mooring line

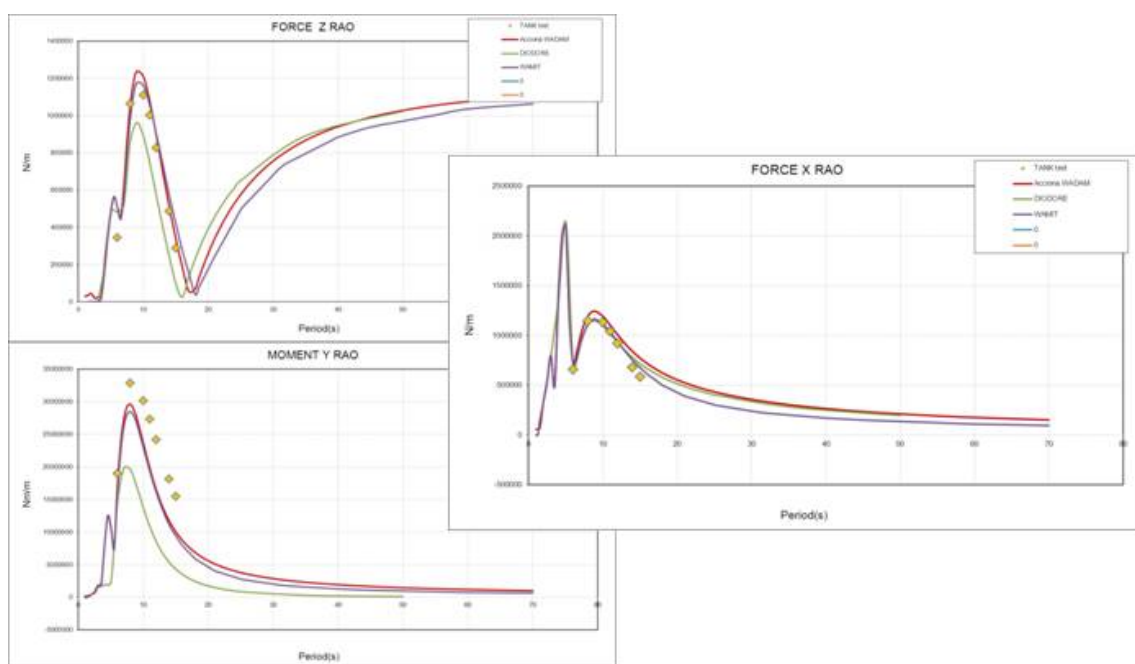


Figure 55 Tanks test comparison to numerical model

A tank test has been performed by Acciona Energía, using non-HiPRWind resources, in order to be able to verify several aspects of the mooring configuration. The numerical model was confirmed with such tank test. The Captive Model Test was compared against the Potential Code.

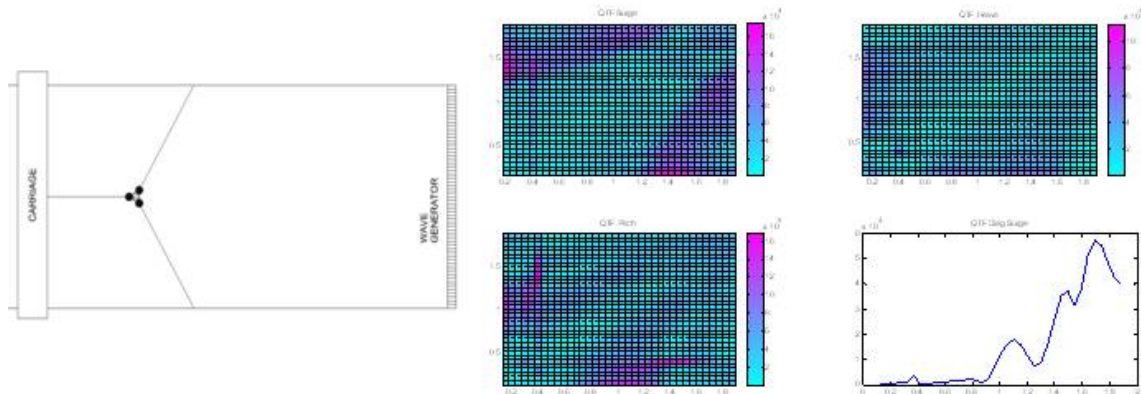


Figure 56 Tank test configuration and QTF results

The QTF diagonal term was used to determine the drift forces required for the mooring design. A fatigue analysis has been performed for the chain that will be shown in the following calculation in 2.2.15.2.

Annual partial damage for the chain connections has been analyzed and a design life of 20 years was confirmed. A Geotechnical study including 3 field surveys (Detailed bathymetry, Geophysics, Magnetometry) were performed by Acciona Energía using non-HiPRWind resources. Results from those field surveys and data were used for the final mooring design and anchoring definition:

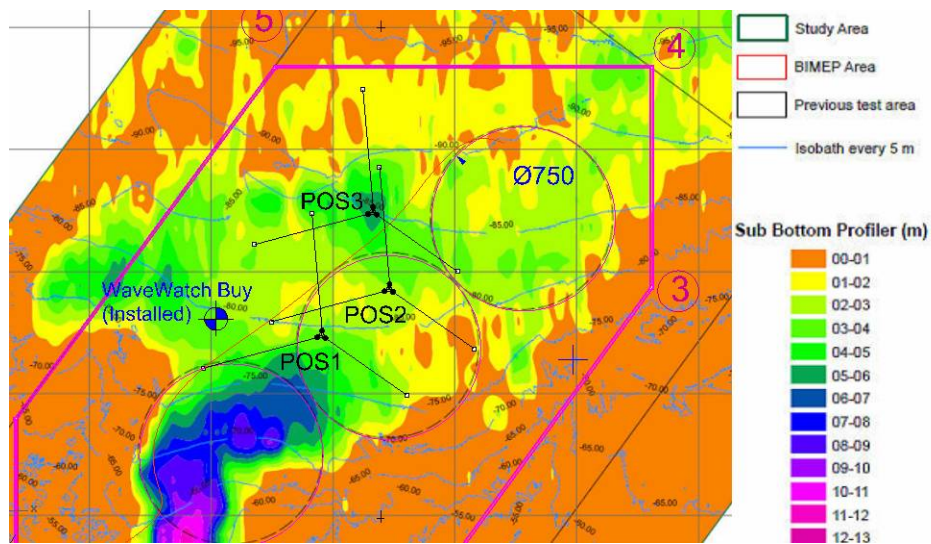


Figure 57 GIS with bathymetry of BIMEP area

3 Alternatives for the positioning of the structure were studied. The installation procedure for the anchors and the mooring depend very much on the ground conditions encountered at the site. Different scenarios were investigated to define the most suitable solution considering all the involved parameters. Compare also with 2.2.15.2

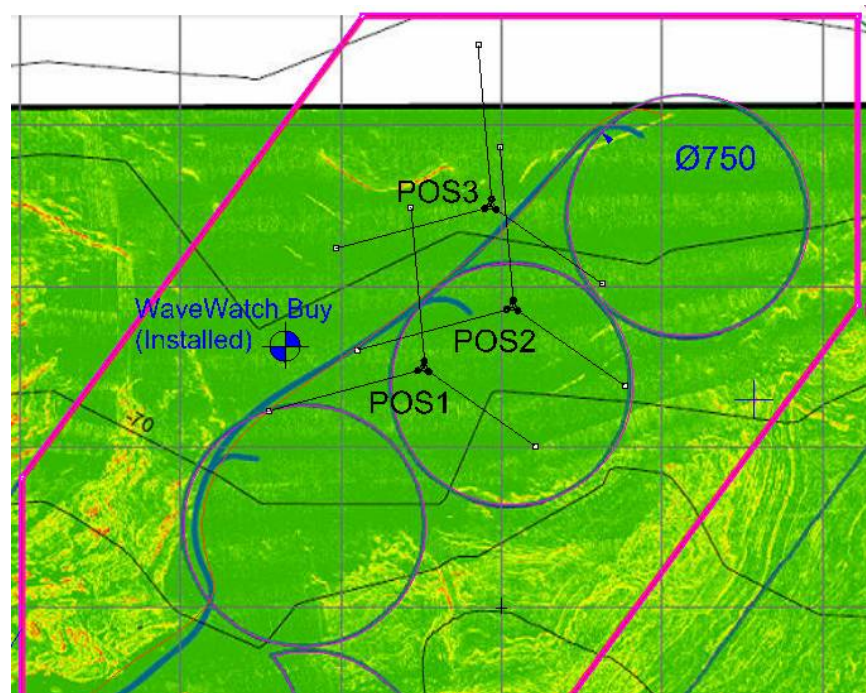


Figure 58 Slopes in the area of depletion

Finally the preferred position will be POS1 with a Medium depth range of 80 meters [75-85m] and a sand layer thickness of 3-4 m at the anchors with the highest load.

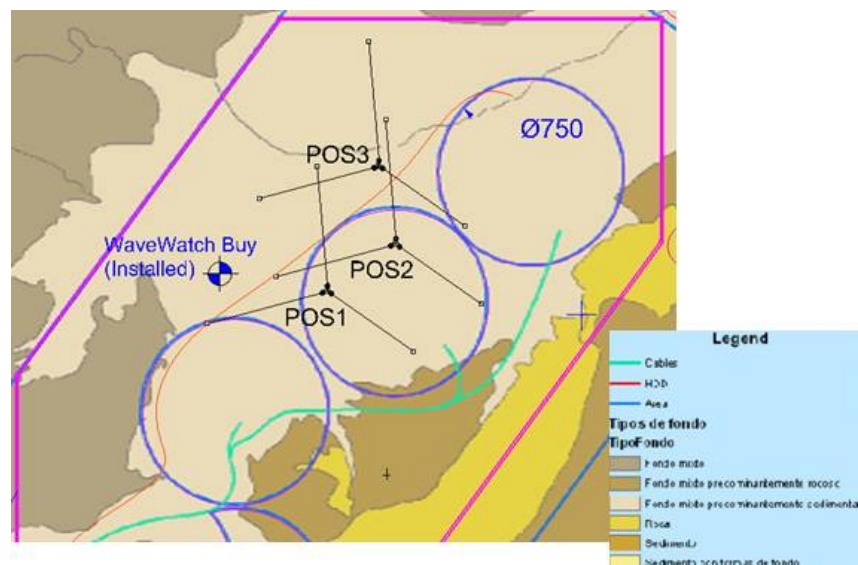


Figure 59 Seabed composition, sediment structure

Time-domain simulation for hooking-up the third mooring line has been evaluated. Compare also with 2.2.15.1.

2.2.15.1 Mooring installation

The final design for the fairleads for the mooring arrangement has been designed. The following concept was chosen on the third column to allow for the tensioning of the third chain and to enable the installation. The following sequence was used for the design of the mooring fixation equipment and the required appurtenances for the installation of the mooring chains. Three short chain segments are fixed

to the structure and will be transported during the towing on board of the floating structure. Their ends are sustained so that they can easily be picked up by the installation vessel.

The three main lines are fixed to their anchors and left with buoys that keep the ends afloat. The chain sections attached to the buoys are marked red in the respective following figures.



Figure 60 Constellation at arrival of floater on site

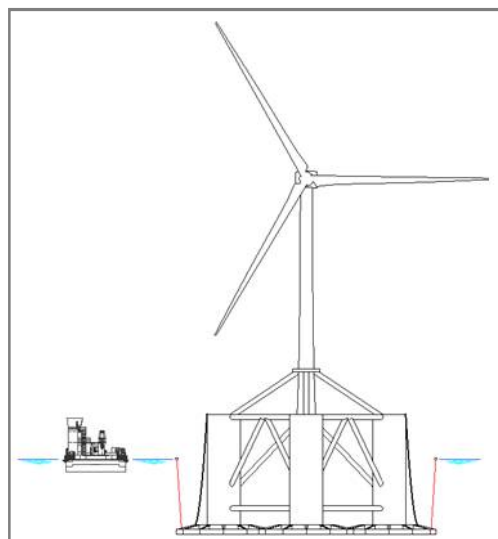


Figure 61 Preinstalled chain segments, red part buoy sustained

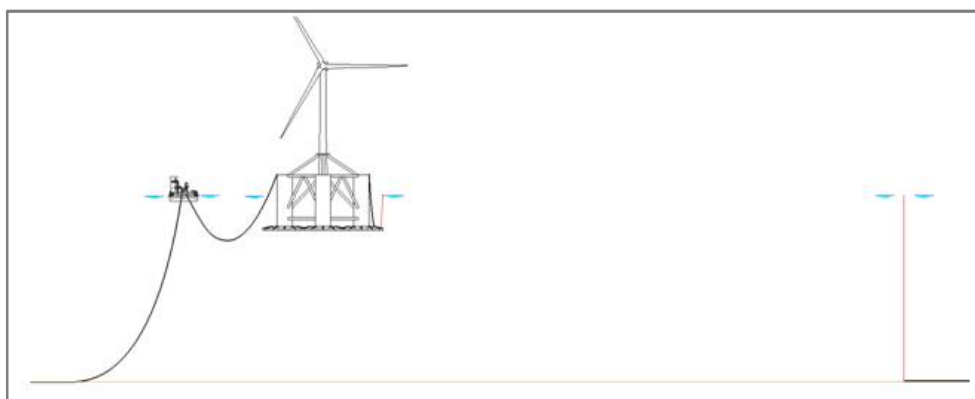


Figure 62 Connection operation first line

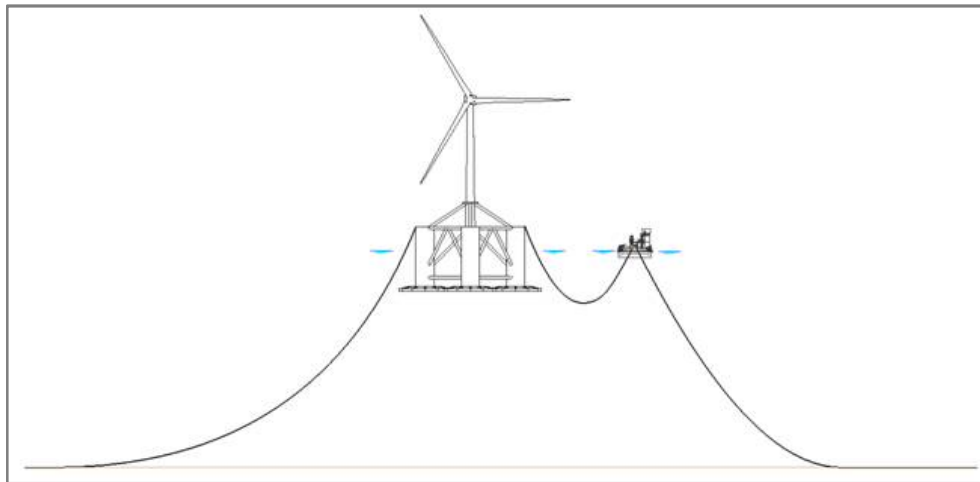


Figure 63 Connection operation second line

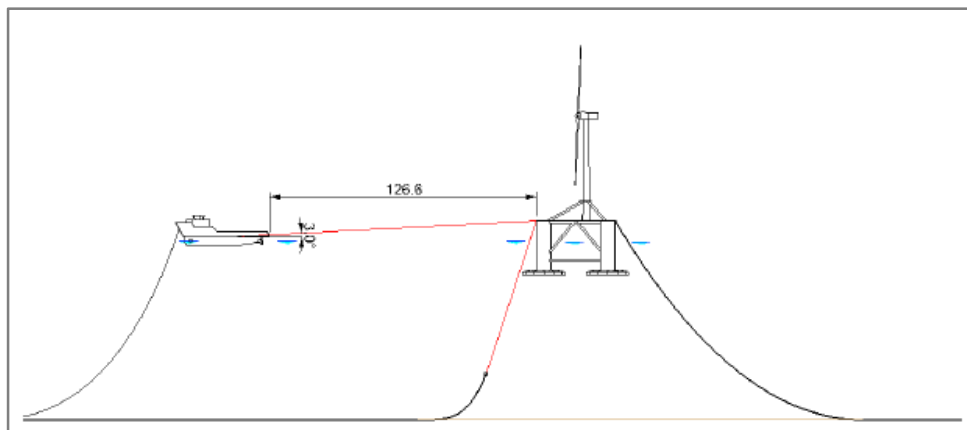


Figure 64 Start connection operation third line

It can be appreciated how the first anchoring line can be attached rather easily bringing the structure alongside the first chain. The second one can also be connected without mayor problems as there is still limited force on the mooring line. Only for the third line the tension rises to a level that makes it difficult to attach the structure towing it into final position, since the weight of the chain will drag the buoy into a position that cannot be reached pulling the structure. A sheave solution that allows pulling the third line into position while the installation vessel will be anchored has been developed.

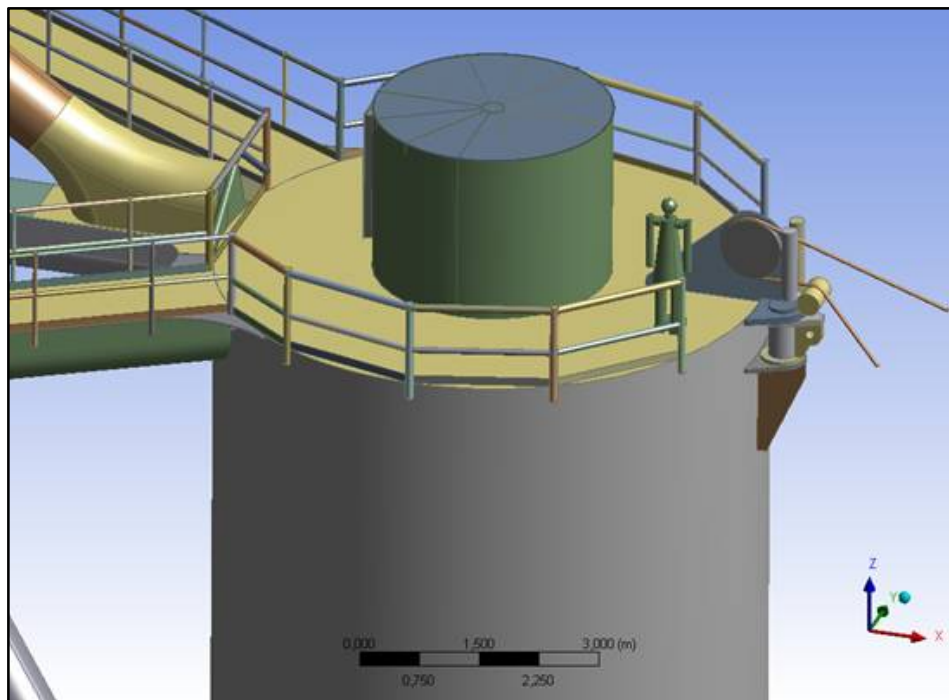


Figure 65 Mooring line fixture and tensioning detail of CAD model

In the drawing above the method on how to connect the third mooring line can be seen. Since the use of a second tug to achieve the pre-tensioning is rather expensive a way was sought and found to achieve the attachment of the mooring line with a winch that is installed on the same vessel that picks up the mooring lines for connection toward the structure. There is the need to have some sheave plate on top of the structure to be able to achieve the necessary tensioning of the third mooring line. The pre-tensioned chain is then after being connected to the Mooring pad eye released into the final constellation.

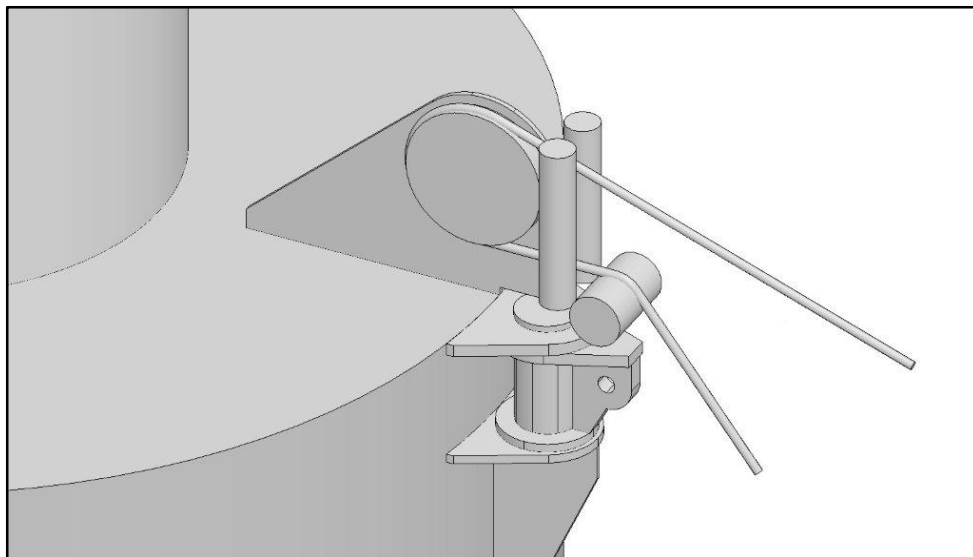


Figure 66 Mooring line fairlead

The connection point for the mooring chain can be seen below the roller with 300mm diameter.

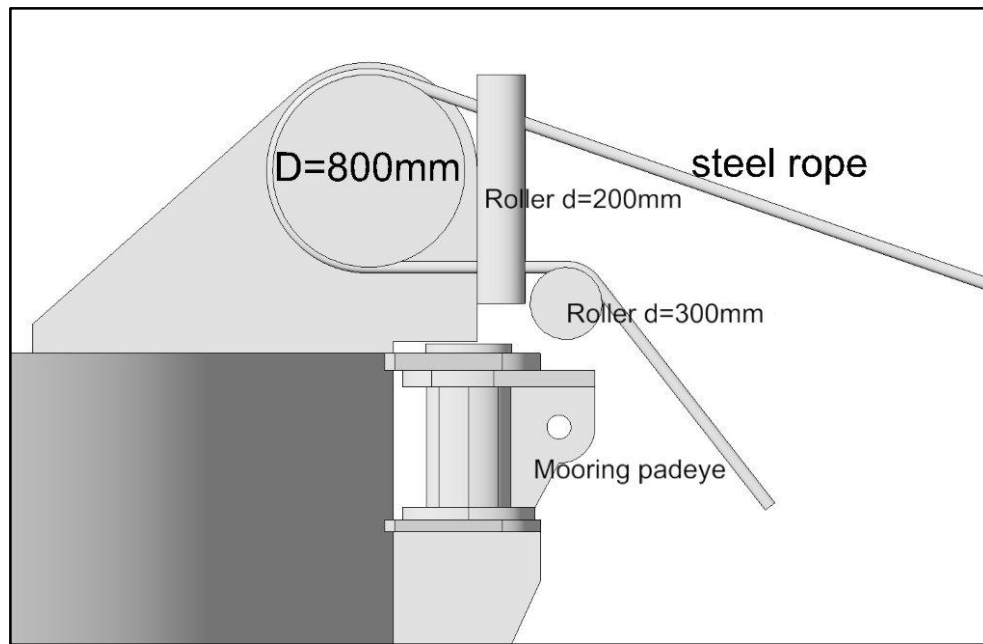


Figure 67 Third Mooring line tensioning roller

For the connection operation a complete design was necessary with the complete procedure defined.

The modeling and design for the mooring line tensioning equipment was finished after several iterations to reduce unwanted forces and also taking the manufacturing process and related restrictions into account.

2.2.15.2 Calculations for the Mooring chains

The mooring system will keep the position of the FWT in an average 80 meters water depth. The mooring system consists of 3 mooring lines (catenary type) none equally spread. Each line is composed of a combination of 84 mm and 92 mm grade R5, drag anchors and proper accessories to provide connection between different components of the moorings and the structure. The mooring lines are split in two parts of different chain sizes, the bottom chain being 92 mm diameter and the upper (catenary) chain being of 84 mm diameter. The connection points between the moorings and the structure (namely fairleads), are set at the top of each column, 10m above the mean sea level (MSL). Next figure shows a top view of the arrangement of the spread mooring system, including heading angles of the mooring lines, lengths of chain segments, and the position of the fairleads and anchors in a local rectangular coordinate system.

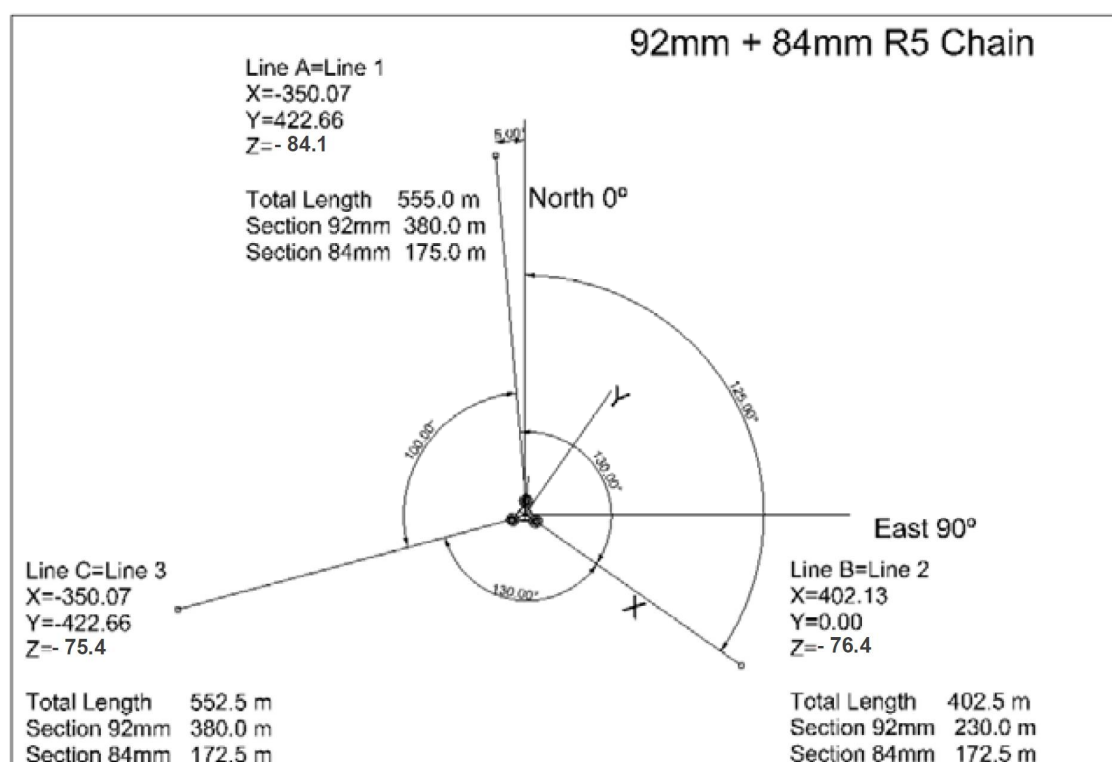


Figure 68 Chain characteristics

Next table resumes the position of the fairleads and anchors in the local coordinate system.

Table 8: Fairlead and anchor points in local coordinates frame for averaged position

	Fairlead			Anchor		
	X	Y	Z	X	Y	Z
Line 1	-12,353	20,18	10	-350,1	422,7	-84,1
Line 2	23,71	0	10	402,1	0	-76,4
Line 3	-12,35	-20,18	10	-350,1	-422,7	-75,4

The following table resumes the characteristics of the chains:

Table 9: 84mm and 92mm chain characteristics

Type	Studless	Studless
Diameter (mm)	84	92
Grade	R5	R5
Weight in air (Kg/m)	141.12	170.53
Weight in water (Kg/m)	122.69	148.26
Proof Load (KN)	5866	6916
MBL (KN)	8418	9924

2.2.15.2.1 Design Premises

The design life of the structure is assumed to be 2 years. A safety factor of 10 on fatigue is required by Bureau Veritas (BV), for a minimum required fatigue life of 20 years.

Design Environmental Conditions

The following tables show the probability of occurrence of all sea states according to their significant wave heights, peak periods and wind speeds in the wind turbine installation area, taking into account the misalignment between wind and waves. See [12].

Table 10: Load cases and probability of occurrence

Windspeed	Hs (m)	Tp (s)	Misalignment (deg)	Num Points	P(dir=300)	P(dir=330)	P(dir=0)	Total
v0-3	1.99	10.52	50.9	87215	59.5%	29.7%	9.7%	98.9%
v3-5	2.08	10.49	49.6	125851	58.4%	30.5%	9.9%	98.8%
v5-7	2.26	10.55	48.4	121392	59.5%	28.9%	9.6%	98.0%
v7-9	2.54	10.61	46.8	89807	61.7%	27.6%	7.5%	96.8%
v9-11	2.92	10.70	44.1	54062	66.6%	25.7%	3.6%	95.9%
v11-13	3.93	10.87	41.7	30826	68.3%	26.8%	1.7%	96.8%
v13-15	3.86	11.07	37.1	17072	64.4%	32.9%	0.6%	97.9%
v15-17	4.42	11.45	33.5	9261	59.7%	39.1%	0.2%	99.0%
v17-19	4.96	11.88	30.7	4647	54.1%	45.4%	0.0%	99.5%
v19-21	5.65	12.66	29.4	1789	54.3%	45.2%	0.0%	99.6%
v21-23	6.37	13.43	29.1	595	56.1%	43.0%	0.0%	99.2%
v23-25	7.15	14.25	29.5	171	56.1%	43.9%	0.0%	100.0%
v25-30	8.02	14.57	28.4	72	48.6%	51.4%	0.0%	100.0%

Wind Speed Bin	Hs1 (m)	Tp1 (s)	Probability Hs1, Tp1	Hs2 (m)	Tp2 (s)	Probability Hs2, Tp2	Hs3 (m)	Tp3 (s)	Probability Hs3, Tp3
v0-3	1.42	8.97	39.04%	1.96	11.45	47.30%	2.78	13.35	13.66%
v3-5	1.48	8.85	39.32%	2.03	11.48	45.33%	2.85	13.38	15.35%
v5-7	1.58	8.76	37.57%	2.16	11.52	43.79%	3.01	13.45	18.63%
v7-9	1.77	8.71	36.85%	2.38	11.52	41.07%	3.29	13.54	22.08%
v9-11	2.03	8.75	36.19%	2.76	11.51	38.79%	3.67	13.61	25.02%
v11-13	2.33	8.91	34.57%	3.15	11.51	38.39%	4.18	13.72	26.33%
v13-15	2.69	9.08	32.19%	3.55	11.49	39.93%	4.74	13.83	27.89%
v15-17	3.01	9.22	25.54%	4.02	11.52	40.33%	5.24	13.87	34.13%
v17-19	3.32	9.37	18.79%	4.43	11.58	38.99%	5.65	13.88	42.22%
v19-21	3.94	10.22	20.46%	5.24	12.49	41.53%	6.45	14.78	38.01%
v21-23	4.69	11.13	23.87%	6.01	13.44	40.84%	7.30	15.61	35.29%
v23-25	5.24	12.19	26.90%	7.29	11.76	43.27%	7.96	16.19	29.82%
v25-30	5.03	9.00	31.94%	7.85	12.00	45.83%	8.81	17.00	22.22%

The scatter diagram table of the load case document [7] has been taken for the analysis of fatigue of the mooring system. This document presents the Hs and Tp values for each wind speed along with data on the probability of occurrence of the directional distribution of sea states from various wave directions. The scatter tables were split to obtain three damage equivalent Hs and Tp pairs. The current is supposed constant with a value of 1m/s going from west to east in all the load cases proposed. The value of the current was taken into account in order to provide a conservative design method because this value corresponds to a value of almost a return period of about 10 years. The wind velocity taken into account in the load cases definition is the maximum wind speed of each wind speed bin. Quadratic drag coefficients explained in the BV mooring verification document [13] are used for each bin of wind. Those coefficients take into account the forces and moment from the wind turbine and from the floater above MSL, the drag coefficients take into account the high peak forces at around 11m/s and the “grid loss” of the machine at 25m/s. The following wind coefficients have been taken into account for each load case:

Table 11: Velocity coefficients of wind turbine

Bins	Velocity Coefficients
Vel. 0-13m/s	11 m/s
Vel. 13-17m/s	15 m/s
Vel. 17-19m/s	18 m/s
Vel. 19-23m/s	22 m/s
Vel. 23-30m/s	25 m/s

Finally, 117 load cases have been defined for the fatigue study of the mooring system. These sea states are described in [7].

2.2.15.2.2 Fatigue Methodology

A model of the floater and mooring lines has been built up in the time domain software OrcaFlex. The hydrodynamic behavior of the floater is driven by the hydrodynamic database described in document in [6], mainly Response Amplitude Operators (RAOs), Inertias, Added Mass, Damping, Quadratic Transfer functions (Newman's approximation), Wind and Current coefficients.

The mooring lines are modeled based on concentrated masses method, which simplifies the mathematical formulation and allows rapid and efficient development of the program to include additional terms of strength and system constraints. The lines are segmented and represented as mass points with linear spring to represent the axial and bending stiffness. Hydrodynamic loads in the moorings are modeled using the extended form of the Morison equation with the coefficients defined by the user. The 117 sea states have been run during 3 hours in the time domain.

The environment is introduced using Jonswap spectrum to represent the behavior of waves, API spectrum for wind at different speeds. The current is supposed constant in all the load cases. The fatigue life of the mooring system is computed by calculating the cumulative damage produced by the stresses incurred in each sea state.

The tensions obtained in lines for each sea state are separated in ranges of tensions using rainflow half-cycle method. This method separates the tension results of each line in ranges of tension of a half cycle for a simulation of three hours. Then, the damage caused by each half cycle is calculated through the rule of Palmgreen-Miner. This gives the value of damage to the designated load case, which is scaled to the total exposure time of the sea state. These damages will be called "partial damages" and include the probability of occurrence of each sea state.

Once done, the partial damage values of total load cases are summed to give the overall total damage per year. So, once calculated this value, the fatigue life is obtained calculating the inverse of the total annual damage.

The T-N fatigue curve for studless chains in Ref. [8] is considered to calculate the damage that each sea state will causes in each line.

$$N \cdot R^m = K$$

Where:

m= 3

K= 316

N: number of cycles to failure

R: ratio of tension range (double amplitude) to minimum breaking load

m: slope of the T-N curve. m = 3 (studless chain)

K: Intercept of the T-N the curve. K = 316 (studless chain)

The effect of corrosion is taken into account considering the corroded chain diameter at midlife. Considering a corrosion/wear rate of 0.4 mm/year in diameter, the loss of diameter after 1 year is $0.4 \times 1 = 0.4$ mm. Thus the MBL used are the ones corresponding to 91.6 mm and 83.6 mm chains which are 6492 kN and 5502 kN respectively.

2.2.15.2.3 RESULTS

The fatigue life is computed for all the chain segments along the lines using the method of counting rainflow cycles, which has been discussed in section 2.2.15.2.2. There are however two locations of interest, the connection points between lines and structure, and the connection point between chains. The following tables show the annual total damages and the associated fatigue lives of the chains at these two locations.

Connection between chains.

Table 12: Annual damages and fatigue lives at connection between chains.

Line number	Total Annual Damage	Life (years)	Life after SF=10 (years)
1	0.00482	207.29	20.7
2	0.00105	945.89	94.5
3	0.02327	43	4.3

Connection between lines and structure.

Table 13: Annual damage and fatigue life at connection between lines and structure.

Line number	Total Annual Damage	Life (years)	Life after SF=10 (years)
1	0.00408	244.7	24.47
2	0.00102	984.1	98.4
3	0.0206	48.50	4.85

Based on the above the minimum fatigue life computed is 43 years in Line 3, which is higher than the minimum required life of 20 years. Therefore the chains fulfill the fatigue life requirement. It is obtained that the fatigue damage at the connection between chains is higher than the fatigue damages at the fairleads. However highest peak tensions are obtained at the fairleads. The connectors final design will be defined when the installation procedure and the boats to do the operations will be defined. This is done because it is possible that the mooring lines will have to be divided into different parts, but this is still not known. When the number and the type of the connectors will be defined, a separate FEA study for each connector will be done. The connectors will be manufactured in R5 and are oversized to withstand higher loads than the MBL of the chain.

The following graphs show the partial annual damage caused by each sea state at the connection between chains.

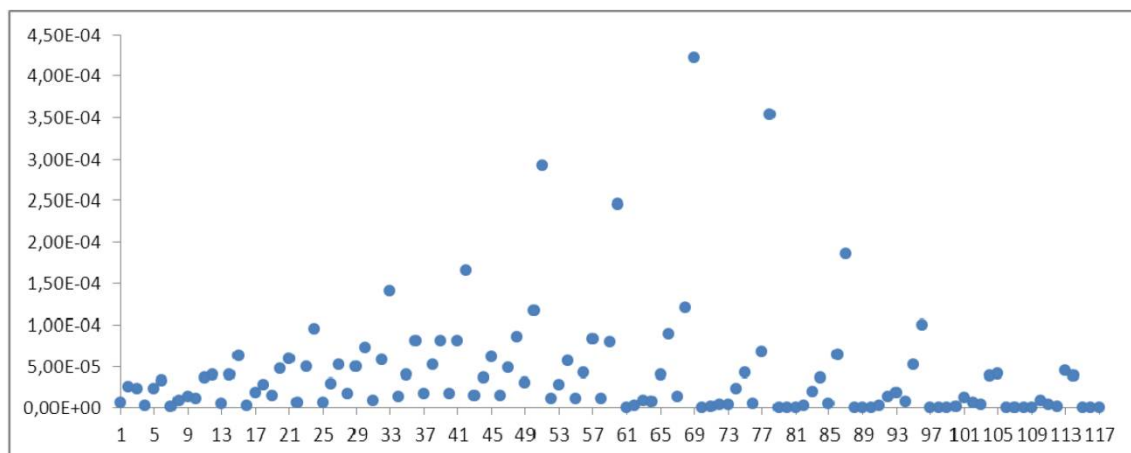


Figure 69 Annual partial damages at connection between chains. Line 1.

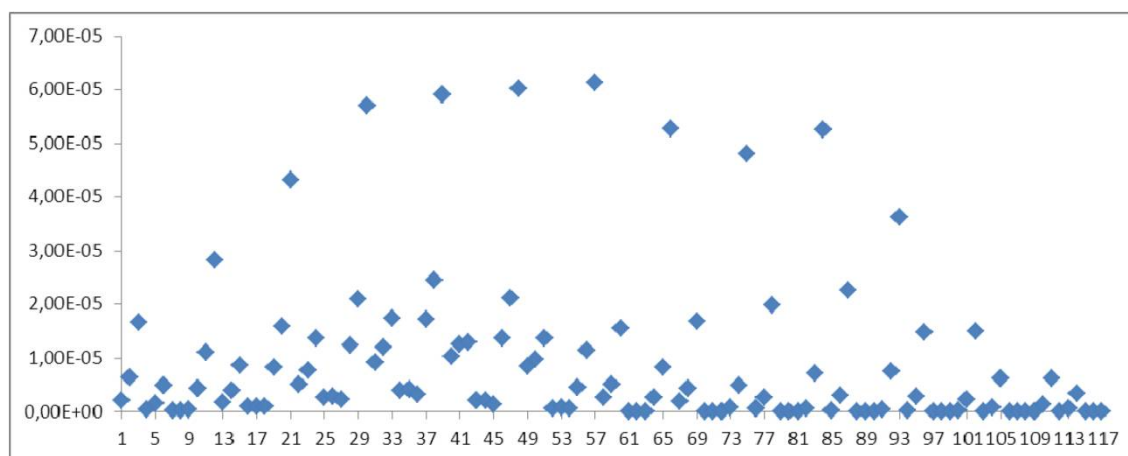


Figure 70 Annual partial damages at connection between chains. Line 2

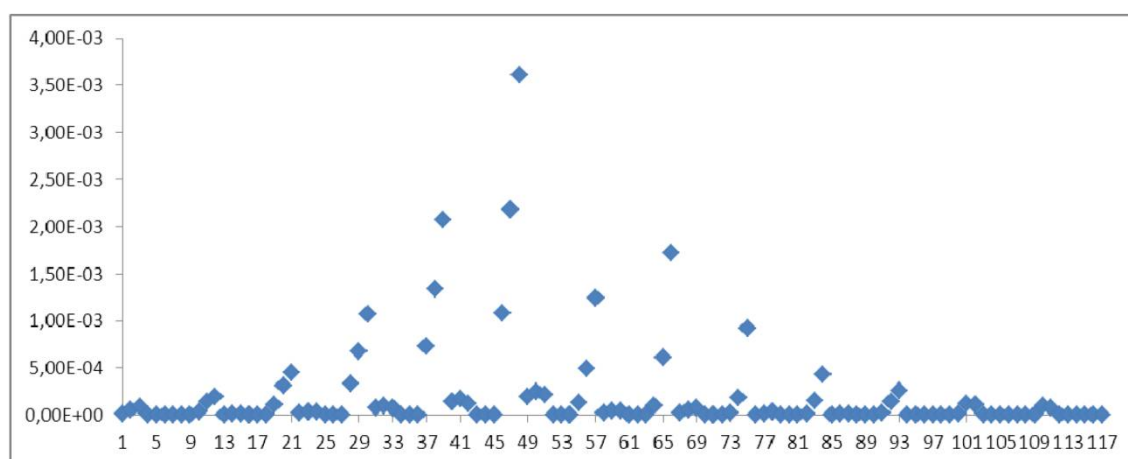


Figure 71 Annual partial damages at connection between chains. Line 3.

The following table shows the sea states that contribute with the largest damages.

Table 14: Largest partial damages at connection between chains.

Line #	Seastate #	Hs (m)	Tp (s)	Wind speed (m/s)	Misalignment (degree)	Annual exposure time (hours)	Partial damage
1	69	5.24	13.87	17	330	20.14	4.22E-4
2	57	4.74	13.83	15	300	50.54	6.14E-5
3	48	4.18	13.72	13	300	93.09	3.61E-3

The following graphs show the partial annual damage caused by each sea state at the connection between lines and structure.

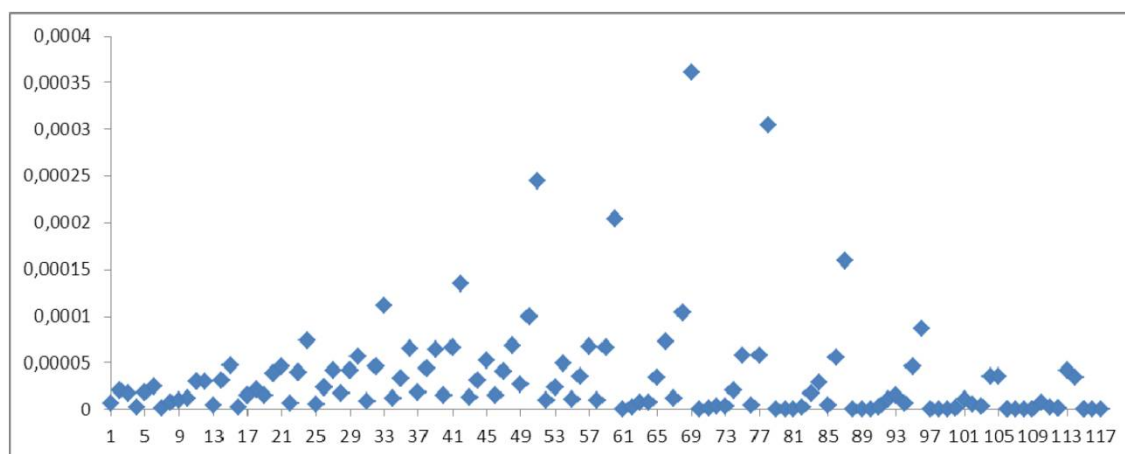


Figure 72 Annual partial damages at connection between structure and line 1.

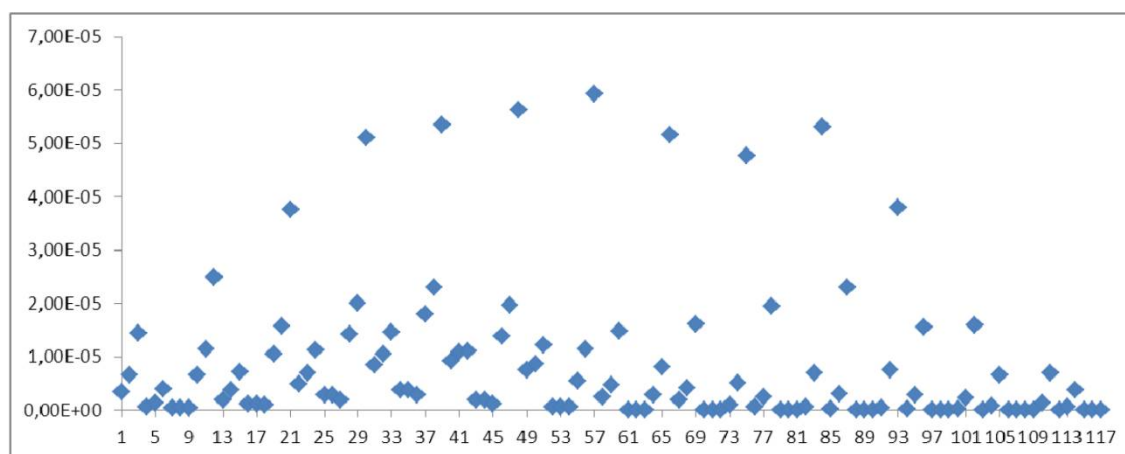


Figure 73 Annual partial damages at connection between structure and line 2.

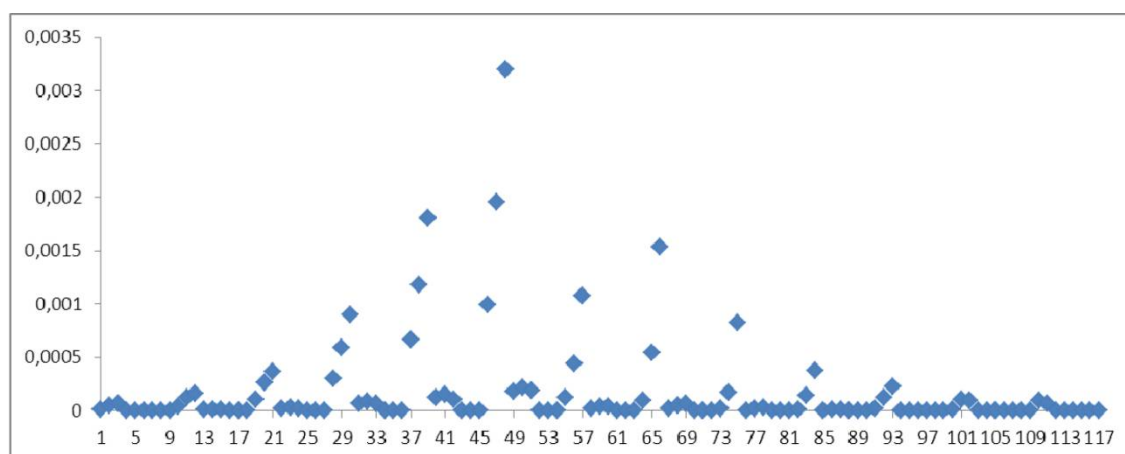


Figure 74 Annual partial damages at connection between structure and line 3.

The following table shows the sea states that contribute with the largest damages.

Table 15: Largest partial damages at connection lines and structure.

Line #	Seastate #	Hs (m)	Tp (s)	Wind speed (m/s)	Misalignment (degree)	Annual exposure time (hours)	Partial damage
1	69	5.24	13.87	17	330	20.14	3.61E-4
2	57	4.74	13.83	15	300	50.54	5.94E-5
3	48	4.18	13.72	13	300	93.09	3.19E-3

Fatigue Damage to Mooring lines

The tables in **Error! Reference source not found.** show the annual partial damages in each line at the fairlead and the connection between chains where higher damages occur.

The following tables show the peak tensions in each line at the fairlead and the connection between chains.

2.2.15.2.4 Conclusions

Based on the analyses carried out, the following conclusions can be achieved:

- The chains of the mooring system of the HiPRWind floating wind turbine fulfill the fatigue life requirement of 20 years, being the minimum fatigue life computed 43 years.
- The highest fatigue damage occurs at the connection between chains in line #3, close to the touchdown point, and not at the fairlead point where highest tensions occur.
- Sea state #48 is the one that contributes with the largest damage to line #3.

2.2.16 Towing

For the Towing operation available vessels and configurations for the towing were investigated and the complete towing for the trajectory from the site of manufacturing towards the site of implementation was investigated and the ports of refuge were determined as well as the met-ocean conditions for the trajectory during the year.

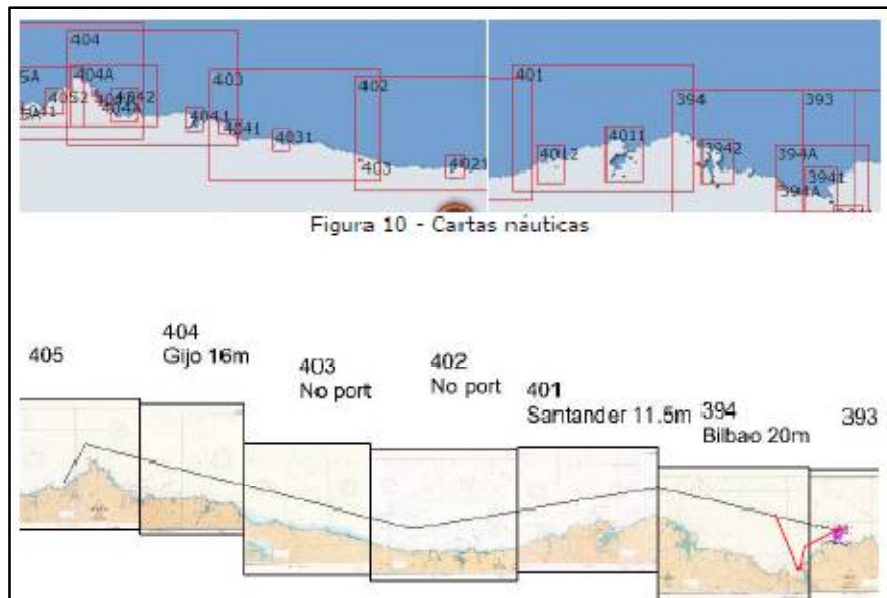


Figure 75 Route for towing operation

The respective scenarios for towing were established and the required marine operations for the ballasting operations were considered. The required coastal towing requirements according to DNV standards were considered as well as the contingency times for the weather windows to reach a port of

refuge. The BIMEP conditions turned out to be more severe than those stated in the DNV standard and needed to be considered for the towing speed and the respective required tugs.

	Rango de velocidades (nudos)	Distancia en remolque (millas náuticas)	Distancia en barcaza (millas náuticas)	Puesta a flote (horas)	Tiempo de traslado total
Alternativa 1	3,0 – 3,5	140	0	0	2 + [2] días
Alternativa 2	5,0 – 6,0	8	137	5	1,5 + [2] días

Figure 76 Calculations for alternative towing scenarios

For the Towing operation towing brackets were designed that allow the attachment of the towing lines. Tank tests have been undertaken by Acciona Energía, using non-HiPRWind resources in order to compare different towing speeds, drag forces of the structure and stability and sea state limits.

			BF2	BF4	BF6	BF8
Draft	Wind	m/s	3	8	13.5	20
	Hs	m	0.25	1.25	4	6.5
	Speed	kts	3.5	3.5	3	3
	Total Hydrodynamic Resistance	kN	739	739	543	543
	Wind resistance	kN	1.4	9.9	28.4	62.4
	Wave resistance	kN	2.6	13.1	42.0	68.3
	TOTAL resistance	kN	743	762	613	674
	Total Hydrodynamic Resistance	kN	630	630	463	463
	Wind resistance	kN	1.8	12.9	36.9	81.1
	Wave resistance	kN	2.6	13.1	42.0	68.3
	TOTAL resistance	kN	635	656	542	612

Figure 77 Towing speeds for different drafts and wind speeds

The towing bracket is located on the column wall above the transit water surface. In the proposal the bracket is positioned 17,5m above keel, 2m above operating WL. However, the final vertical position will have to be decided by the towing contractor. Positions can be selected coinciding with ring stiffeners as explained below. Compare with Figure 79. These positions are: (9,5m * 11,5m * 15,5m * 17,5m * 21,5m)

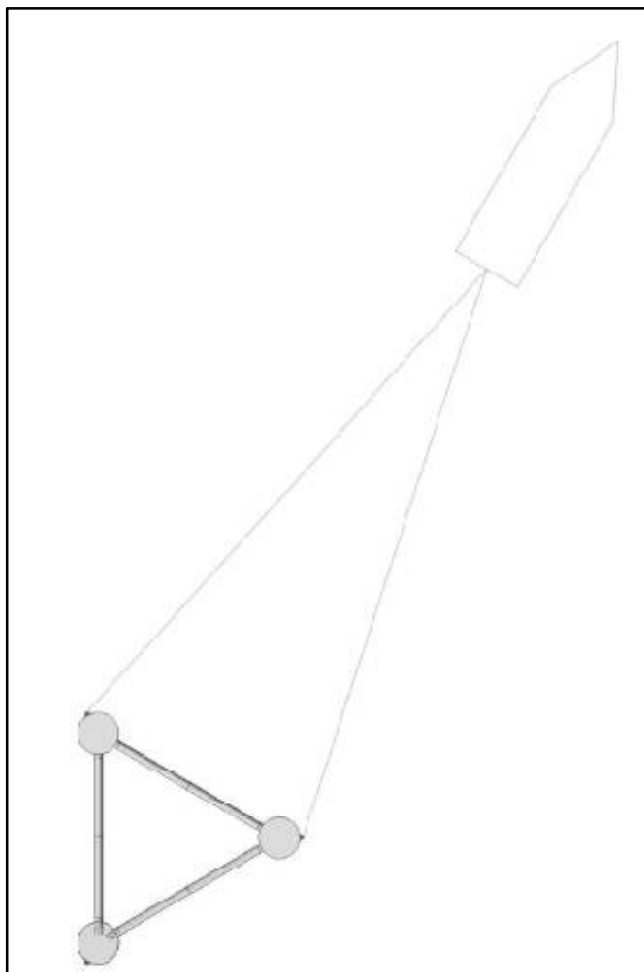


Figure 78 Towing arrangement

To obtain a simple solution, the towing bracket is located in the crossing point of a ring stiffener and the bulkhead.

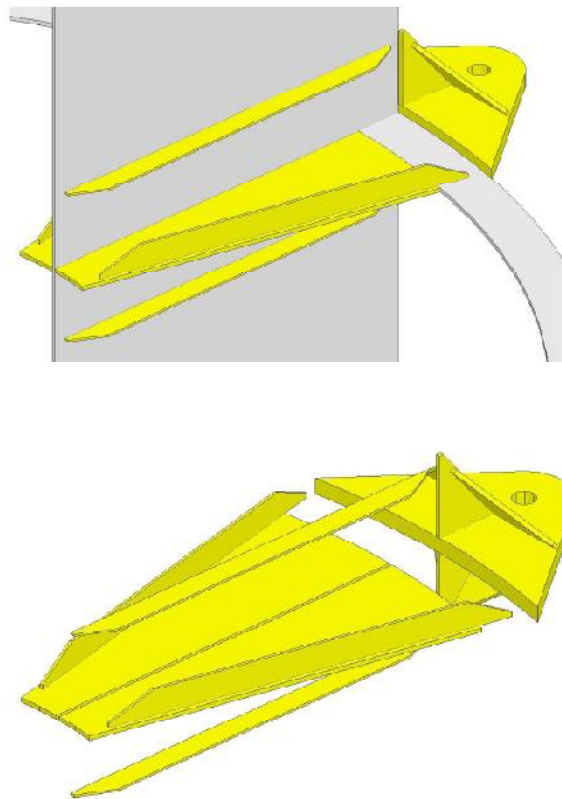


Figure 79 Towing bracket components

With a towing force in radial direction the load is transferred mainly to the bulkhead. With the load in transverse direction (< 90 degrees) a moment is created which is counteracted by the internal web plate which transfers a reaction force to inner column wall. The bracket is arranged in the horizontal plane, with a shackle which can rotate ± 90 degrees from the radial direction. The transverse direction can be related to a bridle arrangement as illustrated in Figure 78 Towing arrangement. The transfer of loads from the bracket through the shell and to the internal structure requires full penetration welds.

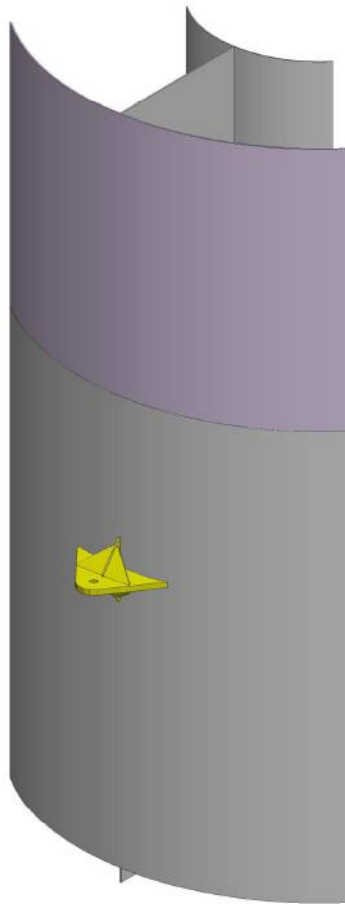


Figure 80 Towing bracket integrated in column wall at height of ring stiffener

The bracket is arranged in the horizontal direction. However the towing load direction can be out of horizontal plane due to the level difference of the towing bracket and the tug deck. Pitch and heel angles may also contribute to the out of plane load direction. In the design an angle of ± 4.5 degree has been applied.

According to the final constellation of the marine operation and the vessel that will be chosen as tug, the design will have to be checked once more to verify, that the assumed angles chosen do reflect the real towing situation and that the brackets will therefore be suitable. In general it can be assumed that even in the unlikely case that the angle is bigger than assumed, the towing bracket can then be located in the crossing point of a ring stiffener and the bulkhead at a different height to limit the angle again without major inconveniences.

2.2.17 Dynamic CABLE

The HiPRWind Deliverable D1.2 Dynamic Cable Design deals with the final design of the dynamic cable. Apart from this a preliminary dynamic cable analysis has been performed to estimate the effects on the structural design of the floating platform with different layout configurations. This was done in order to estimate the loads and feasibility of all these configurations and to be able to deduce the structural components that would be required for their installation. Also to be able to guarantee the secure fixture of the cable on the floating platform and to avoid damage caused by fatigue due to wave forces on the cable and on the fixation of the cable at the floating platform.

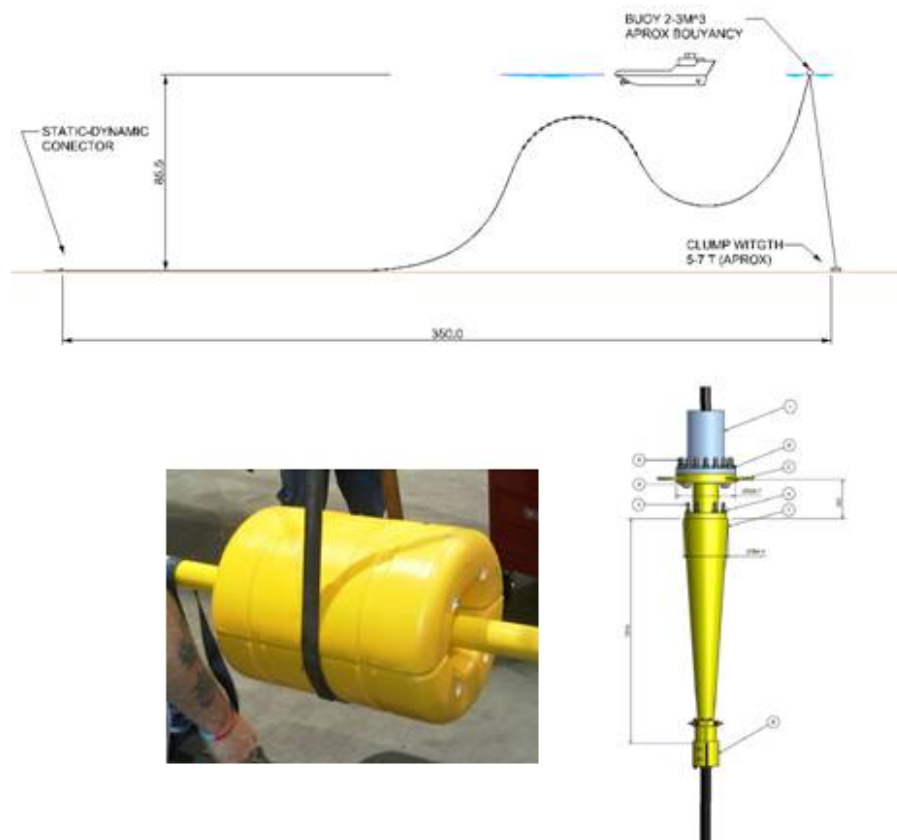


Figure 81 Dynamic cable study

The results from the environmental data for extreme conditions had to be taken into consideration. The design for the cable entry has posed difficulties as to allow for the dynamic behavior of the structure and to avoid failures due to fatigue.

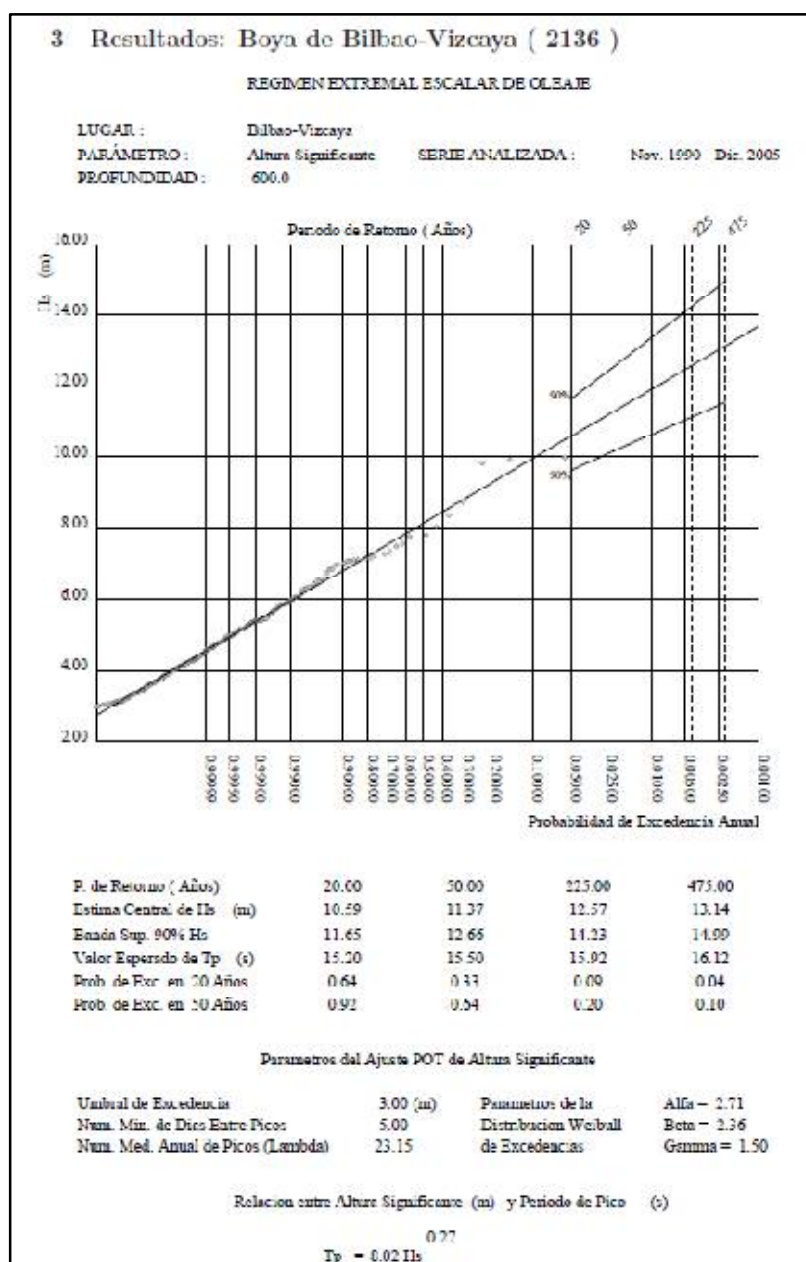
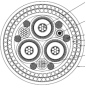
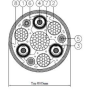

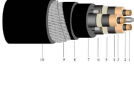


Figure 82 Results for extreme conditions for the design calculations from Bilbao-Biscay buoy (2136)

Commercial systems for bending restrictors have been investigated together with different cable types and different configurations for the location of the cable into the structure were evaluated.

Documents from a series of different vendors have been evaluated and analyzed to determine the best way for the cable entry. Different designs were evaluated concerning the cable entry route inside the structure with all respective consequences for the cable installation, the connection towards the electrical components in the interior and also with respect to O&M aspects concerning the access to the connection points, also important for the installation and decommissioning activities.

Table 16 Table with offers from different cable suppliers

Concept	Units	Supplier 1	Supplier 2	Supplier 3	Supplier 4
Outside diameter	m	87	105	87	102
Outer Sheath material	-	Polyethylene (4 mm nominal thickness)	PE	HDPE (ST7)/Yellow. Nominal thickness: 4.0 mm	Cubierta exterior: PE extruido.
Outer Sheath color	-	Black	?	Yellow	Black
Cable armouring	-	Galvanised steel wire	3 Steel Wire Rops (22 mm diameter) and 1 center wire rope (33 mm diameter)	Armour bedding material HDPE (ST7)/Black. Nominal thickness: 2.5 mm. Double layer Armour. Galvanised steel wires. Nominal diameter of the wires: 3.5 mm. 1st layer number of wires: 55. 2nd layer number of wires: 63	Armadura: doble corona de hilos de acero galvanizado.
MBR Manufacture, storage & load-out	mm	910	2400	1014	?
MBR Duct pull in (installation)	mm	3620	2400	1305	?
MBR deployment (operation)	mm	2610	2400	1205	?
Weight in air	kg/km	18240	22985, 17982	16000	17700
Weight in water (unfloated)	kg/km	11570	13965, 34149	9900	12400
Minimum brk load	kN	720	?	347	?
Tension capacity installation	kN	?	535	?	?
Tension capacity operation	kN	?	368	?	?
Cable maximum safe working load	kN	180	?	?	?
Max conductor temperature	°C	90	?	?	?
Unilateral cross sectional properties					
BI (breaking stiffness)	kNm ²	?	0	22.2	?
BI (bending stiffness)	kNm ²	?	0	25	?
GI (torsional stiffness)	Nm ²	?	0	?	?
Photo					
Power Cores		3 OFF 8.7/15 KV Power Cores to IEC60502-2, each comprising: -Circular stranded (class 2) conductor -Extruded semiconducting conductor screen. -Extruded XLPE insulation. -Semiconducting insulation screen. -Copper wire metallic screen	3 Power Cable 35 mm ² OD=23.0 mm	500f m of a 3x35 mm ² Cu 8.7/15kV dynamic cable with 24 optical fibers (cable cross-section optimised for the rated 1.5 MW at an operating voltage of 13.2 kV). -water blocked / circular/RM. -Class 2 -Nominal diameter: 7.1 mm -copper tapes thickness: 0.1 mm -Insulation material: HEP, nominal thickness: 5.5 mm, minimum thickness: 4.85 mm. Diam over insulation: approx. 19.8 mm. -Longitudinal water tightness material: SC swelling tapes. -Inner and outer semicond nominal thickness: 0.6 mm -Outer sheath: HDPE (ST7)/Black. Nominal thickness: 2 mm. Diameter (approx.): 27 mm	500 metros cable Eprotenax HMM 3x35mm ² 8.7/15 kV (Incluye 2 conductores de corriente continua 220 V). -1. Conductor: Cuerda redonda de hilos de cobre según IEC 60028. Diam: 7 mm -2. Semiconductora interna: Capa extrusionada de material conductor. -3. Aislamiento: Eléctrico propileno (EP), Esp. Nom. = 4.5 mm. Diam=19 mm -4. Semiconductora externa: Capa extrusionada de material conductor. -5. Pantalla: metálica trenza de cobre estañado -6. Cubierta: PE. Reunión de tres almas, mas 2 conductores de c.c. (opcional), mas 1 cable de FO. -7. Releño: compuesto extruido. -8. Asiento de armadura: cubierta de PE extruido. -9. Armadura: doble corona de hilos de acero galvanizado.
Fibre Optic		1 OFF Fibre Optic cable comprising: -24 off 9/125 micron minge mode fibres to ITU-T G.652. -Supported strain free withing a gel filled stainless steel tube. -Extruded polyethylene armour bedding. -Galvanised steel wire armour	16+2 Fibre Optic OD=12.0mm	Optical Fiber Cable Fiber count: 24 Fiber type: G.652B/D Armour: ACS wires (nº/diameter): 6/3,60 mm	El cable dinámico dispondrá de un cable con 24 fibras ópticas. Vease ficha tecnica en la oferta
Armour		-Armour wire bedding of extruded polyethylene (2.6 mm nominal thickness). -Doble layer of galvanised steel wire (4 mm diameter)	3 Steel Wire Rops (22 mm diameter) and 1 center wire rope (33 mm diameter)	Double layer Armour. Galvanised steel wires. Nominal diameter of the wires: 3.5 mm. 1st layer - Number of wires: 55. 2nd layer - Number of wires: 63	Armadura: doble corona de hilos de acero galvanizado.
220V Auxiliary cable		2 off 220V Auxiliary control cable, each comprising: -70 mm ² copper circular stranded (class 2) conductor. -Conductor includes water blocking materials. -Extruded XLPE insulation.	2 Electrical Cable 500/1000 V 70 mm ² OD=12.7 mm	Not included in this offer? To be included	Vease ficha tecnica de la fibra optica en oferta
Other characteristics			3 PVC Intermediate Conduit and 6 PVC Outer Conduit	Max. DC resistance at 20°C -Conductor 0.524 OHM/km -Metallic screen 2.6 OHM/km Short-circuit capacity (1 s) Conductor 5 kA Metallic screen 1 kA	Vease ficha tecnica en la oferta
Standard and tests applied to cable design and fabrication		?	?	?	Norma : IEC 60502-2 Código : 2006.4365 Los ensayos a realizar al cable y terminales tras su fabricación, son los de Rutina y Sobre Muestra especificados en la norma IEC 60 502-2.

The data for different cables from different vendors has been analyzed in respect to the implications for the respective cable configuration, fixture and routing as well as possible installation scenarios. Compare with Table 16. The finalization of this design for the dynamic cable is still outstanding and will depend on the final decisions for marine operations and cable vendor. Minor secondary structures will depend on this decision as well and will have to be added to the final version of this document.

3 References

1. DNV RP-B401, January 2005
2. GL Wind Guideline for the Certification of Offshore Wind Turbines, edition 2005, chapter 3.5
3. BV Corrosion Protection of Steel Offshore Units and Installations, Recommended Practice; NR 423 DTO R00 E
4. BV Rules for the Classification of Offshore Units, Part B – Structural Safety, Chapters 1-2-3, NR 445.B1 DT R02 E;
5. EN ISO 12944, Parts 3 and 5
6. Hydrodynamic data, 120816_HiPrwind_Hydrodynamic_report
7. Fatigue Load cases 110044bt03aLoadCaseDefinition.pdf
8. Classification of Mooring Systems for Permanent Offshore Units NI493-DTM-R01-E July 2008
9. Rules on Materials and Welding for the Classification of Marine Units BV NR 216 January 2011
10. Classification and Certification of Floating Offshore Wind Turbines NI572 BV Guideline Note, November 2010.
11. Design and Analysis of Stationkeeping Systems for Floating Structures. Third Edition API RP 2SK. October 2005.
12. OrcaFlex v 9.1a User manual OrcinaLtd.
13. Mooring data, 120816_HiPriwind_BV_Mooring_Verification_rev4.docx
14. Anderson H S, 2011: 'Local analysis of lower and diagonal brace connection at columns'. Olav Olsen Project no 11229, Memo no 01, Version 1.
15. Anderson H S, (03/01/2012, 12:34): 'HiPRWind – updated detail information', Email to J de Lauzon, cc to J Pascual Vergara, M Pachot, F Surmont, S Smith, M Joosten and D Sveen. Attachments: 'localAnalysis_s3_v2.pdf', 'HiPRWindTowerSupportSimplifications.pdf', 'connectionsS3.zip' and 'towerSupport.zip'.
16. DNV, 2003: 'Fatigue Design of Offshore Steel Structures'. DNV Recommended Practice DNV-RP-C203.
17. Egana I, (04/11/2011, 10:39): 'Project HiPRWind. Definition of the floating platform in Bladed', Email to S Smith and D Sveen. Attachment: '111102_Bladed_definition_platform.xls'.
18. Egana I, (22/12/2011, 11:36): 'Cycle counting for fatigue analysis, project HiPRWind WP1', Email to M Joosten, S Smith, D Sveen and cc J Pascual Vergara. Attachment: 'Markov.zip'.
19. Smith S, Maddox S, He W, Zhou D and Saraswat R, 2010: 'Computer Based Fatigue Analysis for Welded Joints – Third Progress Report'. TWI Report 955a/2010.
20. Smith S, Maddox S, 2010: 'Computer Based Fatigue Analysis for Welded Joints – Fifth Reporting Period – Draft Revisions to BS 7608'. TWI Report 955b/2010.
21. Sveen D, (10/04/2012, 13:06): 'RE: Fatigue analyses of the support braces column connection', Email to S Smith and H S Anderson, cc to J Pascual Vergara and M Joosten.
22. Sveen D, (25/04/2012, 14:26): 'RE: Fatigue analyses of the support braces column connection', Email to M Joosten, J Pascual Vergara and H S Anderson, cc to S Smith, I Egana, M Pachot, J de Lauzon and F Surmont.
23. 2012-04-19 - "HiPRWind Main Structure Specification rev.2 April 2012.pdf"
24. 2011-12-19 - "WTG FLOATER SEMI Rev-01 191211.xls"
25. Recommended practice, DNV-RP-C103 Column Stabilized Units, October 2010
26. FP7 Project - Hi PR WIND – WP1 – BV – Design check under extreme conditions 26/04/2012 3 / 22 Hi PR WIND / WP1